2017

A Mechanistic Study of Micro RNA 21 Induced Hepatic Fibrosis and Use Of Sparstolonin B In Remediation Of Environmental NAFLD

Diptadip Dattaroy

University of South Carolina

A MECHANISTIC STUDY OF MICRO RNA 21 INDUCED HEPATIC FIBROSIS AND USE OF SPARSTOLONIN B IN REMEDIATION OF ENVIRONMENTAL NAFLD.

by

Diptadip Dattaroy

Bachelor of Science
St. Xavier's College (Autonomous), Kolkata,2010

Master of Science
University of Calcutta,2012

_____

Submitted in Partial Fulfillment of the Requirements

For the Degree of Doctor of Philosophy in

Environmental Health Sciences

The Norman J. Arnold School of Public Health

University of South Carolina

2017

Accepted by:

Saurabh Chatterjee, Major Professor

Daping Fan, Committee Member

Geoff Scott, Committee Member

R Sean Norman, Committee Member

Cheryl L. Addy, Vice Provost and Dean of the Graduate School

DEDICATION

To my beloved parents, Mr. Dipak Kumar Dattaroy and Mrs. Shyamalika Dattaroy. Their

boundless love, efforts and sacrifices made me what I am today.

ACKNOWLEDGEMENTS

First and foremost, I offer my sincerest appreciation to my supervisor, Dr. Saurabh Chatterjee for supporting me throughout my thesis with his wisdom and knowledge whilst encouraging me to think outside the box and become independent. His guidance, helped me throughout my PhD and without him this thesis would not have been completed.

I would also like to thank the rest of my PhD committee members: Dr. Daping Fan, Dr. Geoff Scott and Dr. Sean Norman, for their invaluable advice and encouragement.

I have been blessed with a cheerful group of lab colleagues. Without their support and motivation, this work wouldn't have been possible. I would like to thank Mr. Varun Chandrashekaran for his help and continuous encouragement which helped me to strive towards my goal in research.

Last but not the least, I would like to thank my family and friends for their unconditional love and care which have always uplifted me against all odds.

ABSTRACT

Due to the increased prevalence of obesity, non-alcoholic fatty liver disease (NAFLD) has become a major public health problem in the Western world and Asian countries. Approximately a third of the general population in the US has NAFLD. NAFLD includes a spectrum of histological characteristics ranging from simple steatosis to steatohepatitis, fibrosis and cirrhosis and can be characterized into to two major phenotypes: nonalcoholic fatty liver (NAFL) and nonalcoholic steatohepatitis (NASH). Water disinfection byproducts like trihalomethanes can act as crucial risk factors for NAFLD progression. Here I have studied the molecular mechanisms of a water disinfection byproduct, Bromodichloromethane, in induction of hepatic inflammation and fibrogenesis. I found that Bromodichloromethane (BDCM) can induce hepatic fibrogenesis and NASH by inducing leptin mediated activation of NADPH oxidase and subsequent increase in microRNA21 expression, resulting in augmented hepatic TGFβ signaling. I also explored the hepatoprotective effects of a plant derived TLR4 antagonist *Sparstolonin B* (SsnB) and found that it inhibited BDCM induced TLR4-Flottilin co-localization, decreased microRNA21 expression and reduced the expression of a myriad of inflammatory markers in liver when administered *in vivo*. Similar effects of SsnB were also observed in cell culture model of kupffer cells. Anti-fibrotic and anti-proliferative mechanisms of SsnB were observed in a BDCM induced mice NASH model and in hepatic stellate cell (HSC) culture. Mechanistically, SsnB decreased activation and pro-fibrogenic proliferation of HSCs. SsnB could inhibit hedgehog signaling pathway,

decreased proliferation and induced apoptosis in HSCs. SsnB decreased TGFβ signaling by upregulating BAMBI and decreased STAT3 activation in HSCs. SsnB also changed the morphology of fibrogenic stellate cells by downregulating focal adhesion adaptor protein and stress fibers. Thus, my research unravels novel molecular mechanisms of hepatic fibrogenesis in NASH and proposes the use of Sparstolonin B to ameliorate hepatic inflammation and fibrosis in NASH.

TABLE OF CONTENTS

LIST OF FIGURES

CHAPTER 1

INTRODUCTION

Non-alcoholic fatty liver disease (NAFLD) is becoming the most common chronic liver disease in the world with the increased prevalence of obesity and metabolic syndrome(1). The prevalence of NAFLD is around 30% adult population, 80-90% of obese adults, 30-50% diabetic patients and around 90% in patients having hyperlipidemia. In children, the prevalence of NAFLD is 3-10% rising up to 40-90% in obese children(2). Ranging from simple fat deposition or steatosis in the liver to nonalcoholic steatohepatitis (NASH), NAFLD involves a continuum of histological characteristics. Not all individuals having steatosis develop severe diseases, however, NASH can lead to cirrhosis and end-stage liver diseases(3). In the United States, NASH is the second most common liver diseases among the adults who are awaiting liver transplant. The mortality of NASH affected patients can also increase by cardio-vascular damage. According to the multiple hit hypothesis of NASH, steatosis makes the liver vulnerable to secondary hits which are responsible for inducing hepatic inflammation, fibrosis and end stage liver diseases (3). Increased consumption of high fat diet, excess lipolysis from adipose tissue, decreased fat export in VLDL (very low-density lipoprotein) form, augmented de novo lipogenesis, reduced free fatty acid β-oxidation- all these factors can lead to hepatic steatosis. Insulin resistance plays an important role to aggravate this

process by initiating considerable metabolic dysregulation (4). Circulatory cytokines, hypoxia and death of adipocytes can trigger inflammation in the steatotic liver. Interleukin-6 (IL-6), tumor necrosis factor-α (TNFα), and CC-chemokine ligand-2 (CCL2) secreted from inflamed adipocytes can regulate insulin resistance, induce macrophage infiltration and other pro-inflammatory cascades (5). However, adiponectin secreted by adipocytes is an anti-inflammatory adipokine that enhances insulin sensitivity, helps in expansion of healthy adipocytes, prevents ectopic lipid deposition and regulates hepatic β-oxidation of fatty acids (6). Leptin is another adipokine and it maintains homeostatic control of adipose tissue mass (7). NAFLD is associated with leptin resistance (8). NASH patients have been found to have higher serum leptin levels than controls. Leptin has fibrogenic potential. However, serum adiponectin level decreases in NASH patients compared to healthy controls. Leptin has been found to augment inflammation, activate hepatic stellate cells, increase TGFβ signaling and induce insulin resistance. However, adiponectin decreases hepatic stellate cell proliferation, decreases inflammation and fibrogenesis (9). De novo Lipogenesis, Insulin resistance, lipotoxicity, mitochondrial dysfunction, Endoplasmic Reticulum stress-all these factors can facilitate the transition from simple steatosis to NASH (4). Several environmental pollutants can act as secondary mediators and induce injury in steatotic liver. Studies in mice, human adults and also children have shown that air pollution can induce insulin resistance, increase oxidative stress in obese liver and thus plays a chief role on the development of NAFLD (10). Inhaled particulate matter can increase systemic inflammation, increase the levels of triglyceride, LDL, VLDL and increased pro-inflammatory cytokines. In the liver, the particles can induce kupffer cell activation,

activate JNK, NF-kB, TLR4 signaling pathways, affect PPAR activity, alter glucose and fat metabolism etc.(11). Heavy metal containing particulate matters, when hit the liver, can affect lipid metabolism and trigger oxidative stress in the liver (12). Dioxin contaminants which are generated during incineration of domestic and industrial wastes, can escape in the nature from the incinerators. They are known to induce steatohepatitis by down regulating hepatic carboxylesterase 3 (CES3), activating signal transducer and activator of transcription 3 (STAT3), transforming growth factor (TGFβ), IL-6, and SMAD signaling pathways (13). Liver plays an important role in detoxification of drugs, hormones and environmental pollutants. Industrial chemicals, drinking water byproducts like trihalomethanes (THMs) are known to be associated with fatty liver disease and hepatic injury. Trihalomethanes are short lived halogenated compounds which are formed when disinfectants come in contact with natural organic matter. Bromodichloromethane (BDCM), trichloromethane (TCM), dibromochloromethane (DBCM) and tribromomethane (TBM) are four THMs found in disinfectant treated water and humans are exposed to them through ingestion, inhalation and dermal as THMs may enter human body through drinking water, showering, swimming, mopping etc. (14). Several experimental and epidemiological studies found the association between trihalomethane expore with hepatic injury and disbetes mellitus (14). A current cross-sectional study utilizing the U.S. NHANES 1999–2006 data has reported that ALT levels (a marker of liver injury) was increased in individuals exposed to higher than the median blood brominated trihalomethane levels (15). As liver metabolizes the xenobiotic compounds in circulation and process the absorbed contents from the gastrointestinal tract, it is the primary target organ for human THM exposure which was supported by some previous

3

studies from our lab where low acute exposure of bromodichloromethane (BDCM) in diet induced obese mice was found to generate free radicals followed by CYP2E1 mediated metabolism resulting in oxidative stress, protein free radical formation and lipid peroxidation. BDCM induced oxidative stress also promotes glucose transport, glycolysis and gluconeogenesis resulting in dysfunctional lipid metabolism and NASH development (16-18). Increased hepatic leptin followed by BDCM exposure in obese mice augmented hepatic inflammation, kupffer cell activation and hepatic fibrogenesis resulting in NASH progression (16, 19). In the first chapter of my thesis, I explored the pro-fibrogenic role of BDCM where BDCM induced NADPH oxidase induced mir21 expression in liver and increased TGFβ signaling (20).

Alteration of the gut microbiota and induced permeability of intestinal barrier can also trigger hepatic inflammation and metabolic disorders. Endotoxins like Lipopolysaccharide (LPS) augments NASH pathogenesis as observed in many studies (21, 22). Stimuli by pathogen associated molecular patterns (PAMPS) are responded by innate immune response through toll like receptors (TLRs) and NOD-like receptors (NLRs). Apart from inflammation though gut leaching, tissue injury and cell death can also induce sterile inflammation and activate TLR4 in liver giving rise to NASH related liver injury (3). TLR family of receptors can get activated by damage associated molecular patterns (DAMPs) released during oxidative stress induced tissue injury (23). Interestingly, BDCM induced NADPH oxidase activation can produce peroxinitrite which can induce TLR4 recruitment in the lipid rafts, augment TLR4 signaling, increase IL-1β production, sinusoidal injury and kupffer cell activation resulting in NASH (24). TLR4 activation can lead to increased IKK and JNK activation, increased NFkB

translocation into nucleus etc., which leads to inflammation, fibrosis, insulin resistance and other metabolic dysregulation during NASH (25-27).

Our collaborators have characterized and published studies of a TLR4 antagonist, Sparstolonin B (SsnB) derived from a Chinese herb, *Sparganium stoloniferum*, an herb historically used in traditional Chinese herbal medicine as an anti-inflammatory, anti-tumor agent. As identified by NMR and X-ray crystallography, SsnB is a polyphenol with structural similarities to isocoumarins and xanthone-all these compounds are known for anti-inflammatory, anti-oxidant and anti-tumor properties (28). SsnB has been shown to disrupt TLR4 and TLR2 dependent downstream signaling pathways, including NfkB and MAPK (28). We are the first group to test the therapeutic effect of this compound in NASH. In the second chapter of my thesis I report that SsnB attenuates of liver inflammation in early NASH through inhibiting TLR4 migration into the lipid rafts (19). As chronic inflammation and TLR4 activation leads to increased stellate cell activation and excessive extracellular matrix deposition in NASH liver (27), we aim to use SsnB to reduce NASH related liver fibrosis by abrogating the TLR4 signaling. The third and fourth chapters of this thesis examine the molecular mechanism of SsnB in attenuation of stellate cell (HSC) activation, proliferation and fibrosis. It is important to target hepatic stellate cell to attenuate liver fibrosis and cirrhosis. These cells are also involved in liver cancer and acute liver injury. We found that SsnB significantly decreased stellate cell activation and proliferation by downregulating pro-fibrogenic cell signaling pathways. We have also observed that SsnB inhibits the focal adhesion adaptor protein, causes loss of stress fibers and induces apoptosis in HSCs. Thus, my research provides a novel (i) mechanistic and (ii) therapeutic approach for NASH-prevention/remediation.

5

CHAPTER 2

MICRO RNA 21 INHIBITION OF SMAD 7 ENHANCES

FIBROGENESIS VIA LEPTIN MEDIATED NADPH OXIDASE IN

EXPERIMENTAL AND HUMAN NONALCOHOLIC

STEATOHEPATITIS[1]

Running title: Oxidative stress-miR21 regulation of liver fibrosis

Key words: NAFLD, ob/ob, NF-kB, SMAD7, SMAD2/3 colocalization, TGF-β

Author for correspondence:

*Dr. Saurabh Chatterjee, Ph.D. 1Environmental Health and Disease Laboratory, Department of Environmental Health Sciences, University of South Carolina, Columbia 29208 USA. Email: schatt@mailbox.sc.edu; Tel: 803-777-8120; Fax: 803-777-3391

Abstract:

Hepatic fibrosis in NASH is the common pathophysiologic process resulting from chronic liver inflammation and oxidative stress. Though significant research has been carried out on the role of leptin induced NADPH oxidase in fibrogenesis, the molecular mechanisms that connect leptin-NADPH oxidase axis in upregulation of TGF-β signaling has been unclear. We aimed to investigate the role of leptin mediated upregulation of NADPH oxidase and its subsequent induction of miR21 in fibrogenesis. Human NASH livers and a high fat (60% kCal) diet fed chronic mouse model where hepatotoxin bromodichloromethane was used to induce NASH, were used for this study. To prove the role of Leptin-NADPH oxidase-miR21 axis, mouse deficient in genes for leptin, p47phox

7

and miR21 were used. Results showed that wild type mice and human livers with NASH had increased oxidative stress, increased p47phox expression, augmented NF-kB activation and increased miR21 levels. These mice and human livers showed increased TGF-β, SMAD2/3-SMAD4 colocalizations in the nucleus, increased Col1α and α-SMA expression with a concomitant decrease in protein levels of SMAD7. Mice that were deficient in leptin or p47phox had decreased activated NF-kB and miR21 levels suggesting the role of leptin and NADPH oxidase in inducing NF-kB mediated miR21 expression. Further miR21 KO mice had decreased co-localization events of SMAD2/3-SMAD4 in the nucleus, increased SMAD7 levels and decreased fibrogenesis. Taken together the studies show the novel role of leptin-NADPH oxidase induction of miR21 as a key regulator of TGF-β signaling and fibrogenesis in experimental and human NASH.

2.1 INTRODUCTION

Pathogenesis of NASH is not clearly understood and perceived to comprise of an inflammatory phase of high circulatory leptin, increased oxidative stress, elevated inflammatory cytokines resulting in hepatocellular injury and subsequent progression into fibrosis (29). Most NASH pathophysiology is accompanied by a late stage fibrosis (30-32). Hepatic fibrosis in NASH most likely occurs from chronic liver inflammation associated with rise in pro inflammatory cytokines and oxidative stress (33). Fibrosis is closely linked to accumulation of extracellular matrix (ECM) proteins, mainly type I collagen, which also can occur in many chronic liver diseases(33). The accumulation of ECM proteins distorts the hepatic architecture by forming a fibrous scar and the subsequent development of nodules of regenerating hepatocytes can lead to condition known as cirrhosis (34). Since NASH might arise almost always from a preexisting

condition of obesity, type 2 diabetes, insulin resistance, the higher circulatory levels of adipose tissue cytokines leptin and TNF-α has been predicted to play a significant role in hepatic fibrogenesis (35). We and others have shown in rodent models of NASH that higher leptin is closely associated with fibrosis in NASH (36-38).

Leptin, a product of the ob gene, is synthesized in the liver and the adipose tissue (39). We have shown that mice fed with a high fat diet and challenged with low doses of hepatotoxins cause increase in both hepatic and circulatory levels of leptin (17, 40). An early study by Honda H *et al.* showed that leptin deficiency is responsible for resistance to thioacetamide induced fibrogenesis whereas subsequent studies have highlighted the role of leptin in stellate cell activation, leptin induced TGF-β production via Kupffer cells and leptin signaling induced collagen production and extracellular matrix formation (40-45).

Although leptin has been found to play a distinct role in the stellate cell activation and TGF-β production, molecular mechanisms involving reactive oxygen species, especially the role of NADPH oxidase were revealed recently (33). NADPH oxidase , both the phagocytic and non-phagocytic isoforms has been detected in the liver cell types (46). Hepatic stellate cells has been found to express the NADPH oxidase isoform 2 (NOX2) and deletion of one of its cytosolic subunits have resulted in decreased fibrosis in rodent models of NASH (33). Further published reports from our laboratory have identified the role of peroxynitrite, a highly reactive nitroso species formed by superoxide and nitric oxide in NASH (40). We further showed that NADPH oxidase was crucial for peroxynitrite formation that was again dependent on leptin (40).

It is also critical that high circulatory levels of leptin accompanied by leptin resistance are common in patients with liver fibrosis (47). Quiescent hepatic stellate cells in humans express very low levels of p47phox, a regulatory subunit of NADPH oxidase but they are highly activated in culture activated stellate cells isolated from patients with liver fibrosis (48).

Although significant research has been carried out on the leptin induced NADPH oxidase in fibrogenesis, the molecular mechanisms that connect leptin-NADPH oxidase axis in upregulation of TGF-β signaling has been unclear. Reactive oxygen species production by NADPH oxidase, primarily in the form of superoxide or hydrogen peroxide has been shown to induce nuclear translocation of NF-kB (49). Our unpublished reports indicate that NF-kB activation led to epigenetic modulations in the form of upregulation of micro RNA 21 in NASH. Micro RNA 21 (miR21) is a small noncoding RNA that has been found to have a distinct role in inflammation and their regulatory functions in NASH pathophysiology are slowly emerging (50, 51).

miR21 upon induction target several proteins either by binding entirely to the complementary sequence of mRNA of the target protein resulting in a nonfunctional mRNA or binding partially to cause a translational defect (52). Regulatory protein SMAD7 which plays an important role in TGF-β signaling, is a target of miR21 and has been shown to reverse the regulatory effect of this protein (53, 54). Importantly, TGF-β signaling is crucial to the fibrogenesis in NASH and has been shown conclusively in many studies (55, 56).

In this study, we test the hypothesis that high circulatory leptin induced NADPH oxidase-NF-kB activation causes miR21 mediated SMAD 7 inhibition resulting in increased TGF-β signaling. The resultant inhibition of SMAD 7 a regulatory SMAD leads to uninterrupted TGF-β function causing fibrogenesis in NASH. The results obtained via the use of a rodent model of NASH, human tissues and transgenic mice lacking leptin, p47phox and miR21 show that leptin induced NADPH oxidase causes activation of NF-kB and subsequent upregulation of miR21. Lack of miR21 led to significantly less fibrogenesis, TGF-β production, and downstream signaling of TGF-β pathway.

2.2 MATERIALS AND METHODS

Obese mice: Adult male, pathogen-free, 6 weeks old mice with C57BL/6J background (Jackson Laboratories, Bar Harbor, Maine) were used as model for diet induced obesity. The animals were fed with high-fat diet (60% kcal) from 6 weeks to 16 weeks to develop diet induced obesity (DIO). After completion of 16 weeks, all experiments were conducted. Mice which contained disrupted ob gene (leptin) (B6. V-Lepob/J) (Jackson Laboratories) (ob/ob), another group of leptin knockout mice (ob/ob) treated with leptin (leptin supplemented group, ob/ob + Leptin), disrupted p47 phox gene(B6.129S2-Ncf1tm1shl N14) (Taconic, Cranbury, NJ) (p47 phox KO) and mice with disrupted microRNA21 gene (B6;129S6-Mir21atm1Yoli/J) (miR21 KO) were fed with a high-fat diet and treated identically to DIO mice. The mice were housed one per cage in a temperature-controlled room at 23-24°C with a 12-h/12-h light/dark cycle with libitum access to food and water. All animals had been treated in strict accordance with the NIH guideline for Humane Care and Use of Laboratory Animals and local IACUC standards.

All experiments were approved by the institutional review board at NIEHS, Duke University and the University of South Carolina.

Induction of liver injury in obese mice (Toxin Model): Bromodichloromethane (BDCM) (2.0m mole/kg, diluted in corn oil) was administered through intraperitoneal injection in 16 weeks old DIO mice (n=6). Liver tissues were collected and pooled after 24 hour exposure of BDCM (DIO+BDCM (24h)) and after 48 hour exposure of BDCM (DIO+BDCM (48h)). The other group of DIO mice was administered two doses of BDCM (1.0 mmole/kg, diluted in corn oil)/ week for one week (DIO+BDCM (1w)) and for four weeks (DIO+BDCM (4w))(n=4). 16 weeks old high fat diet fed DIO mice, administered with 100ng GdCl3 per day via intraperitoneal route for 4 weeks were also administered with BDCM (1.0mmole/kg, diluted in corn oil) through the intraperitoneal route (GdCl3 treated). 16 weeks old high fat diet fed gene specific knockout mice (ob/ob, p47 phox KO, miR21 KO) mice were administered with BDCM (1.0mmole/kg, diluted in corn oil) through the intraperitoneal route (n=3). DIO mice was treated with corn oil (diluent of BDCM) to use as control. After completion of the treatments, all mice were sacrificed for liver tissue for the further experiments. The tissues were pooled and used for the study.

Human tissues: Human liver tissues both from NASH and normal individuals were obtained from NIH repository at University of Minnesota and University of Pittsburg. Each experiment was carried out using 3 experimental group and 3 control samples.

Histopathology: Liver sections were collected from each animal and fixed in 10% neutral buffered formalin. These formalin-fixed, paraffin embedded tissues were cut in

5µm thick sections. These sections were deparaffinized using standard protocol and stained with Picro-Sirius red. Picro-Sirius red staining of liver sections was done by using Nova ultra sirius red stain kit following manufacturer's protocol (IHC world, Woodstock, MD) and they were observed using 20x objectives under the light microscope.

Immunohistochemistry: Formalin-fixed, paraffin embedded tissues were cut in 5µm thick sections. Each section was subjected to deparaffinization using standard protocol. To describe briefly, these sections were washed with two changes of 100% xylene twice for 3 min followed by xylene: ethanol (1:1) for 3 min, and rehydrated through a series of ethanol (twice with 100%, 95%, 70%, and 50%), twice with distilled water. The sections were finally rinsed twice with PBS. Epitope retrieval of the deparaffinized sections was carried out using epitope retrieval solution and steamer (IHC-World, Woodstock, MD) by following the manufacturer's protocol. The primary antibodies 1) anti-3 nitrotyrosine, 2) anti-TGFβ, 3) anti-CTGF, 4) anti-EDAFN, 5) anti-α-SMA, 6) anti-Col 1α1 were purchased from Abcam (Cambridge, MA) and used in recommended dilutions. Species specific biotinylated conjugated secondary antibody and streptavidin conjugated with HRP were used from Vectastain Elite ABC kit (Vector Laboratories, Burlingame, CA) to perform antigen-specific immunohistochemistry following manufacturer's protocols. 3, 3' Diaminobenzidine (Sigma-Aldrich, St.Louis, MO) was used as a chromogenic substrate. Tissue sections were counter-stained by Mayer's hematoxylin (Sigma-Aldrich). Phosphate buffer saline was used for washing thrice between the steps. Sections were mounted in Simpo mount (GBI Laboratories, Mukilteo, WA) and observed under a 20x objective. Morphometric analysis was done using CellSens Software from Olympus America.

Immuno-fluorescence dual-labelling microscopy: Formalin-fixed, paraffin embedded tissues were cut in 5μm thick sections. Each section was subjected to deparaffinization using standard protocol. Epitope retrieval of the deparaffinized sections was carried out using epitope retrieval solution and steamer (IHC-World, Woodstock, MD) by following the manufacturer's protocol. The primary antibodies anti-SMAD2/3, anti-SMAD4, and anti-gp-91phox, anti-p47phox (purchased from Cell Signaling Technology, MA and Santa Cruz biotechnology, Inc. Santa Cruz, CA) and used at recommended dilutions. Species-specific anti-IgG secondary antibodies conjugated with Alexa Fluor 488, Alexa Fluor633 (Invitrogen, California, USA) were used together against anti-SMAD4 and anti-SMAD2/3 respectively. Alexa Fluor 488 and Alexa Fluor 568 were used together against anti-p47phox and anti-gp91phox respectively. The sections were mounted in a ProLong gold antifade reagent with DAPI (Life technologies, EU, OR). Images were taken under 20x/60x oil objectives using Olympus BX51 microscope.

Quantitative Real-Time Polymerase Chain Reaction Analysis (qRT-PCR): Real-time reverse transcription-polymerase chain reaction was done to measure gene expression (mRNA) levels in the liver tissue samples. Total RNA was isolated from each liver tissue by homogenization in TRIzol reagent (Life Technologies, Carlsbad, CA) according to manufacturer's instruction and was purified by using RNeasy mini kit columns (Qiagen, Valencia, CA). iScript cDNA synthesis kit (Bio-rad, Hercules, CA) was used to convert 1μg of purified RNA to cDNA following the manufacturer's standard protocol. qRTPCR was performed with the gene specific primers by using SsoAdvanced universal SYBR Green supermix (Bio-Rad, Hercules, CA) and CFX96 thermal cycler (Bio-Rad, Hercules, CA). Threshold Cycle (Ct) values for selected genes were normalized against 18S

(internal control) values in same sample. For each gene and each tissue sample, each reaction was carried out in triplicates. Liver sample from DIO mice was used as control to compare with all other liver samples in the toxin model of NASH. The relative fold change was calculated by the 2-ΔΔCt method. The primers used for Real time PCR in 5'to 3' orientation are Human p47phox (Forward: GTACCCAGCCAGCACTATG, Reverse: CCTGGCTTTGCTTTCATCTG) and Mouse p47phox (Forward: GGTCGACCATCCGCAACGCA, Reverse: TGTGCCATCCGTGCTCAGCG).

miR21 expression levels in liver tissues: Total miRNA was isolated from liver tissue by homogenization in Qiazol reagent (Qiagen, Valencia, CA) following the manufacturer's instructions. The purification was done by using miRNeasy mini kit columns (Qiagen, Valencia, CA). 1000ng of purified miRNA was converted to cDNA using miScript cDNA synthesis kit (Qiagen, Valencia, CA) following the manufacturer's protocol. qRTPCR was performed with microRNA specific primers (Qiagen, Valencia, CA) using miScript SYBR Green PCR master mix (Qiagen, Valencia, CA) and CFX96 thermal cycler (Bio-rad, Hercules, CA). Threshold Cycle (Ct) values for the selected gene was normalized against RNU6-2 (internal miR expression control) values in the same sample.

Western Blotting: 30 mg of each liver tissue was homogenized in 500 µl of RIPA buffer (Sigma Aldrich) in the presence of phosphatase and protease inhibitor (Pierce, Rockford, IL) by using dounce homogenizer. After centrifuging the homogenate, the supernatant was collected for further experiments. 30 µg of protein from each sample was loaded on 4–12% bis-tris gradient gel (Invitrogen, California, USA) for SDS PAGE. By using precut nitrocellulose/filter paper sandwiches (Bio-Rad Laboratories Inc., California, USA) and Trans – Blot Turbo transfer system (Bio-Rad), proteins were transferred to

nitrocellulose membrane. Blots were blocked with 5% non-fat milk solution. Primary antibody against SMAD7 and β-actin (purchased from Abcam) were used at recommended dilutions and incubated overnight at 4ºC. Species specific secondary antibody conjugated with HRP was used. Pierce ECL Western Blotting substrate (Thermo Fisher Scientific Inc., Rockford, IL) was used. The blot was developed by using BioMax MS Films and cassettes (with intensifying screen, Kodak). Densitometry analysis of the images was done using Lab Image 2006 Professional 1D gel analysis software from KAPLEAN Bioimaging Solutions (Liepzig, Germany).

NF-kB transcription factor binding assay: Nuclear fraction of each liver samples were isolated by using NF-kB assay kit and following manufacturer's standard protocol (Five photon Biochemicals). DNA binding activity of the transcription factor NF-kB present in those nuclear extracts was detected using enzyme-linked immunosorbent assay (ELISA) method (Abcam's NF-kB p65 Transcription Factor Assay Kit) following manufacturer's standard protocol.

Statistical Analyses: In vivo experiments were repeated two-three times with an average of 3 mice per group with other in vivo experiments having 4-6 mice/group (n=3/4/6 wherever applicable; data from each group of mice was pooled). The statistical analysis of data was done by analysis of variance (ANOVA) followed by Bonferroni post-hoc correction for performing intergroup comparisons. Quantitative data from Western blots, depicted by the relative intensity of the bands were analyzed by performing student's t test. $*p<0.05$ and $\#p<0.01$ are considered statistically significant.

2.3 RESULTS

Leptin induces NADPH oxidase subunit p47phox and membrane association with gp91phox in NASH of both mice and humans. We have shown previously that leptin induces p47phox in early steatohepatitis leading to the formation of peroxynitrite and corresponding inflammation and Kupffer cell activation (57). To prove the role of leptin in induction of p47phox in fibrogenesis of NASH, experiments were performed in both mice model of NASH and human tissue samples from NASH patients. Results showed that DIO+BDCM group that shows typical NASH lesions had a 1.6-fold increase in p47phox mRNA expression as compared to DIO group alone ($P<0.05$) (Figure 2.1 A). Leptin knockout (ob/ob) mice showed a significant decrease in p47phox expression as compared to DIO+BDCM group ($P<0.05$), while leptin supplementation in leptin knockout (ob/ob+Leptin) mice resulted in a significant upregulation of p47phox mRNA as compared to only leptin knockout (ob/ob) mice ($P<0.01$). Human NASH (Hu NASH) tissues showed a significant increase p47phox mRNA expression as compared to controls (Hu CTRL) ($P<0.05$) (Figure 2.1 B). p47phox subunit of NADPH oxidase requires its association with its membrane counterpart gp91phox for activation of this enzyme. We studied the membrane association of these two subunits by immunofluorescence microscopy in both mice and human tissue samples. Results were analyzed based on the number of colocalization/overlay events (shown by yellow) per 300 cells counted (Figure 2.1 C and D). Results showed that DIO+BDCM group had a significant increase in the colocalization events as compared to DIO group only ($P<0.01$) (Figure 2.1 C and D). Leptin knockout (ob/ob) mice had a significant decrease in the number of colocalization events as compared to DIO+BDCM group ($P<0.01$). Leptin supplemented Leptin

17

Knockout mice (ob/ob+Leptin) had a significant increase in the colocalization events as compared to leptin knockout (ob/ob) mice (P<0.05) (Figure 2.1 C and D). Human NASH samples showed a significant increase in the p47phox/gp91phox colocalization as compared to human controls (Figure 2.1 C and D) (P<0.05). The above results suggest that leptin induced p47phox expression in NASH and aided in the membrane association of p47phox and gp91phox that assumes significance in causing oxidative stress in NASH.

Leptin induced NADPH oxidase activation causes peroxynitrite mediated oxidative stress in both NASH of mice and humans. We have previously shown that peroxynitrite mediated oxidative stress plays a crucial role in activating Kupffer cells in early steatohepatitic lesions in NASH (57). To prove that leptin-induced activation of NADPH oxidase in causing oxidative stress through peroxynitrite formation, experiments were performed in vivo to estimate 3-nytrotyrosine (3 N-Tyr) immunoreactivity in these tissues (Figure 2.2). Results showed that 3-nitrotyrosine immunoreactivity was significantly increased in DIO+BDCM group as compared to DIO group (P<0.05) (Figure 2.2 A and B). Leptin knockout (ob/ob) mice had a significant decrease in 3-nitrotyrosine immunoreactivity as compared to DIO+BDCM group (P<0.05). Leptin supplemented leptin knockout (ob/ob+Leptin) mice showed a significant increase in the 3-nitrotyrosine immunoreactivity as compared to leptin knockout (ob/ob) mice (P<0.05). Human NASH samples (n=3) showed a significant increase in 3-nitrotyrosine immunoreactivity as compared to human controls as shown by morphometry analysis of the slides (P<0.05) (Figure 2.2 B). All morphometric analysis of the stained liver sections was expressed as percentage area of immunoreactivity (Figure 2.2 B). The results suggested that leptin was significantly associated with increase in 3-nitrotyrosine

18

immunoreactivity and peroxynitrite might be a prominent player in causing oxidative stress.

Leptin induced NADPH oxidase activation mediates NF-kB translocation to the nuclei and upregulation of miR21. NADPH oxidase mediated oxidative stress has been shown to induce NF-kB translocation (49). NF-kB translocation and its binding to miR21 promoter are crucial for many inflammatory events in disease progression (58). To prove that leptin, through its activation of NADPH oxidase in vivo causes NF-kB translocation and binding to DNA, we performed experiments with liver tissue of both mice and humans. Results showed that NF-kB activation and DNA binding was significantly increased in DIO+BDCM group as compared to DIO group only (P<0.05) (Figure 2.3 A). Leptin knockout (ob/ob) mice showed a significant decrease in the NF-kB activation and binding as compared to DIO+BDCM group (P<0.05). p47phox knockout mice which cannot participate in NADPH oxidase mediated oxidative stress also showed a significant decrease in NF-kB activation and binding to DNA as compared to DIO+BDCM group (P<0.05) (Figure 2.3 A). Human NASH samples from liver showed a significant increase in NF-kB activation and binding to DNA as compared to corresponding control tissues (P<0.01) (Figure 2.3 B). DIO+BDCM group had a significant increase in miR21 levels (4 fold) as compared to DIO group (P<0.01) (Figure 2.3 C). Leptin knockout (ob/ob) or p47phox knockout mice had a significant decrease in miR21 levels as compared to DIO+BDCM group (P<0.01) (Figure 2.3 C). However Leptin supplementation to leptin knockout (ob/ob+Leptin) mice had a significant increase in miR21 levels as compared to leptin knockout (ob/ob) mice and had comparable levels of miR21 with DIO+BDCM group (P<0.01) (Figure 2.3 C). Human liver samples that had NASH etiology, had

19

significantly higher miR21 levels (4.5 fold) as compared to human control tissues (P<0.01) (Figure 2.3 D). The above results suggested that leptin mediated NADPH oxidase activation was significantly associated with increased miR21 levels in NASH. The results assume significance since miR21 mediated repression of its target proteins can play a major role in disease pathology.

Leptin mediated NADPH oxidase activation and its corresponding induction of miR21 represses regulatory SMAD protein in both mice and human NASH. miR21 has been found to repress many functional proteins in disease pathology (59). SMAD7, a regulatory protein in the TGF-β signaling cascade has been shown to be a target for miR21 (54). We studied the role of Leptin-NADPH oxidase axis in mediating miR21-induced SMAD7 repression. Results showed that protein levels of SMAD7 were significantly elevated during the initial phases of NASH development (DIO+BDCM, 48h) as compared to DIO group. The protein levels of SMAD7 decreased significantly at 1w and at the termination of the study (4w) that showed full-blown NASH symptoms and correlated well with fibrotic lesions (P<0.05) (Figure 2.4.A and C). miR21 knockout mice showed a significant increase in SMAD7 protein expression as compared to DIO+BDCM group at 4 weeks (P<0.01) (Figure 2.4.B and D). Leptin knockout (ob/ob) mice or p47phox knockout mice or DIO+BDCM mice that were depleted with macrophage toxin GdCl3 did not show any significant protein levels of Smad7 (Figure 2.4.B and D). This is not surprising since these mice did not have oxidative stress and there was no induction of SMAD7 in the initial phases (data not shown). Human NASH tissues showed a significant decrease in SMAD7 protein levels as analyzed by western blot as compared to corresponding controls (P<0.01) (Figure 2.4.B and D). The results

20

suggested that the increased miR21 in mice and human NASH is strongly associated with decreased SMAD7 protein. The results assume significance since SMAD7 plays a crucial role in regulating and inhibiting TGF-β signaling, crucial for fibrogenesis in NASH.

Leptin mediated NADPH oxidase activation and corresponding induction of miR21 regulate TGF-β levels in mice and human NASH. TGF-β has been shown to be key for NASH fibrogenesis (60). To prove the role of leptin mediated NADPH oxidase induction of miR21 in regulating TGF-β levels in NASH, experiments were performed with liver slices of mice and human NASH tissues and assessing the immunoreactivity by using immunohistochemistry. Results showed that DIO+BDCM group had a significantly increased level of TGF-β as compared to DIO group ($P < 0.01$) (Figure 2.5A and B). Leptin knockout (ob/ob), p47phox knockout and miR21 knockout mice had a significant decrease in TGF-β immunoreactivity as compared to DIO+BDCM group ($P < 0.01$) (Figure 2.5A and B). Leptin supplementation to leptin knockout (ob/ob+Leptin) mice showed a significant increase in TGF-β immunoreactivity as compared to leptin knockout (ob/ob) mice alone ($P < 0.05$) (Figure 2.5A and B). Human NASH liver slices showed a significant increase in TGF-β immunoreactivity as compared to control tissues as shown by percentage area covered by the immunoreactive staining (morphometric analysis) ($P < 0.05$) (Figure 2.5A and B). The results suggested that leptin mediated NADPH oxidase activation and miR21 induction plays a crucial role in TGF-β levels in the livers of NASH.

Leptin mediated NADPH oxidase activation and corresponding induction of miR21 in NASH are crucial for regulation of SMAD2/3-SMAD4 assembly in the nucleus, a key event in TGF-β signaling pathway. TGF-β signaling through SMAD2/3 is crucial

21

for collagen deposition and fibrogenesis (61-63). It has been shown previously that SMAD2/3 binds with SMAD4 and translocate to the nucleus. The nuclear colocalization of the SMAD2/3-SMAD4 heterodimer complex is key event in TGF-β functional pathway. TGF-β induces heteromeric complexes of SMADs 2, 3 and 4, and their concomitant translocation to the nucleus, which is required for efficient TGF-β signal transduction (62). To study the role of leptin mediated NADPH oxidase activation and miR21 induction in TGF-β signal transduction pathway, experiments were performed using liver tissue slices. Immunoreactivity to SMAD2/3, SMAD4 and their nuclear colocalizations were assessed by immunofluorescence microscopy. Results showed that the number of colocalization events in the nucleus were significantly higher in DIO+BDCM group as compared to DIO group (P<0.01) (Figure. 2.6A and C). The colocalization events in the leptin knockout (ob/ob), p47phox knockout and miR21 knockout mice were significantly decreased as compared to DIO+BDCM group (P<0.01 and P<0.05). Leptin supplementation to leptin knockout (ob/ob+ Leptin) mice significantly increased the number of nuclear colocalization events as compared to leptin knockout (ob/ob) mice alone (P<0.05). Human NASH samples showed significant increase in SMAD2/3, SMAD7 nuclear colocalizations as compared to Human liver controls (P<0.05) (Figure. 2.6A and C). The results were analyzed based on the number of nuclear colocalizations per 300 cells (Figure. 2.6C). 60X oil micrographs of DIO+BDCM group in the mouse model and Human NASH liver are shown in Figure.2.6B. The results show that increased TGF-β induced signaling through SMAD2/3 and SMAD 4 is regulated by leptin mediated NADPH oxidase and its subsequent upregulation of miR21.

22

Leptin mediated NADPH oxidase activation and subsequent miR21 induction regulate the levels of TGF-β signaling proteins Connective Tissue Growth factor (CTGF) and EDA-Fibronectin in mice model of NASH and human NASH livers. In fibrotic liver, connective tissue growth factor (CTGF) is constantly expressed in activated hepatic stellate cells (HSCs) and acts downstream of TGF-β to modulate extracellular matrix production (64). On the other hand fibronectin (FN) is a major component of the extracellular matrix and occurs in two main forms: plasma and cellular FN. The latter includes the alternatively spliced domain A (EDA) (65). EDA-Fibronectin has been shown to participate in TGF-β mediated fibroblast differentiation and fibrogenesis (66). To prove the role of leptin mediated NADPH oxidase activation and subsequent induction of miR21 in TGF-β signaling, immunohistochemical analysis of the mice liver and human liver tissues were performed. Results showed that there was a significant increase in the immunoreactivity of CTGF and EDA-Fibronectin (EDAFN) in DIO+BDCM group as compared to DIO group (P<0.01and P<0.05) (Figure.2 7A ii and B ii) (Fig.2 7C and D for morphometric analysis). On the other hand leptin knockout (ob/ob), p47phox knockout and miR21 knockout mice had a significant decrease in the CTGF and EDA Fibronectin levels as compared to DIO+BDCM group (Figure.2 7A iii, v and vi) (2.7B iii, v and vi) (Figure.2.7C and D for morphometric analysis) (P<0.05). Leptin supplementation in leptin knockout (ob/ob+Leptin) mice showed a significant increase in the levels of immunoreactivity of both these crucial proteins (P<0.05) (Figure.2 7A iv and 2.7B iv) (Figure.2 7C and D for morphometric analysis). Human NASH livers had a significant increase in the immunoreactivity of CTGF and EDA-fibronectin as compared to control livers (P<0.05) (Figure.2 7A viii and B viii)

23

(Figure.2.7C and 2.7D for morphometric analysis). The above results show that Leptin mediated NADPH oxidase activation and subsequent miR21 inhibition of SMAD7 is closely associated with increased TGF-β signaling resulting in higher CTGF and EDA-fibronectin levels in NASH.

Leptin mediated NADPH oxidase activation and miR21 induction cause stellate cell activation and collagen deposition in NASH. Stellate cell activation is a key event for NASH progression (16). α-SMA is a biomarker for stellate cell activation (67). Importantly, increased fibrogenesis and TGF-β signaling results in higher collagen 1α1 level in tissues. To show the role of leptin mediated NADPH oxidase in stellate cell activation and fibrogenesis, immunohistochemical analyses of mice and human liver tissues were performed. Results showed that immunoreactivity to α-SMA and Col1α were significantly high in DIO+BDCM group as compared to DIO group (P<0.01) (Figure 2.8A ii and 2.8B ii) (morphometric analysis Figure. 2.8C and 2.8D). Leptin knockout (ob/ob), p47phox knockout and miR21 knockout mice had significantly decreased immunoreactivity of α-SMA and Col1α as compared to DIO+BDCM group (P<0.01) (Figure. 2.8A iii, v and vi; 2.8B iii, v and vi) (morphometric analysis Figure.2.8C and 2.8D). Leptin supplementation in leptin knockout (ob/ob+Leptin) mice showed a significant increase in the levels of both α-SMA and Col1α as compared to leptin knockout mice (ob/ob) group alone (P<0.05)(Figure.2.8A iv and 2.8B iv) (morphometric analysis Figure. 2.8C and 2.8D). Human NASH liver exhibited a significant increase in α-SMA and Col1αas shown by increased immunoreactivity to these proteins and morphometric analysis of the tissue staining (P<0.05) (Figure. 2.8A viii and 2.8B viii) (morphometric analysis Figure.2.8C and 2.8D). The results suggested

that leptin-mediated NADPH oxidase and the subsequent induction of miR21 regulated the stellate cell activation and corresponding collagen deposition in both mice and human NASH livers.

Leptin mediated NADPH oxidase activation and miR21 induction cause fibrogenesis in NASH. A. Analysis of picrosirius staining for collagen showed increased reactivity in DIO+BDCM group, especially in the periportal regions as compared to DIO group (Figure.2.9 A ii). Leptin knockout (ob/ob) or p47phox knockout or miR21 knockout mice showed a minimal fibrotic stain as compared to DIO+BDCM group (Figure.2.9 A iii, v and vi). Leptin supplementation sharply increased periportal staining of picrosirius red (Figure.2.9 A iv) whereas human tissues for NASH showed higher picrosirius red staining compared to controls (Figure. 2.9 A viii). To show a correlation between the levels of tissue leptin and fibrotic stage, leptin immunoreactivity in mouse liver homogenates at 24 h, 48h, 1wk and 4wk as assessed by western blot followed by normalizations against β-actin (Figure 2.9 B and C) and by picro sirius red staining depicting fibrosis at 24h, 48h, 1w and 4 w in DIO+BDCM group (Figure 2.9 D).. Results showed that increased leptin concentrations correlated well with periportal and bridging fibrosis at 4 weeks following the toxin exposure in an underlying condition of steatosis (NASH model).

2.4 DISCUSSION

In this study we report for the first time the role of leptin-mediated NADPH oxidase in inducing miR21 in preclinical NASH model as well as in human NASH patients. We also show the mechanistic role of miR21 in repressing SMAD7, a crucial regulator of TGF-β

signaling, thus modulating fibrogenesis in NASH (Figure.2.10). Significantly, the miR21-modulation of TGF-β signaling, fibrogenesis and NASH progression were mediated by NADPH oxidase in our present study. The study assumes huge clinical significance since the role of NADPH oxidase has been shown in fibrogenesis by us and others but the link between NADPH oxidase based oxidative stress signaling through posttranscriptional epigenetic changes and TGF-β signaling remained largely elusive in vivo.

An earlier report from our laboratory showed that leptin-mediated NADPH oxidase activation activated Kupffer cells largely through the formation of peroxynitrite in an early stage of steatohepatitic injury (57). Through the present study, we advanced our understanding about the role of leptin-mediated NADPH oxidase based oxidative stress in a full blown NASH model and in human NASH livers. The present study used a rodent model of NASH that had a hepatotoxin bromodichloromethane (BDCM) as a second hit (16). All our investigations were carried out at a time point where NASH symptoms were confirmed using clinical indicators. NADPH oxidase subunit p47phox induction and subsequent activation were observed in these liver tissues (Figure 2.1. A-D). The induction and subsequent activation of NADPH oxidase was dependent on the presence of leptin since leptin knockout mice (ob/ob) or leptin supplementation (100 ng, daily for 4 weeks) in leptin knockout (ob/ob+Leptin) mice had opposite outcomes (Figure 2.1). Based on our previous reports in the same model, we also established the nature of the oxidizing species since we observed significant increase in 3-nitrotyrosine immunoreactivity, a measure for generation of highly reactive peroxynitrite (Figure.2 2A and B).

Highly reactive oxidizing species has been shown to induce changes in the epigenetic foci and cause increases in the expression of non-coding RNAs (68). There are several miRNAs that are known to be induced in an inflammatory condition (58, 59). NASH has been shown to induce several miRNAs with specific functions targeted towards its progression (69-71). miR21 is induced in an inflammatory microenvironment and has been shown to be induced in disease pathophysiology following the binding of nuclear transcription factor NF-kB to its promoter (58). In the present study we show that NF-kB binding activity to the DNA was significantly higher in DIO+BDCM group (NASH mouse model) and human NASH livers (Figure 2.3A and B). The activation NF-kB was dependent on leptin and NADPH oxidase activation since leptin knockout (ob/ob) mice and p47phox knockout mice had significantly lower NF-kB activation (Figure 2.3A). Human livers had significant increase in NF-kB activation, an index of oxidative stress and inflammatory signaling pathway (Figure 2.3B). Coupled with the NF-kB activation our studies also showed that the miR21 levels in the NASH livers were significantly elevated (Figure 2.3C and D). The levels of the miR21 were dependent on the NADPH oxidase subunit p47phox and leptin. The results correlate well with observations reported previously about NF-kB mediated miR21 induction in vitro through a binding of NF-kB to miR21 promoter region(72). However the above phenomenon could not be established in the in vivo models of NASH due to procedural complications involving transfection in primary cells from the NASH mice at this point. Thus it can be justified to assume that NF-kB translocation in the NASH livers might bind to miR21 promoter causing its induction, apart from the other functions that it is predicted to perform in NASH (Figure 2.3C and D).

A recent review by Noetel et al. describe the current knowledge of the role of miR21 in liver fibrosis (51). Inflammatory microenvironment in the NASH livers are predicted to promote TGF-β signaling which in turn can stimulate SMAD2/3 phosphorylation and their association with SMAD4. Further the above events can up-regulate miR21 which by suppressing SMAD7 can further add to the increased TGF-β-mediated profibrogenic responses, events that are known in other fibrotic mechanisms in the lung and kidney (54, 70). We are not aware of any reports that establish a direct role of NADPH oxidase activation-induced miR21 in TGF-β signaling and subsequent liver fibrosis. To prove the role of miR21-induced SMAD7 repression and SMAD2/3-SMAD4 interactions, we used miR21 knockout mice in parallel to p47phox and leptin knockout (ob/ob) mice. Results showed that miR21 knockout that show significantly lower inflammation in similarly used NASH models (unpublished data), had higher SMAD7 levels when treated identically with high fat diet and hepatotoxin challenge as compared to DIO+BDCM (Figure. 2.4B and D). Interestingly SMAD7 proteins were significantly decreased in human NASH livers as compared to controls (Figure. 2.4B and D). Leptin knockout (ob/ob) and p47phox knockout mice had a small increase in protein levels as compared to DIO+BDCM at 4 weeks but the reported increase was not statistically significant (Fig. 4D). This might be due to the genetic makeup of these mice and a very low level of inflammation that trigger SMAD 7 protein expression. Also, it's worth reporting were the levels of TGF-β in leptin, p47phox and miR21 knockout mice (Figure.2.5A and B). Results showed that these knockout mice had significantly decreased TGF-β levels as compared to DIO+BDCM group (Figure.2.5). The results also establish that TGF-β levels

28

are significantly regulated upstream of miR21 induction and leptin, NADPH oxidase and miR21 are linked to cause an upregulation of TGF-β.

TGF-β signaling is crucial for fibrogenesis in NASH. SMAD2/3 association with SMAD7 in the nucleus is a crucial event in this process (63). This important mechanistic association and its regulation by miR21 have never been shown in liver fibrosis in vivo or in human NASH livers. We show by immunofluorescence imaging ex vivo, the colocalization of SMAD2/3-SMAD4 in the nuclei of NASH livers (Figure.2.6). Murine and Human NASH livers had a significant increase in the number of colocalization events as compared to corresponding controls whereas leptin, p47phox and miR21 knockout mice had significantly less number of colocalization events as compared to NASH groups (Figure.2.6C). The results described in this study assume great significance since we show that NADPH oxidase through miR21 not only repressed SMAD7 as a profibrogenic mechanism but also contributed partly to enhance SMAD2/3-SMAD4 association in the nucleus, a key event in liver fibrogenesis. The leptin-mediated NADPH oxidase induction of miR21 also played a significant role in the downstream events of TGF-β signaling pathway by regulating the levels of CTGF and the intracellular form of fibronectin (EDA-Fibronectin) (Figure.2.7).

Finally, we studied the implications of the leptin mediated NADPH oxidase activation and subsequent miR21 upregulation in stellate cell activation, collagen levels and fibrosis, key events in NASH pathogenesis. Predictably, our results showed a direct involvement of leptin-mediated NADPH oxidase and miR21 role in fibrogenesis since leptin knockout (ob/ob), p47phox knockout or miR21 knockout mice had significantly decreased levels of α-SMA, Col1α and picrosirius red staining as compared to mouse and

29

human NASH models (Figure 2.8 and 2.9). Importantly NASH pathogenesis for proving stellate cell activation and fibrosis in both preclinical and clinical settings rely on the levels of α-SMA, Col1α and picrosirius red staining.

In summary, we show that leptin mediated NADPH oxidase upregulated the levels of miR21 through NF-kB activation predictively by binding to the miR21 promoter in vivo, observations that have been reported previously. The resultant upregulation of miR21 caused fibrogenesis in NASH by SMAD2/3-SMAD4 association in the nucleus and SMAD7 repression. Our results will help advance the current knowledge about the mechanisms of NADPH oxidase mediated fibrogenesis in NASH and will stimulate newer studies that can help develop therapeutic approaches for this clinically silent disease.
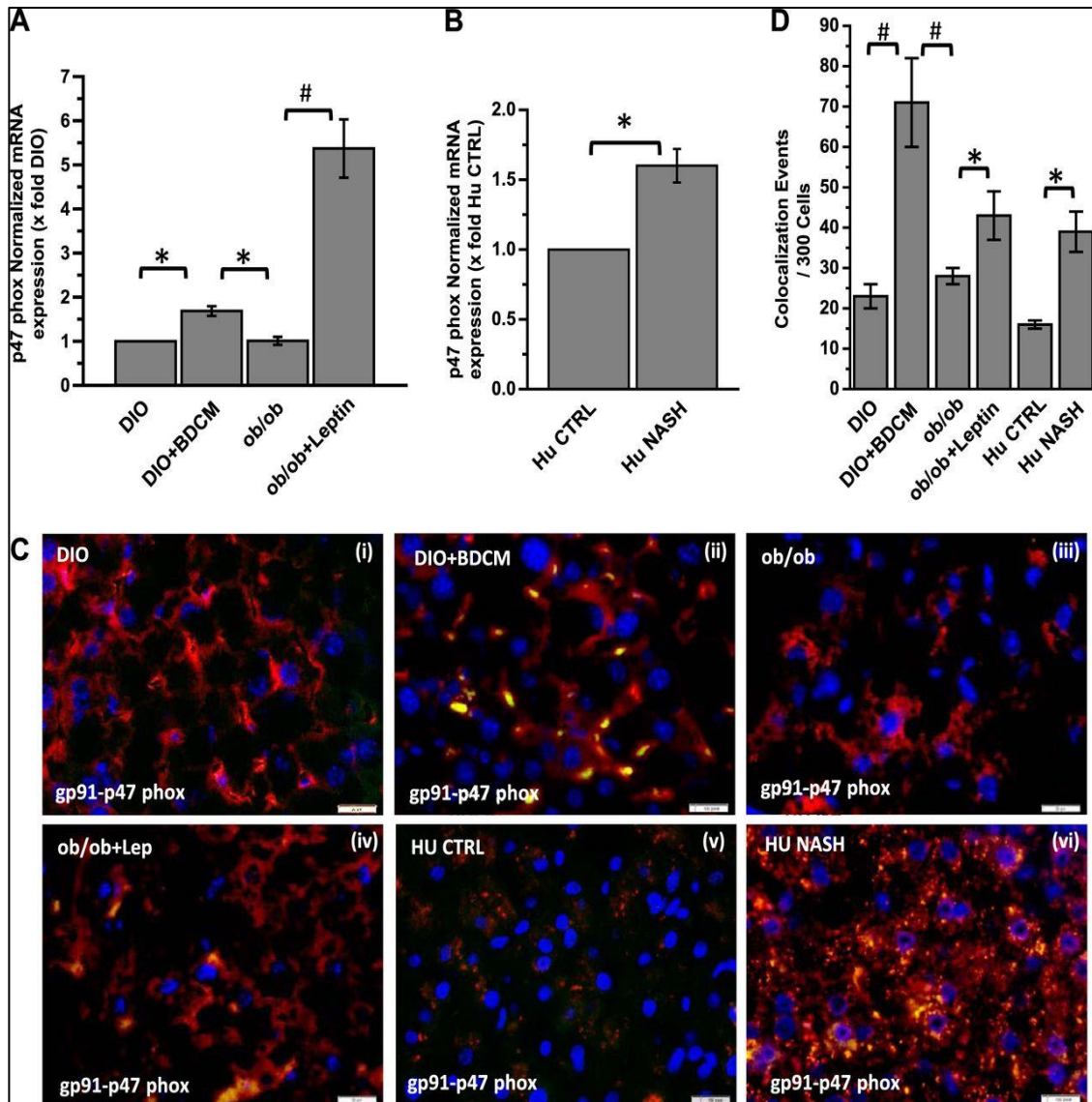
Figure 2.1 Leptin induces NADPH oxidase subunit p47phox and membrane association with gp91phox. A: qRT-PCR analysis of p47phox mRNA expression of diet-induced obesity (DIO), DIO + bromodichloromethane (BDCM), ob/ob, and ob/ob + leptin mice samples normalized against DIO. B: qRT-PCR analysis of p47phox mRNA expression of human (Hu) nonalcoholic steatohepatitis (NASH) samples normalized against Hu control (CTRL). C: immunofluorescence dual-labeling microscopy depicting gp91phox (red)-p47phox (green) colocalization (yellow) in DIO (i), DIO + BDCM (ii), ob/ob (iii), ob/ob + leptin (iv), Hu CTRL (v), and Hu NASH (vi) liver samples taken at ×60 (oil) magnification. D: morphometric analysis of colocalization events of C, shown in colocalization events/300-cell unit. *P < 0.05 and #P < 0.01 are considered statistically significant.

31

Figure 2.2 Leptin-induced NADPH oxidase activation causes peroxynitrite-mediated oxidative stress in NASH of both mice and humans. A: 3-nitrotyrosine (3 N-Tyr) immunoreactivity as shown by immunohistochemistry in liver slices from the DIO (i), DIO + BDCM (ii), ob/ob (iii), ob/ob + leptin (iv), Hu CTRL (v), and Hu NASH (vi) groups, respectively. Images were taken at ×20 magnification. B: morphometric analysis of the immunoreactivity of A. *P < 0.05 is considered statistically significant.
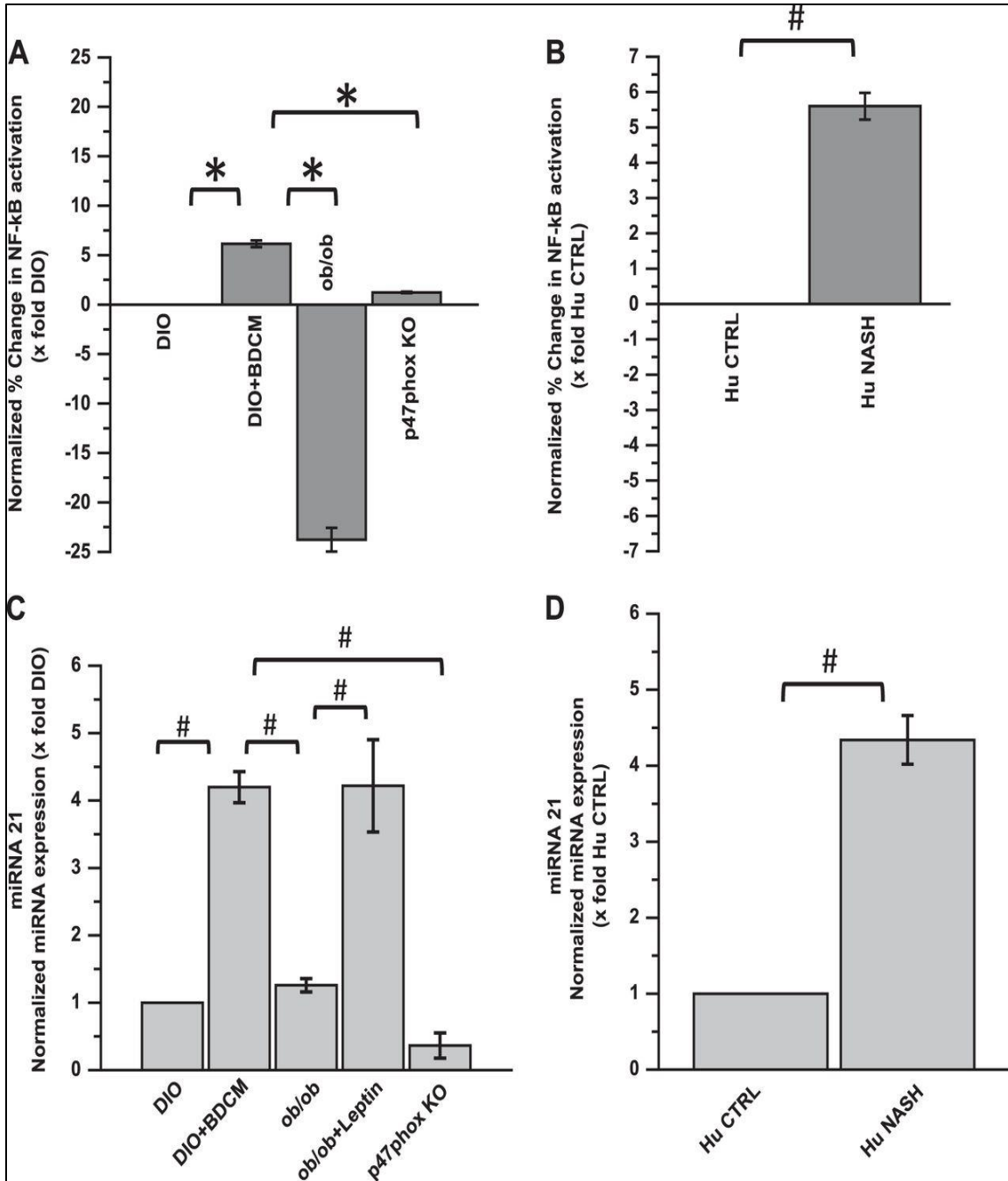
Figure 2.3 Leptin-induced NADPH oxidase activation mediates NF-κB activation and upregulation of micro-RNA 21 (miR21). A: normalized % change of NF-κB activation in DIO, DIO + BDCM, ob/ob, and p47 phox knockout (KO) samples. B: normalized % change of NF-κB activation in Hu CTRL and Hu NASH samples. C: qRT-PCR analysis of miR21 expression of DIO, DIO + BDCM, ob/ob, and ob/ob + leptin mice samples normalized against DIO. D: qRT-PCR analysis of miR21 expression of Hu NASH samples normalized against Hu CTRL. *P < 0.05 and #P < 0.01 are considered significant.

33
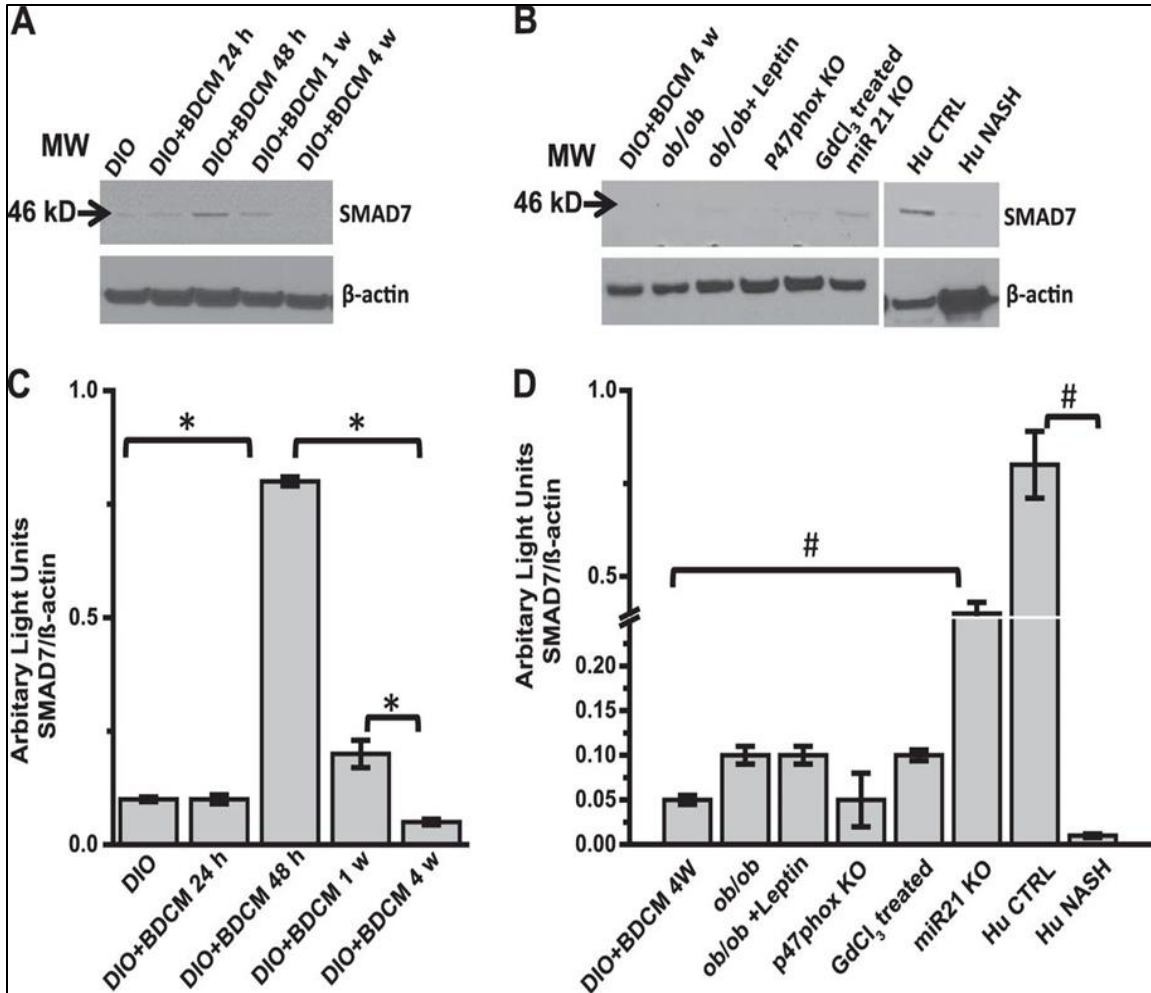
Figure 2.4 Leptin-mediated NADPH oxidase activation and its corresponding induction of miR21 repress regulatory SMAD7 protein both in mice and human NASH. A: Western blot analysis of SMAD7 from liver homogenates of DIO, DIO + BDCM 24 h, DIO + BDCM 48 h, DIO + BDCM 1 wk (w), and DIO + BDCM 4 w groups, respectively. B: Western blot analysis of SMAD7 from liver homogenates of DIO, DIO + BDCM 4 w, ob/ob, ob/ob + leptin, p47phox KO, GdCl3-treated sample, miR21 KO, Hu CTRL, and Hu NASH groups, respectively. C: immunoreactive band analysis of SMAD7 normalized against β-actin. y-Axis depicts the SMAD7/actin ratio from DIO, DIO + BDCM 24 h, DIO + BDCM 48 h, DIO + BDCM 1 w, and DIO + BDCM 4 w groups. D: immunoreactive band analysis of SMAD7 normalized against β-actin. y-Axis depicts the SMAD7/actin ratio from DIO, DIO + BDCM 4 w, ob/ob, ob/ob + leptin, p47phox KO, GdCl3-treated sample, miR21 KO, Hu CTRL, and Hu NASH groups. *P < 0.05 and #P < 0.01 are considered statistically significant.
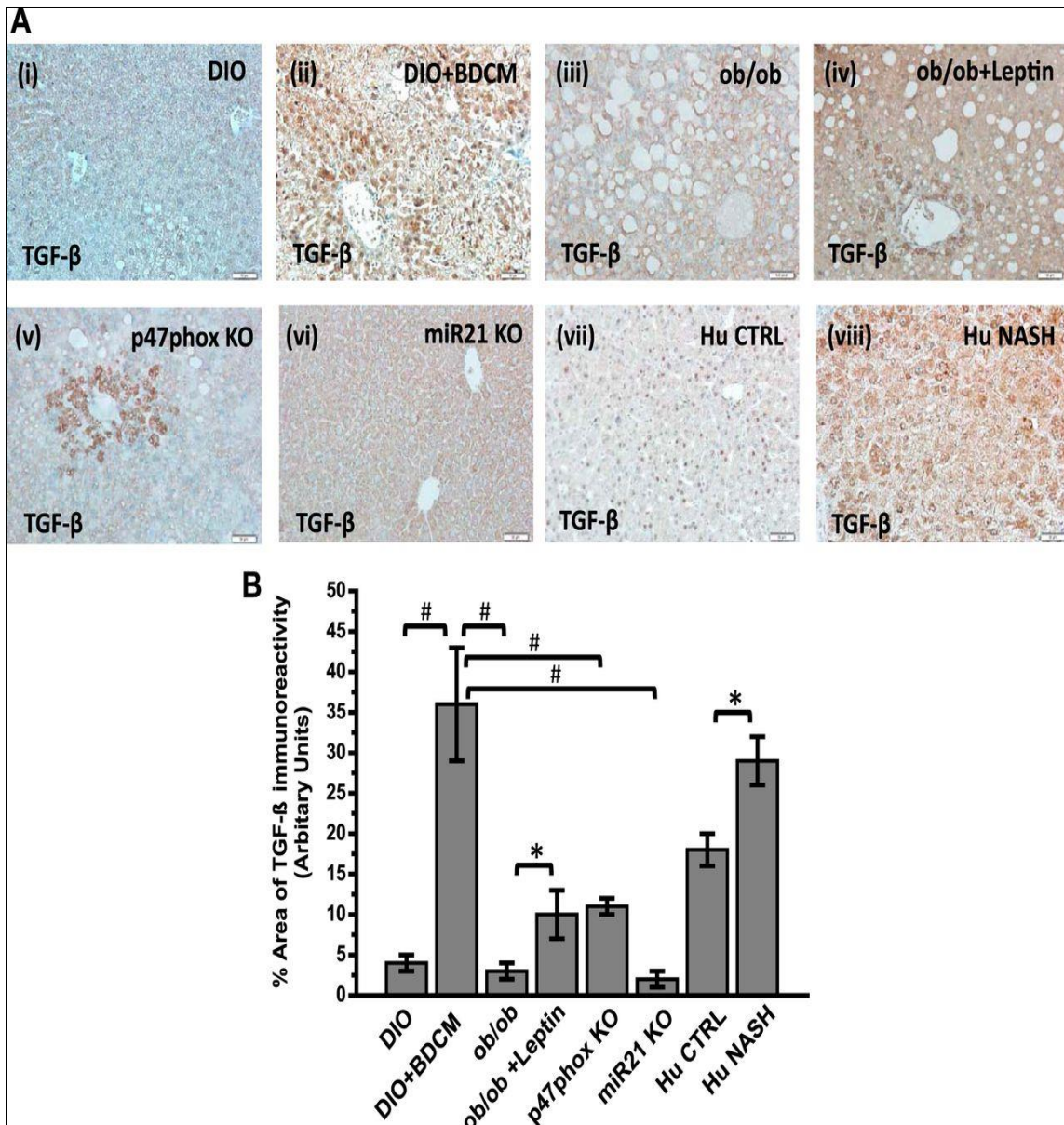
Figure 2.5 Leptin-induced NADPH oxidase activation and corresponding induction of miR21 regulate transforming growth factor (TGF)-β levels in mice and human NASH. A: TGF-β immunoreactivity as shown by immunohistochemistry in liver slices from the DIO (i), DIO + BDCM (ii), ob/ob (iii), ob/ob + leptin (iv), p47phox KO (v), miR21 KO (vi), Hu CTRL (vii), and Hu NASH (viii) groups, respectively. Images were taken at ×20 magnification. B: morphometric analysis of the immunoreactivity of A. *P < 0.05 and #P < 0.01 are considered statistically significant.
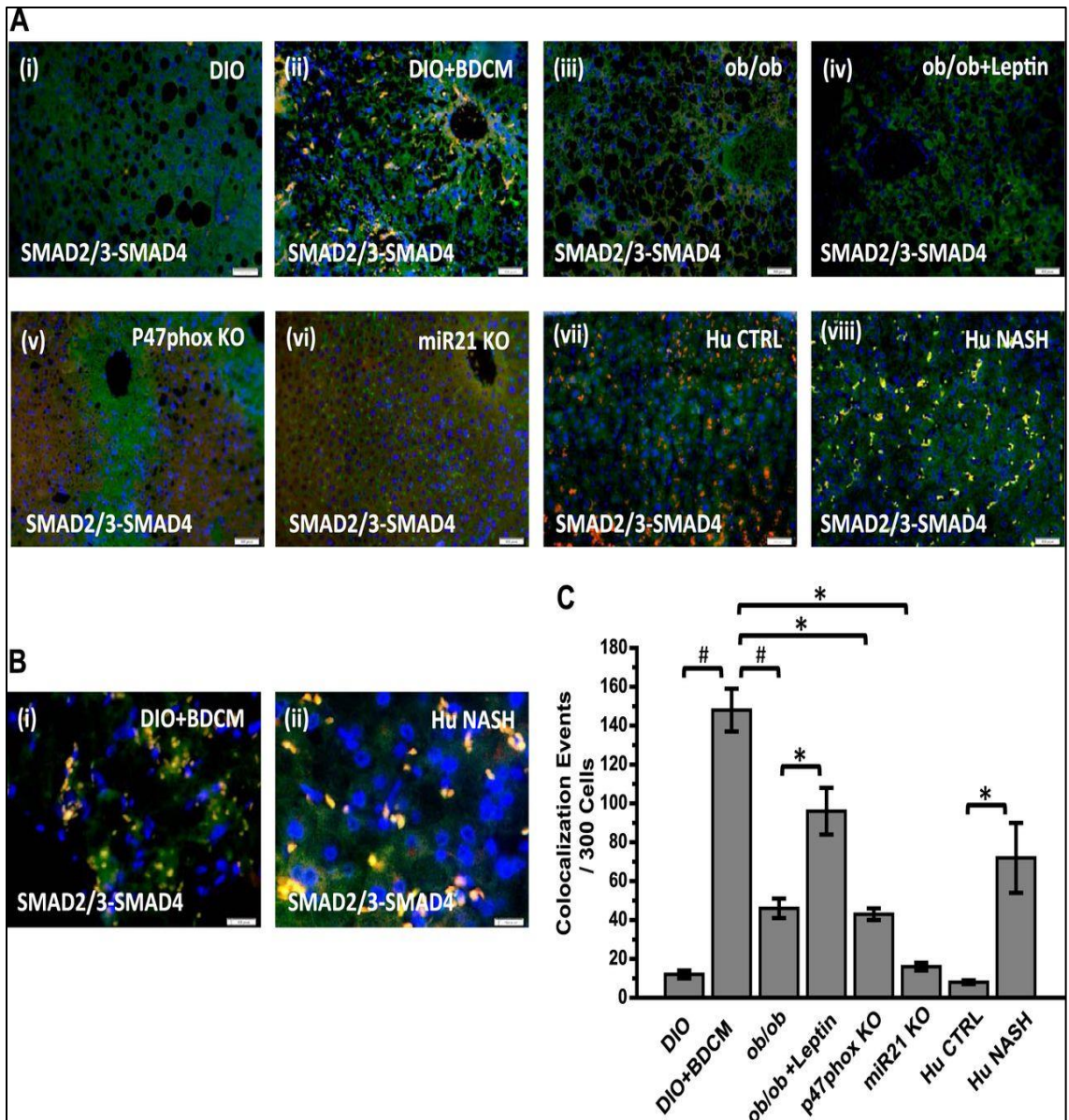
Figure 2.6 Leptin-mediated NADPH oxidase activation and corresponding induction of miR21 are crucial for regulation of SMAD2/3-SMAD4 assembly in the nucleus. A: immunofluorescence dual labeling depicting SMAD2/3 (red)-SMAD4 (green) colocalization (yellow) in the DIO (i), DIO + BDCM (ii), ob/ob (iii), ob/ob + leptin (iv), p47phox KO (v), miR21 KO (vi), Hu CTRL (vii), and Hu NASH (viii) liver samples, taken at ×20 magnification. B: immunofluorescence dual labeling of DIO + BDCM (mouse) (i) and Hu NASH (human) (ii) liver samples depicting SMAD2/3 (red)-SMAD4 (green) colocalization (yellow) taken at ×60 (oil) magnification. C: morphometric analysis of colocalization events of A, shown in colocalization events/300-cell unit. *P < 0.05 and #P < 0.01 are considered statistically significant.

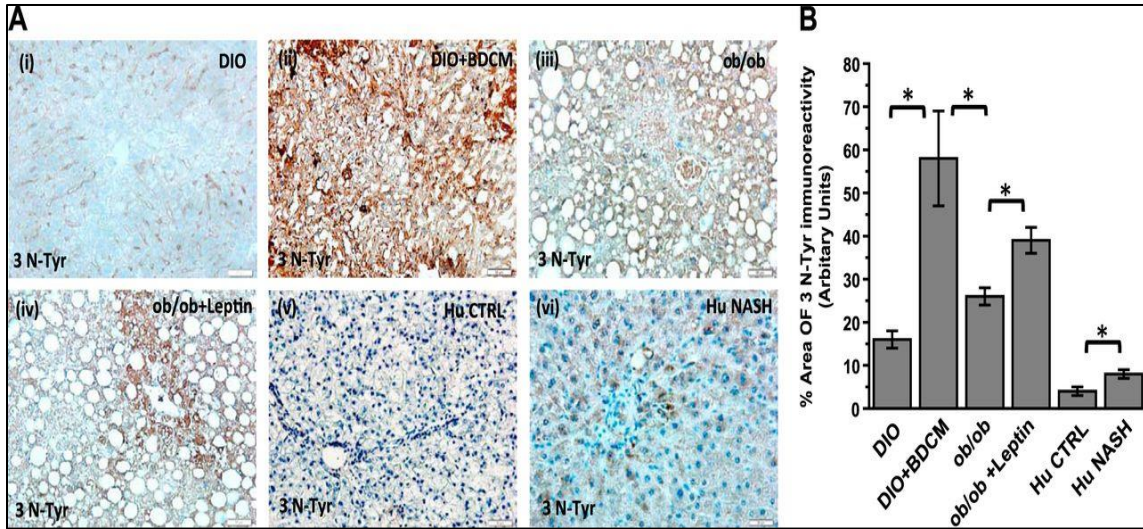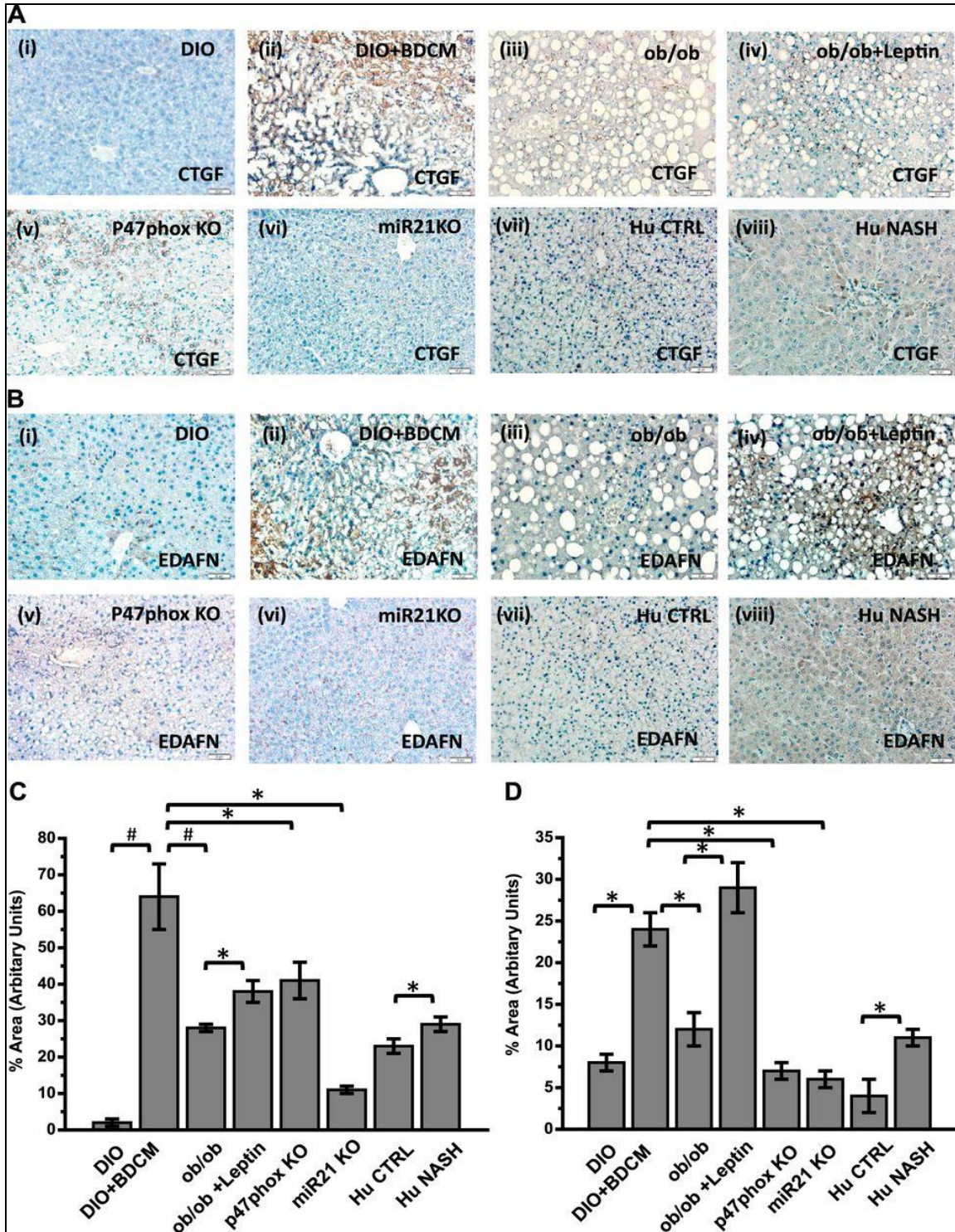Figure 2.7 Leptin-mediated NADPH oxidase activation and subsequent induction of miR21 regulate TGF-β signaling proteins. Connective tissue growth factor (CTGF) and extra domain A-fibronectin (EDAFN) in mice and human NASH. A: CTGF immunoreactivity as shown by immunohistochemistry in liver slices from the DIO (i),

DIO + BDCM (ii), ob/ob (iii), ob/ob + leptin (iv), p47phox KO (v), miR21 KO (vi), Hu CTRL (vii), and Hu NASH (viii) groups, respectively. Images were taken at ×20 magnification. B: EDAFN immunoreactivity as shown by immunohistochemistry in liver slices from the DIO (i), DIO + BDCM (ii), ob/ob (iii), ob/ob + leptin (iv), p47phox KO (v), miR21 KO (vi), Hu CTRL (vii), and Hu NASH (viii) groups, respectively. Images were taken at ×20 magnification. C: morphometric analysis of the immunoreactivity of A. D: morphometric analysis of the immunoreactivity of B. *$P < 0.05$ and #$P < 0.01$ are considered statistically significant.
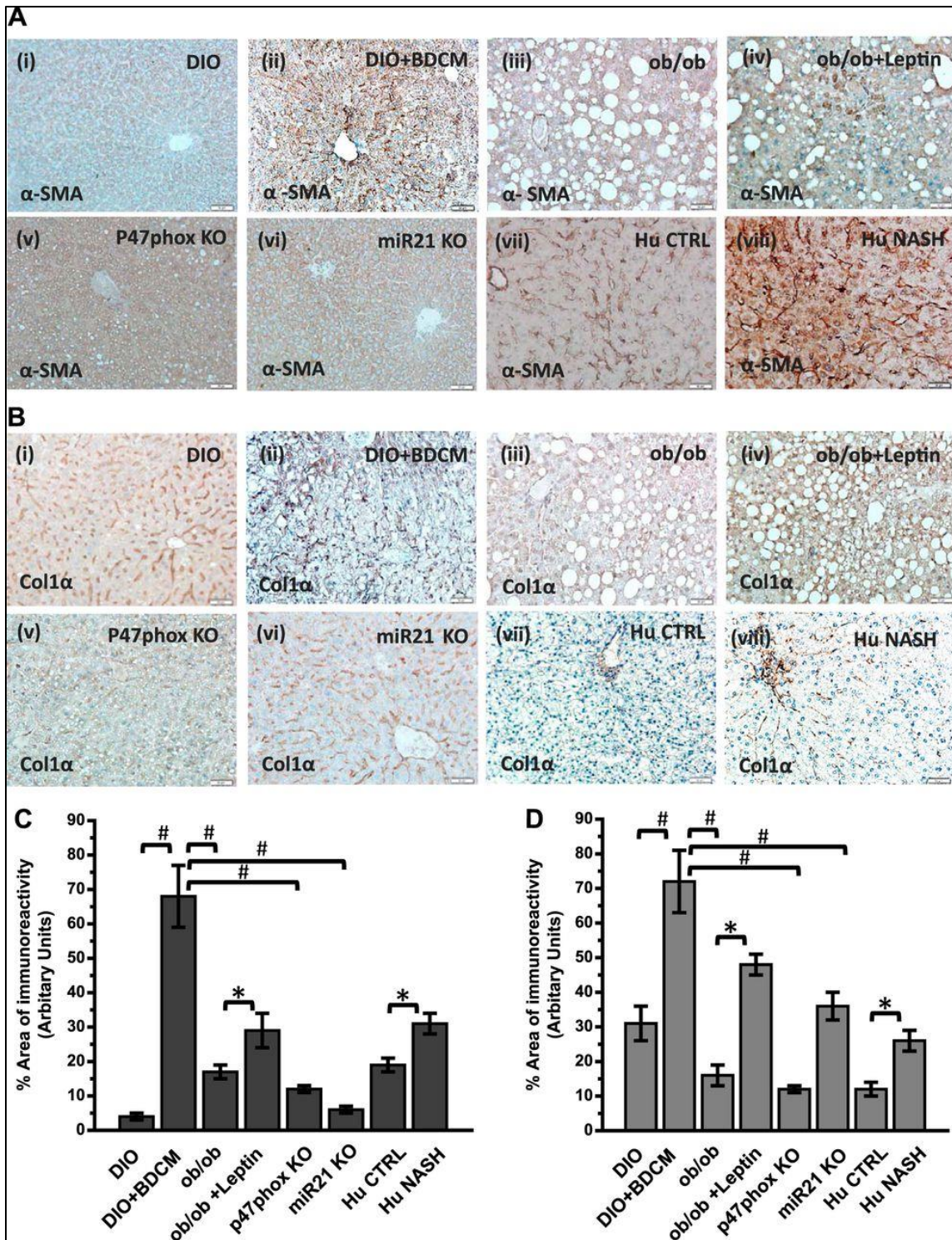
Figure 2.8 Leptin-mediated NADPH oxidase activation and miR21 induction cause stellate cell activation and collagen deposition in NASH. A: α-smooth muscle actin (SMA) immunoreactivity as shown by immunohistochemistry in liver slices from the DIO (i), DIO + BDCM (ii), ob/ob (iii), ob/ob + leptin (iv), p47phox KO (v), miR21 KO (vi), Hu CTRL (vii), and Hu NASH (viii) groups, respectively. Images were taken at ×20

magnification. B: Col1α1 immunoreactivity as shown by immunohistochemistry in liver slices from the DIO (i), DIO + BDCM (ii), ob/ob (iii), ob/ob + leptin (iv), p47phox KO (v), miR21 KO (vi), Hu CTRL (vii), and Hu NASH (viii) groups, respectively. Images were taken at ×20 magnification. C: morphometric analysis of the immunoreactivity of A. D: morphometric analysis of the immunoreactivity of B. *P < 0.05 and #P < 0.01 are considered statistically significant.

Figure 2.9 Leptin-mediated NADPH oxidase activation and miR21 induction cause fibrogenesis in NASH. A: picrosirius red (PSR) staining of DIO (i), DIO + BDCM (ii), ob/ob (iii), ob/ob + leptin (iv), p47phox KO (v), miR21 KO (vi), Hu CTRL (vii), and Hu NASH (viii) liver slices. Fibrosis is depicted by red staining. Images were taken at ×20 magnification. B: leptin immunoreactivity in mouse liver homogenates at 24 h, 48 h, 1 wk, and 4 wk as assessed by Western blot followed by normalizations against β-actin in C. D: PSR staining depicting fibrosis at 24 h, 48 h, 1 wk, and 4 wk in the DIO + BDCM group. *P < 0.05 is considered statistically significant.
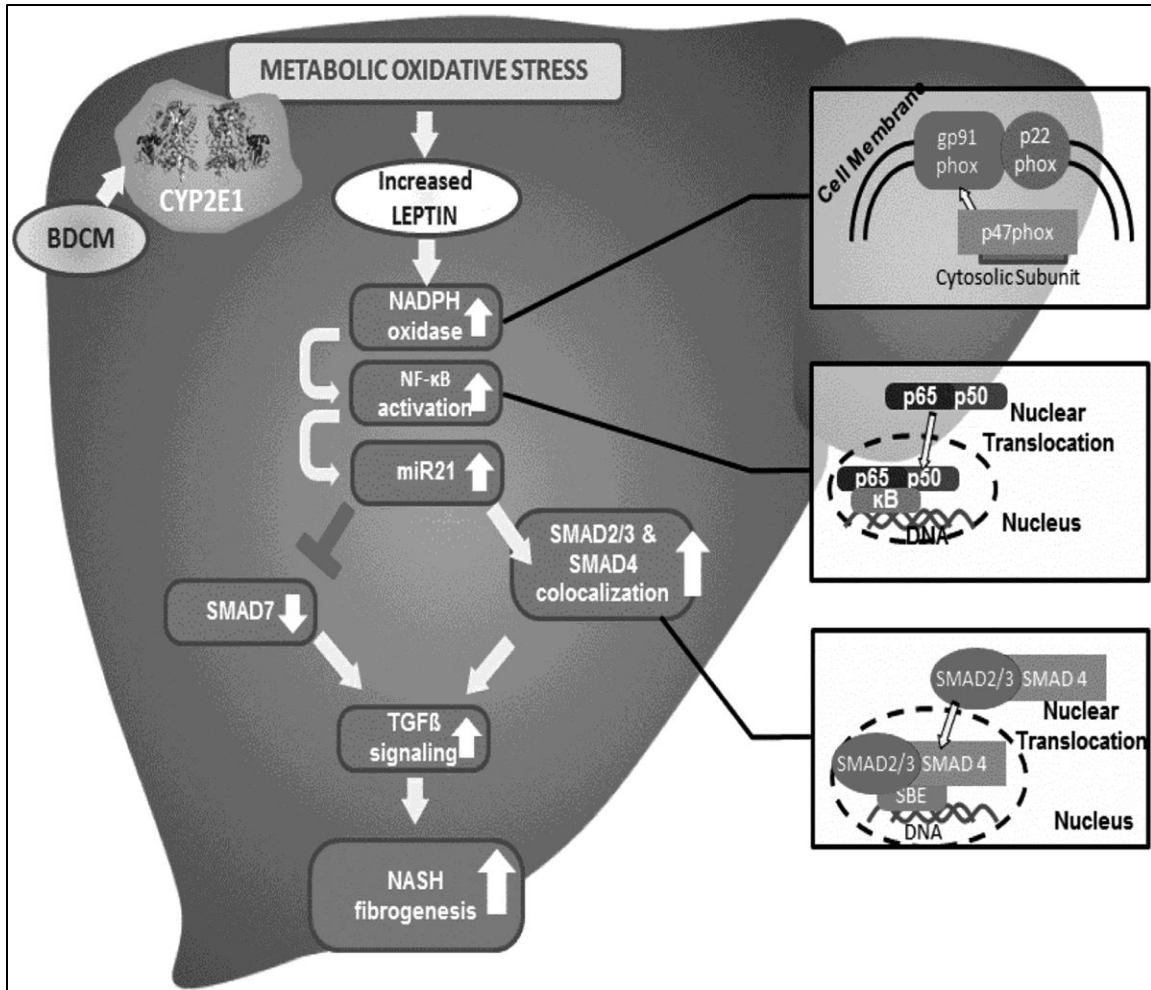
Figure 2.10 Schematic representation of the role of leptin-induced miR21 in modulating TGF-β pathway in NASH fibrogenesis. SBE, SMAD binding element.

CHAPTER 3

SPARSTOLONIN B ATTENUATES EARLY LIVER INFLAMMATION

IN EXPERIMENTAL NASH BY MODULATING TLR4-TRAFFICKING

IN LIPID RAFTS VIA NADPH OXIDASE ACTIVATION.[2]

Running Title: SsnB mitigates TLR4 trafficking in NASH.

Author for correspondence:

**Dr. Saurabh Chatterjee, Ph.D. Environmental Health and Disease Laboratory, Department of Environmental Health Sciences, University of South Carolina, Columbia 29208 USA. Email: schatt@mailbox.sc.edu; Tel: 803-777-8120; Fax: 803-777-3391

Key words: SsnB, inflammation, NADPH oxidase, p47phox, peroxynitrite

Abstract:

Although significant research data exist on the pathophysiology of nonalcoholic steatohepatitis (NASH), finding an efficient treatment regimen for it remains elusive. The present study used sparstolonin B (SsnB), a novel TLR4 antagonist derived from the Chinese herb Sparganium stoloniferum, as a possible drug to mitigate early inflammation in NASH. This study used an early steatohepatitic injury model in high-fat-fed mice with CYP2E1-mediated oxidative stress as a second hit. SsnB was administered for 1 wk along with bromodichloromethane (BDCM), an inducer of CYP2E1-mediated oxidative stress. Results showed that SsnB administration attenuated inflammatory morphology and decreased elevation of the liver enzyme alanine aminotransferase (ALT). Mice administered SsnB also showed decreased mRNA expression of proinflammatory cytokines TNF-α, IFN-γ, IL-1β, and IL-23, while protein levels of both TNF-α and IL-1β were significantly decreased. SsnB significantly decreased Kupffer cell activation as evidenced by reduction in CD68 and monocyte chemoattractant protein-1 (MCP1) mRNA and protein levels with concomitant inhibition of macrophage infiltration in the injured liver. Mechanistically, SsnB decreased TLR4 trafficking to the lipid rafts, a

phenomenon described by the colocalization of TLR4 and lipid raft marker flotillin in tissues and immortalized Kupffer cells. Since we have shown previously that NADPH oxidase drives TLR4 trafficking in NASH, we studied the role of SsnB in modulating this pathway. SsnB prevented NADPH oxidase activation in vivo and in vitro as indicated by decreased peroxynitrite formation. In summary, the present study reports a novel use of the TLR4 antagonist SsnB in mitigating inflammation in NASH and in parallel shows a unique molecular mechanism of decreasing nitrative stress.

Keywords: SsnB, inflammation, NADPH oxidase, p47phox, peroxynitrite

3.1 INTRODUCTION

Nonalcoholic steatohepatitis (NASH), a hepatic manifestation of metabolic syndrome, arises from an underlying condition of obesity (73).

After nearly three decades there remains a void of drugs approved for the treatment of NASH. Although sufficient progress in the understanding of pathophysiology, diagnosis, and stages of the disease has been made, a treatment regimen to cure this metabolic disease remains a challenge. Several treatment modalities have been tried, yet no single approach has been found to be effective in treating NASH (74). Lipid-lowering drugs like fibrates and statins have some effect, while insulin sensitizers (metformin, thiazolidinediones), endocannabinoid receptor agents, ursodeoxycholic acid, and green tea polyphenols have mixed effects (75). Results from both preclinical and clinical trials distinctly point to a combinatorial approach (caloric restriction, anti-inflammatory, and antioxidant) as a therapeutic remedy for NASH (76-78). Therefore there is a dire need for sustained research and drug discovery efforts that aim at

identifying new targets for therapy and eventually combine those that target concomitant and synergistic pathways of NASH pathogenesis.

As for alcoholic steatohepatitis, Toll-like receptors (TLRs) have been shown to be involved in the pathogenesis of NASH, as reviewed recently (79, 80). A pioneering study by Farhadi et al. (81) reported endotoxemia resulting from possible gut leakiness as a cause for NASH. Later, many reports emerged about the involvement of endotoxin from the gut as a cause for activation of the TLR4 receptors and the downstream inflammatory pathways(81-94). We have recently shown (24) that peroxynitrite, a nitrative species formed from the reaction between superoxide and nitric oxide, is responsible for TLR4 recruitment in lipid rafts. Lipid raft trafficking of TLR4 remains a significant step in TLR4 signaling and inflammation (95, 96). Upon binding to the TLR4 ligand, it is rapidly assembled in the lipid-containing domains, an event that is facilitated by NADPH oxidase (95). Our previously published observations (24) point to the role of peroxynitrite in contributing to the trafficking of TLR4 in rafts primarily following NADPH oxidase activation in NASH livers. Abrogation of TLR4 trafficking significantly decreased inflammation in NASH models and had improved histological outcomes (24). Several research reports in the past have described TLR4 antagonists and their effectiveness in attenuating TLR4-based inflammation in disease models (97). Unfortunately, none could be recommended for therapeutic use in humans. However, the search for an effective TLR4 antagonist continues owing to the importance of the TLR4 pathway in a myriad of diseases.

Extending this endeavor in search of an effective TLR4 antagonist, our collaborators have recently published several research studies that report the effective

TLR4-antagonizing role of sparstolonin B (SsnB), a natural product derivative (28, 98-104). SsnB, an isocoumarin, was isolated from a Chinese herb, Sparganium stoloniferum; its structure was determined by NMR spectroscopy and X-ray crystallography (28). In light of the above evidence of SsnB being a potent antagonist for TLR4-induced inflammation and tissue injury, we tested the hypothesis that administration of SsnB in murine models of NASH and immortalized Kupffer cells will attenuate early inflammation and tissue injury induced by TLR4 activation. In the present study we used a rodent model of NASH in which oxidative stress mediated by CYP2E1, lipotoxicity, and innate immune mediators were used as "second/multiple hits" to cause NASH. Results showed that SsnB significantly attenuated TLR4 trafficking to the lipid rafts, a significant event in TLR4 activation. The effects of SsnB on TLR4 trafficking were also correlated with a significant inhibition of NADPH oxidase activation and peroxynitrite formation, an event that was reported by us to be upstream of TLR4 activation in NASH though TLR4-induced NADPH oxidase activation.

3.2 MATERIALS AND METHODS

Cell culture: Rat immortalized kupffer cell line (Applied Biological Materials Inc., Canada) was maintained in complete Dulbecco's Modified Eagle's Medium (DMEM, Corning, VA) supplemented with 10% fetal bovine serum (FBS, Atlas Biologicals, CO) and 1x Penicillin-Streptomycin solution (Gibco, Life Technologies, NY), and grown at 37°C in a humidified incubator with 5% CO2. HBSS buffer, Tissue culture plastic wares were purchased from Corning (Corning, VA). Sparstolonin B (SsnB) compound was a kind gift from our collaborator Dr. Daping Fan (Cell Biology and Anatomy, University of South Carolina School of Medicine).Stock solution of SsnB was prepared in dimethyl

sulfoxide (DMSO). The final concentration of SsnB on cells was 100μg/ml, 0.1% DMSO. The cells were plated on 12 well plates (100,000/well) using DMEM medium supplemented with 10% FBS. Before treating the cells with LPS (50ng/ml), Leptin (100ng/ml) and SsnB (100μg/ml), cells were serum starved (DMEM with 0.25% FBS) for overnight. All treatments are given for 24 hours in 0.25% FBS containing DMEM medium. Cells treated with 0.1% DMSO were used as control. Cells treated with Leptin (BioVision, CA) and LPS (Sigma, MO) also had 0.1% DMSO. The cell supernatant was collected for Nitiric oxide quantification. Cells were plated on coverslips by putting the coverslips on each well of 12 well plates maintaining the aforementioned conditions and the cells adhered on coverslips were used for immune-fluorescence dual labelling staining after completion of the treatment. Primary mice (C57BL6) hepatic macrophages (ScienCell research lab, Carlsband, CA) were cultured in macrophage specific MaM media supplemented with MAGS, FBS and P/S (ScienCell research lab, Carlsband, CA) as instructed by the manufacturer on poly-L-lysine (ScienCell research lab, Carlsband, CA) coated 12 well plates and incubated at 37°C in a humidified incubator with 5% CO_2 to initiate the culture. The cell culture medium was replaced with fresh media in the next morning and the cells were treated with LPS, LPS and SSnB maintaining the same concentration and incubation time as mentioned above. Cells, treated with 0.1% DMSO were used as control.

Mouse Models: Pathogen free, male, C57BL/6J background mice (purchased from Jackson Laboratories, Bar Harbor, ME) were housed one per cage with a 12-h/12-h light/dark cycle at 23-24°C at libitum access to food and water. These mice were fed with 60% kcal high fat diet (purchased from Research Diets, New Brunswick, NJ) from 6

weeks until 16 weeks to generate a model of steatosis (S). Another group of these high fat diet fed mice, were administered Bromodichloromethane BDCM (1mmol/kg, diluted in corn oil) intraperitoneally, twice a week for 1 week to generate toxin induced early steatohepatitic injury model of mice (SH). BDCM and corn oil were purchased from Sigma-Aldrich (St. Louis, MO).A set of high fat diet fed, BDCM treated mice were administered with SsnB (3mg/kg-bw) intraperitoneally twice for 1 week (SH+SsnB). A group of steatotic mice was also administered with SsnB (3mg/kg-bw) intraperitoneally twice for 1 week (S+SsnB). Age-matched lean control mice (LC) were fed with chow diet having 10% kcal fat. Another group of chow diet fed lean mice was treated with same dosage of BDCM for 1 week (LC+BDCM). All animals were treated in strict accordance with the NIH guideline for Humane Care and Use of Laboratory Animals and local IACUC standards. All experiments were approved by the institutional review board at NIEHS, Duke University and the University of South Carolina at Columbia. After completion of the treatment, mice belonging to all groups were sacrificed for liver tissues and serum samples for further experiments.

Laboratory analysis

Immunohistochemistry: Mice livers were collected and fixed in 10% neutral buffered formalin (Sigma Aldrich, Missouri, USA). These formalin-fixed tissues were paraffin embedded and cut in 5µm thick sections. Using standard protocol (53), these liver sections were deparaffinized. The deparaffinized sections were subjected to epitope retrieval of was performed using epitope retrieval solution and steamer (IHC-World, Woodstock, MD) following the manufacturer's instructions. The endogenous peroxidases were blocked by 3% H_2O_2. Anti-mouse primary antibodies like anti–IL1β, anti–TNFα,

anti-MCP1, anti-F4/80, anti-3 Nitrotyrosine (Abcam, Cambridge, MA) were used in recommended dilutions. Following manufacturer's protocols (Vectastain Elite ABC kit, Vector Laboratories, Burlingame, CA), biotinylated conjugated secondary antibody (species specific) and streptavidin conjugated with HRP were used to perform antigen-specific immunohistochemistry. 3, 3' Diaminobenzidine (Sigma-Aldrich, St.Louis, MO) was used as chromogenic substrate. Mayer's hematoxylin (Sigma-Aldrich) was used as counterstain. Phosphate buffer saline was used for washing three times between the steps. Finally, the sections were mounted in Simpo mount (GBI Laboratories, Mukilteo, WA) and observed under a 20x objective using an Olympus BX51 microscope (Olympus, America). Morphometric analysis was done using CellSens Software from Olympus America (Center Valley, PA).

Haematoxylin and Eosin staining: Formalin-fixed tissues were paraffin embedded liver tissue sections were stained with Haematoxylin and Eosin by the IRF, University of South Carolina, and School of Medicine.

Serum ALT: Serum samples collected from mice were subjected to alanine aminotransferase (ALT) analysis (Discovery Life Sciences, CA) according to manufacturer's instructions.

Nitric oxide quantification assay: After treating the rat kupffer cells with LPS and LPS+SsnB (mentioned before), the cell supernatants were collected. The supernatant collected from the wells, where cells were not treated with LPS or LPS+SsnB, served as a control. Nitrite was measured in these samples by Griess Reagent System (Promega, WI) following the manufacturer's instructions.

49

ELISA: After treating the primary mice hepatic macrophages with LPS and LPS+SsnB (mentioned before), the cell supernatants were collected. The supernatant collected from the wells, where cells were not treated with LPS or LPS+SsnB, served as a control. TNFα concentration was measured in these samples by using Mouse TNF ELISA kit (BD Biosciences, San Jose, CA) following the manufacturer's instruction.

Immunofluorescence dual-labeling

In vivo: Formalin-fixed, paraffin embedded tissues sections were subjected to deparaffinization using standard instructions. Epitope retrieval of the deparaffinized sections was done using epitope retrieval solution and steamer (IHC-World, Woodstock, MD) following the manufacturer's protocol. The primary antibodies anti-gp-91phox, anti-p47phox, Flottilin1, TLR4 (purchased from Santa Cruz biotechnology, Inc. Santa Cruz, CA and Abcam, Cambridge, MA) and used at recommended dilutions. Species-specific anti-IgG secondary antibodies conjugated with Alexa Fluor 488(Invitrogen, California, USA) was used against anti-p47phox, anti-flottilin1 and Alexa Fluor 633 (Invitrogen, California, USA) was used against anti-gp91 phox and TLR4 respectively. The sections were mounted in a ProLong gold antifade reagent with DAPI (Life technologies, EU, OR). Images were taken under 20x and 60x oil objectives using Olympus BX51 microscope.

In vitro: After completion of the treatments under serum starved condition as the aforementioned cell culture section, cells attached on coverslips were fixed using 10% Neutral Buffer Saline. After washing the cells with PBS, containing 0.1% triton x (Sigma, MO) the cells were blocked using 3% BSA, 0.2% Tween (Fisher, NJ), 10% FBS

in PBS. Cells were incubated with primary antibodies anti-gp91 phox, anti-p47 phox, anti-TLR4 (mentioned earlier) and anti-flotillin 2 (Abcam, Cambridge, MA), followed by species specific Alexa Fluor 633 and 488 (mentioned earlier), for immune-fluorescence dual labelling staining. Alexa Fluor 633 was used against anti-TLR4 and anti-gp91 phox. Alexa Fluor 488 was used against anti-flottilin2 and anti- p47 phox. The stained cells attached on the coverslips were mounted on slides using ProLong gold antifade reagent with DAPI (Life technologies, EU, OR) and viewed under 40x and 60x oil objectives using Olympus BX51 microscope.

Quantitative Real-Time Polymerase Chain Reaction: Gene expression (mRNA) levels in the mice liver tissue samples and mouse primary hepatic macrophages were measured by real-time reverse transcription-polymerase chain reaction (qRTPCR). Total RNA was isolated from liver tissues and mouse primary hepatic macrophages using TRIzol reagent (Life Technologies, Carlsbad, CA). Trizol reagent is used to lyse the tissue, RNA extraction and purification are carried out by using RNeasy mini kit columns (Qiagen, Valencia, CA) following manufacturer's protocol. 1µg of purified RNA was converted to cDNA by using iScript cDNA synthesis kit (Bio-rad, Hercules, CA). Quantitative real-time reverse transcription-polymerase chain reaction was performed with the gene specific primers using CFX96 thermal cycler (Bio-Rad, Hercules, CA) and SsoAdvanced universal SYBR Green supermix (Bio-Rad, Hercules, CA). Threshold Cycle (Ct) values for genes of interest were normalized against 18S (internal control) values in same sample. Reaction was carried out in triplicates for each gene and each tissue sample. The relative fold change was calculated by the 2-$\Delta\Delta$Ct method. The mouse specific primers used for Real time PCR in 5'to 3' orientation are IL1β (Forward:

CCTCGGCCAAGACAGGTCGC, Reverse TGCCCATCAGAGGCAAGGAGGA), TNFα (Forward: CAACGCCCTCCTGGCCAACG, Reverse: TCGGGGCAGCCTTGTCCCTT), IFNγ (Forward: TGCGGGGTTGTATCTGGGGGT, Reverse: GCGCTGGCCCGGAGTGTAG), IFNγ (Forward: TGCGGGGTTGTATCTGGGGGT, Reverse: GCGCTGGCCCGGAGTGTAG), IL23 (Forward: AAAGGATCCGCCAAGGTCTG, Reverse: GCAGGCTCCCCTTTGAAGAT), CD68 (Forward: GCTACATGGCGGTGGAGTACAA, Reverse: ATGATGAGAGGCAGCAAGATGG), MCP1(Forward: CACAGTTGCCGGGCTGGAGCAT, Reverse: GTAGCAGCAGGTGAGTGGGGC), P47phox (Forward: GGTCGACCATCCGCAACGCA, Reverse: TGTGCCATCCGTGCTCAGCG), TLR4 (Forward: GGAGTGCCCCGCTTTCACCTC, Reverse: ACCTTCCGGCTCTTGTGGAAGC).

miRNA21 expression levels in liver tissues: Liver tissues were homogenized in Qiazol reagent (Qiagen, Valencia, CA) following the manufacturer's instructions to isolate the total miRNA. The purification was done by using miRNeasy mini kit columns (Qiagen, Valencia, CA). 100ng of purified miRNA was converted to cDNA using miScript cDNA synthesis kit (Qiagen, Valencia, CA) using the manufacturer's protocol. qRTPCR was performed with microRNA specific primers (Qiagen, Valencia, CA) using miScript SYBR Green PCR master mix (Qiagen, Valencia, CA) and CFX96 thermal cycler (Bio-rad, Hercules, CA). Threshold Cycle (Ct) values for the selected gene was normalized against RNU6-2 (internal miRNA expression control) values in the same sample.

Western Blotting: In the presence of phosphatase and protease inhibitors (Pierce, Rockford, IL), 30 mg of each liver tissue was homogenized in 500 µl of RIPA buffer (Sigma Aldrich) by using dounce homogenizer. The homogenate was centrifuged and the supernatant was collected for further experiments. 25 µg of each protein sample was loaded on 4–12% bis-tris gradient gel (Invitrogen, California, USA) for SDS PAGE. By using precut nitrocellulose/filter paper sandwiches (Bio-Rad Laboratories Inc., California, USA) and Trans – Blot Turbo transfer system (Bio-Rad), proteins were transferred to nitrocellulose membrane. Blots were blocked with 5% non-fat milk solution. Primary antibody against PTEN, β-actin (purchased from Abcam, MA) and TLR4 (Santa Cruz Biotechnology, CA) were used at recommended dilutions and incubated overnight at 4ºC. Species specific secondary antibodies conjugated with HRP (Abcam, MA) were used and the blots were incubated at room temperature for 2 hours. Pierce ECL Western Blotting substrate (Thermo Fisher Scientific Inc., Rockford, IL) was used. The blot was developed by using BioMax MS Films and cassettes (with intensifying screen, Kodak). Densitometry analysis of the images was done using Lab Image 2006 Professional 1D gel analysis software from KAPLEAN Bioimaging Solutions (Liepzig, Germany).

Statistical Analyses: The statistical analysis was performed by analysis of variance (ANOVA) which was followed by Bonferroni post-hoc correction for intergroup comparisons $*p < 0.05$ and $\#p < 0.01$ are considered statistically significant.

3.3 RESULTS

SsnB administration attenuates early steatohepatitic injury in obese mice. Feeding high fat diet to C57BL6/J mice for 4 weeks starting from 8 weeks post gestational age causes insulin and leptin resistance, steatosis but does not cause inflammation, tissue injury and fibrosis(40). Nonalcoholic steatohepatitis (NASH) can be a result of multiple hits that may include oxidative stress, increased CYP2E1 activity, cytokine release and/or altered metabolism(105). We used a toxin-induced steatohepatitis and lipotoxicity model in mice to show the therapeutic effects of SsnB(38) . Results showed that SsnB administration markedly decreased necrosis, ballooning, Mallory denk bodies and inflammatory foci in steatohepatitis group (SH) (Figure 3.1 A). SsnB administration significantly decreased the levels of serum ALT as compared to SH group but was significantly higher than the steatosis (S) group (Figure 3.1 B) ($P<0.05$).

NASH is known to have a significant proinflammatory phase primarily arising from activation of pattern recognition receptors (PRRs) in the liver primarily from higher endotoxin levels, HMGB1 or other endogenous ligands(90, 106). To study the effect of SsnB administration to SH mice, liver proinflammatory cytokine gene and protein levels were analyzed by qrtpcr and immunohistochemistry. Results showed that as expected, mRNA expression of TNF-α, IFN-γ and IL1β, which are proinflammatory in nature were significantly elevated in SH group as compared to S only group (Figure.3.2A)($P<0.05$). IL23 is known as a marker for M1 polarization(107, 108). Results showed that mRNA expression of IL23 also was significantly upregulated in SH group when compared to S only group (Figure.3.2A)($P<0.05$). SsnB administration significantly decreased the mRNA expression of proinflammatory markers TNFα, IFNγ, IL1β and macrophage

polarization marker IL23 when compared to SH group (Figure.3.2A)(p<0.05). Since TLR4 activation has been shown to be major event in progression of nonalcoholic steatohepatitis we studied the downstream proinflammatory molecules for this important pathway. Results showed that there was a significant increase in TNF-α and IL1β immunoreactivity in liver slices from SH mice when compared to S group only (Figure.3.2B, C and D)(P<0.05). The localization of the cytokines was unevenly distributed with TNFα localized in the centrilobular regions while IL1β at both Zone1 and Zone 3 respectively (Figure.3.2B). SsnB administration significantly decreased the immunoreactivity of both TNFα and IL1β in liver tissue when compared to SH group mice (Figure3.2B, C and D)(P<0.05).

SsnB administration modulates Kupffer cell activation in early steatohepatitic injury. NASH is associated with activation of the resident macrophages in the liver(40). Kupffer cells has been shown to migrate more towards Zone-3 in liver injury, generate reactive oxygen species, release proinflammatory cytokines and chemokines and play a significant role in inflammatory mechanisms in NASH(44). We examined the role of SsnB in modulating Kupffer cell activation in vivo by studying the mRNA and immunoreactivity of Kupffer cell activation marker CD68 and monocyte chemoattractant protein-1 (MCP-1) in the injured livers. Results showed that SsnB administration significantly decreased mRNA expression of both CD68 and MCP-1 (decrease of more than 12 fold for CD68) (Figure.3.3A) (P<0.05). Immunoreactivity to MCP1 were also significantly decreased in SH mice that were administered SsnB when compared to SH mice alone suggesting a possibility of low leukocyte infiltration in the liver lobule (Figure 3.3B, upper panel, C-morphometric analysis) (P<0.05). To examine the extent of

leukocyte infiltration in the liver lobule immunoreactivity to pan macrophage marker F4/80 was studied using immunohistochemistry. Results showed that there were significant increases in F4/80 immunoreactivity in the injured liver when compared to S group alone while administration of SsnB significantly attenuated the leukocyte infiltration as evidenced by decreased immunoreactivity to F4/80 in the liver (Figure. 3.3 B-down panel, 3D-morphometry) ($p<0.05$).

SsnB administration attenuates miR21 expression and repression of phosphatase and Tensin homologue (PTEN). We have shown previously that steatohepatitic injury following obesity causes a marked increase in miR21 expression, a non-coding RNA that has significant regulatory role in liver inflammation(109, 110). Higher miR21 levels led to decreased GRHL3 and SMAD7 proteins in both human NASH and rodent models of obesity(109, 110). Since TLR4 has been shown to play a role in miR21 induction, we studied the effects of SsnB, a probable TLR4 antagonist in TLR4-induced miR21 pathway. Results showed that SH mice had a significant increase in mir21 expression while administration of SsnB markedly decreased its expression in the murine obese liver (over 3 fold decrease) (Figure 3.4A)($P<0.05$). SsnB administration also decreased the levels of PTEN, a direct target of miR21 in the liver as shown by western blot analysis when compared to SH group (Figure 3.4B and C)($P<0.05$). The results suggested that SsnB might have a role in decreasing miR21 induced repression of PTEN primarily by blocking TLR4 activation however the interpretation of a SsnB role in blocking TLR is speculative at this time.

SsnB targets TLR4 trafficking to lipid rafts. Many studies, including ours have shown a direct role of TLR4 activation in both alcoholic and nonalcoholic steatohepatitis (80,

95, 111). One of the key aspects of TLR4 activation is its trafficking to lipid rich domains on the plasma membrane(95). Upon binding to a specific TLR4 ligand which can include, lipopolysaccharide (LPS), HMGB1 or free fatty acids, TLR4 protein is translocated to lipid containing rafts where the association to adaptor proteins and membrane assembly take place. Our collaborators in this study have shown via direct evidence that SsnB disrupts TLR4 activation and can be a potent TLR4 antagonist. To show the mechanistic insight of SsnB action in steatohepatitic liver injury, we studied the TLR4 trafficking into lipid rafts and its disruption by SsnB. Results showed that SsnB administration significantly decreased the colocalization of TLR4 (red) and lipid raft component flotillin (green) in the plasma membrane of SH mice (Figure 3.5A). The number of colocalization events/microscopic field were significantly decreased in SsnB treated group as compared to SH mice livers (Figure 3.5 B)(P<0.05). The results suggested that SsnB has a significant role in TLR4 trafficking in early steatohepatitic injury and the modulation of TLR4 trafficking might be contributing in part for the attenuation of inflammation seen with SsnB administration. Since resident macrophages play a clear role in liver inflammation in NASH, we studied the TLR4 trafficking in immortalized Kupffer cells following their stimulation with LPS, the classical ligand of TLR4. Results showed that incubation of Kupffer cells with LPS (50ng/ml) significantly increased colocalization of TLR4 with lipid raft marker flotillin while co-incubation with SsnB (100µg/ml) significantly attenuated the TLR4 translocation to the rafts (Figure. 3.6A and B). The SsnB co-incubation resulted in a 3 fold decrease in the colocalization events (Figure. 3.6 B(P<0.05). The colocalization is also shown in higher magnification (Figure. 3.6C)

SsnB targets leptin induced TLR4 trafficking in Kupffer cells. We have shown previously that proinflammatory adipokine leptin regulates Kupffer cell activation via reactive oxygen species generation(40). Leptin increased peroxynitrite generation by increasing NADPH oxidase activation that resulted in higher inflammatory mediation. Since hepatic leptin resistance is a common phenomenon in NASH patients, and selective leptin signaling observed in hepatic stellate cells, we studied the role of leptin in TLR4 trafficking to the lipid rafts in vitro(112, 113). Results showed that leptin administration to immortalized Kupffer cell culture significantly increased the TLR4-Flotillin colocalization as evidenced by yellow spots on the membranes of the incubated cells (Figure 3.7A-40x and C-60x oil images showing clusters of cells with colocalization in the membranes). Analysis of the number of colocalization events showed a significant increase in leptin-treated group when compared to cell-only controls (Figure 3.7A and B)($P<0.05$) with a 4 fold increase recorded in this group. SsnB co-incubation with leptin significantly decreased the colocalization events in these cells (Figure 3.7A and B) ($P<0.05$). The results suggested that similar to LPS, TLR4 trafficking to the lipid rafts was also influenced by leptin, a proinflammatory adipokine with known effects in NASH. Though the mechanism of leptin action via TLR4 ligand binding is highly unlikely in these cells, SsnB modulation of leptin might be an upstream event and can be a common target for SsnB apart from being a strong antagonist for TLR4 activation.

SsnB attenuates NADPH oxidase activation and peroxynitrite generation. Since SsnB administration significantly decreased TLR4-induced hepatic inflammation in obesity both in response to LPS and leptin, we argued about the presence of a significant target upstream of the TLR4 pathway that might be common and conspicuous for both

58

leptin and LPS mediated signaling. We recently showed that TLR4-lipid raft trafficking in NASH was mediated by peroxynitrite generated by the activation of NADPH oxidase(111). To show that SsnB modulated NADPH oxidase activation and peroxynitrite generation, events that are upstream of TLR4 activation, colocalization analysis of NADPH oxidase membrane subunits in the membranes of liver tissue were studied by immunofluorescence microscopy. Results showed that p47 phox (green), a cytoplasmic subunit required for NADPH oxidase activation colocalized with gp91 (red) a membrane subunit in liver tissue (Figure 3.8A-20x and C-60x oil images showing colocalization clusters). Analysis of the number of colocalization events in the liver tissue showed a significant increase in SH treated group while SsnB treated mice liver showed a significant decrease in the colocalization events suggesting a decreased NADPH oxidase activation (Figure 3.8B)(P<0.05). Kupffer cells treated with both leptin and LPS showed a marked increase in the gp91/p47 phox colocalization events while administration of SsnB (100 µg/ml) resulted in a significant decrease of the events (Figure 3.8D). Since NADPH oxidase activation resulted in generation of peroxynitrite in NASH, we examined the formation of 3-Nitrotyrosine, a marker for peroxynitrite generation in the diseased liver and immortalized Kupffer cells. Results showed that 3-nitrotyrosine immunoreactivity as analyzed by immunohistochemistry was significantly increased in SH mice livers as compared to S only group (Figure 3.9A and B)(P<0.05). SsnB administered mice livers showed a significant decrease in the 3-nitrotyrosine immunoreactivity when compared to SH mice livers (Figure 3.9A and B)(P<0.05). Since peroxynitrite generation requires both O_2^- and NO• reactivity in equal diffusion controlled rates, we studied the release of NO• from the Kupffer cell supernatants

incubated with both leptin, LPS and SsnB. Results showed that LPS and Leptin significantly increased NO• release while co-incubation with SsnB significantly attenuated the release of NO• analyzed by Greiss assay (Figure 3.9C)(P<0.05). The results suggested that apart from the strong TLR4 pathway antagonism function of SsnB, it also plays a significant role in NADPH oxidase activation and NO• release in inflammation. The SsnB attenuation of TLR4 pathway might be in part related to its effect on NADPH oxidase activation that is upstream of TLR4 trafficking to lipid rafts.

SsnB attenuates TLR ligand-induced gene expression of inflammatory cytokines, p47 phox, CD68 and cytokine release in mouse primary hepatic macrophages. To see the direct effect of SsnB on mouse primary hepatic macrophages, qRT PCR was performed to measure the pro-inflammatory cytokine gene expression levels. Result showed that as expected, mRNA expression of IL1β, MCP1 and TNFα pro-inflammatory cytokine gene expression were significantly elevated in LPS treated cells compared to untreated control cells. However, co-incubation of LPS treated cells with SsnB, decreases the expression of these genes significantly compared to only LPS treated cells (Figure 3.10A). In another set of experiments, after the mice primary hepatic macrophages were treated with SsnB and LPS for 24 h, the supernatant was collected for measurement of TNFα cytokine concentration by ELISA. As shown in Figure 3.10B, in TNFα level in the control media was almost undetectable. LPS (50 ng/ml) treatment dramatically increased the TNFα cytokine level. However, co-incubation with SsnB significantly reduced the TNFα cytokine level (Figure 3.10B). We have shown previously in Figure 3.8 and Figure 3.9 that SsnB significantly reduces the formation of peroxynitrite and corresponding inflammation and Kupffer cell activation by decreasing the co-localization of gp91/p47

phox and thus attenuates NADPH oxidase activation. To see whether SsnB has any effect in attenuating p47phox gene expression, a quantitative-real time PCR was performed to measure the p47phox gene expression levels. Result showed that mRNA expression of p47 phox gene expression was significantly elevated in LPS treated cells compared to untreated control cells (Figure 3.10C). However, co-incubation with SsnB, decreases the expression of these genes significantly compared to only LPS treated cells.

SsnB treatment does not reduce TLR4 gene expression or protein concentration. To address the question whether SsnB acts by decreasing TLR4 mRNA expression, qRT PCR experiments were performed to quantify the TLR4 mRNA expression both invivo and invitro. Our data shows that SsnB administration may slightly attenuated the up-regulation of TLR4 mRNA levels compared to SH group (Figure.3.11A). Co-incubation of mice primary hepatic macrophages with SsnB also resulted a faint reduction of TLR4 mRNA expression compared to only LPS treated cells (Figure 3.11B). Liang et al., (28) observed the similar incident and described it as a secondary event to the suppression of pro-inflammatory signaling pathways. A western blot experiment was also performed from mice liver homogenates to see if TLR4 protein expression is reduced by SsnB administration. Our data clearly indicates that SsnB administration didn't cause any reduction in total TLR4 protein level (Figure. 3.11C and D). However, it has already been shown by Liang et al., (28) that SsnB possibly acts by attenuating the interaction of MyD88 and TLR4 Toll/interleukin-1 receptor (TIR) domain. Our findings also suggest that SsnB decreases TLR4 trafficking in lipid rafts by preventing NADPH oxidase activation and reducing nitrative stress. Thus there is a possibility that SsnB induced

TLR4 signaling attenuation may not be dependent on the total TLR4 protein concentration.

3.4 DISCUSSION: The present study reports a novel role and mechanistic insight of the TLR4 antagonist SsnB. Using a rodent model of early steatohepatitic injury, we show that SsnB attenuated inflammation in the liver by blocking TLR4 trafficking to the lipid rafts. Further, we deciphered that SsnB could block TLR4 trafficking into the lipid rafts by decreasing NADPH oxidase activation and peroxynitrite generation. The role of TLR4 in NASH and its consequences is being pursued vigorously across the scientific community(79, 80, 114). The potent role of TLR4 activation and its downstream signaling has been reported in both alcoholic and nonalcoholic steatohepatitis(79). In alcoholic steatohepatitis, portal endotoxemia from gut leaching has been accepted as a source for the TLR4 ligand in the liver(87, 115). Various studies have reported free fatty acids and HMGB1 as ligands in TLR4 activation in NASH(95, 116, 117). We recently reported that peroxynitrite generation activates TLR4 signaling by modulating its trafficking into the lipid rafts primarily by an upstream NADPH oxidase activation(111). The results in that study also confirmed an earlier report showing NADPH oxidase as a prime regulator of TLR4 trafficking but could not provide a molecular mediator for its actions (95). Interestingly TLR4 downstream signaling is also known to produce NADPH oxidase activation(118). Our results in this report show a novel role of SsnB, a natural product derivative in modulating TLR4 trafficking into lipid rafts, a mechanism that remained elusive before. SsnB has been shown by our collaborators in numerous in vivo and in vitro studies to be a portent TLR4 antagonist(28, 98-101, 119). SsnB structural analysis and its characterization in terms of mechanism of action showed that it reduced

the association of MyD88 with TLR4 and TLR2 but not with TLR9(28). Inflammatory cytokine signaling emanating from the TLR4 signaling in vitro was specifically blocked by SsnB while LPS-induced septic shock was reversed by its administration in vivo(101). Having known the earlier reported mechanisms of SsnB action we explored its role in NASH induced inflammatory injury. Our rationale was based on the strong inflammatory phase in NASH that is appreciated in both rodent models of NASH and clinical phases(120). Our results showed that SsnB administration in vivo reversed inflammatory pathophysiology primarily evidenced by reduced leukocyte infiltration, decreased necrosis in Zone3 and lower levels of proinflammatory cytokines IL1β and TNF-α. Since Kupffer cell activation is a prime inflammatory event in NASH that also has been shown to play a vital role in activating stellate cells, we examined the levels of CD68 and MCP-1. Results showed a dramatic decrease in the levels of the chemokines and surface expression of CD68. The results were in line with earlier reports from our lab and others that Kupffer cell activation reversal can have a beneficial effect on NASH progression and treatment at least in rodent models of NASH(40, 114). The studies reported here however have not explored the role of SsnB in reversal of Kupffer cell activation since we knew that SsnB might target TLR4 that has been shown previously to activate Kupffer cells(121). Though Kupffer cells respond to LPS mediated TLR4 activation, there are reports of TLR4 expression in hepatocytes, endothelial cells and stellate cells(79, 90).Interestingly, Kupffer cells are primary foci for generating an inflammatory response and SsnB action in these cells might mediate the TLR4 activation.. The SsnB role in preventing TLR4 signaling in Kupffer cells might render a stalling effect on the initial inflammatory phase which may eventually block stellate cell activation and

63

extracellular matrix formation. For the purposes discussed above we used immortalized Kupffer cells to illustrate the mechanism of SsnB deactivation of TLR4 pathway.

We have recently shown that NASH is characterized by an increase in miR21 induced repression of GRHL3 and SMAD7, two key proteins that have a pronounced role in sinusoidal endothelial injury and extracellular matrix formation (109, 110). Interestingly miR21 is a TLR4 inducible non coding RNA and our results in this report of a significant decrease in miR21-induced repression of PTEN confirmed the SsnB targeting of TLR4 pathway(58). It will be of interest in later studies, how SsnB may help in alleviating the miR21-induced repressions of GRHL3 and SMAD 7 in NASH.

To mechanistically explain the role of SsnB in TLR4 deactivation response we studied the trafficking of TLR4 into lipid rafts which is a prime event in TLR4 activation and downstream signaling(95). Lipid raft are lipid rich domains within the plasma membrane that help in assembly of many transmembrane receptors including TLR4(95). This myriad of molecular events and assembly starts with the binding of an appropriate ligand to TLR4. We observed that SsnB administration significantly attenuated the trafficking of TLR4 into lipid rafts as shown by decreased number of colocalization events (TLR4 and flotillin) in NASH livers. Rat immortalized Kupffer cells were also used to show the trafficking process and its attenuation by SsnB following TLR stimulation by LPS. Our results of significant decrease in colocalization events of TLR4 and flotillin in Kupffer cells show that SsnB could exert its TLR4 antagonism by stalling the lipid raft recruitment process. Though SsnB has been shown by our collaborators to interfere in the association of TLR4 with its adaptor MyD88, It can be speculated that SsnB could competitively bind to TLR4 thus restricting the classical ligand LPS to exert

its effects(28). However this observation is highly speculative at this point since SsnB binding to TLR4 in NASH has not been studied. Interestingly TLR4 trafficking to rafts occur on binding of the ligand to TLR4 and it would be interesting to see the molecular aspects of SsnB binding to TLR4 or its restrictive capacity to alter TLR4 ligand binding in future studies.

We have shown previously that proinflammatory adipokine leptin mediates the progression of NASH by activating Kupffer cells, upregulation of non-coding RNAs and activating pattern recognition receptor P2X7r(109, 110). Leptin has been shown recently to upregulate TLR2 expression in monocytes (122). Extending the studies of leptin induced proinflammatory action in Kupffer cells we studied their role in activating TLR4 trafficking in these cells. Results showed that leptin activated TLR4 signaling via promoting the TLR4 trafficking to lipid rafts an event that was attenuated by SsnB co-incubation. These results were significant since it showed that SsnB can target an upstream molecular event in lipid raft trafficking of TLR4, considering the fact that leptin is not a ligand for TLR4 neither has it been shown to have structural similarity to a classical ligand of TLR4. We also have evidence from previous published reports from our lab that (i) leptin targets NADPH oxidase activation and (ii) NADPH oxidase drives TLR4 trafficking via peroxynitrite generation (40, 111). Based on these arguments we conducted studies to show the role of SsnB in NADPH oxidase activation. Our results of a significant increase in colocalization of gp91 (membrane subunit) and p47 phox (cytoplasmic subunit) in SH groups and its subsequent decrease in these events following SsnB administration indicated a novel role of SsnB apart from its proven role as an TLR4 antagonist. Parallel to the in vivo data, Kupffer cells also showed significant attenuation

of NADPH oxidase activation following SsnB administration in response to both leptin and LPS. However it needs to be considered that NADPH oxidase activation primarily depends on membrane assembly of a number of subunits, p47 phox being one of them, a crucial element for NOX2 type NADPH oxidases(33, 46). Finally, SsnB-induced decrease in peroxynitrite marker 3-nitrotyrosine both in vivo and nitric oxide release in vitro showed a clear mechanistic connection between NADPH oxidation, increased nitrative stress and TLR4 activation following SsnB administration. It is worth mentioning here that peroxynitrite induced HMGB1, a TLR4 activator release has been shown(123). A decrease in peroxynitrite formation following NADPH oxidase inhibition by SsnB might be a parallel mechanism of SsnB amelioration of TLR4 pathway and subsequent decrease in early steatoheaptitic injury and inflammation in the liver.

Taken together, our data describe a novel mechanistic role of SsnB in resolving NASH –induced inflammation primarily by blocking TLR4 lipid raft trafficking and NADPH oxidase activation. Future studies featuring SsnB binding kinetics to TLR4 or pathways unique to deactivation of NADPH oxidase might usher new light on probable therapeutic benefits of SsnB.

Conflict of Interest: The authors declare that there is no conflict of interest.
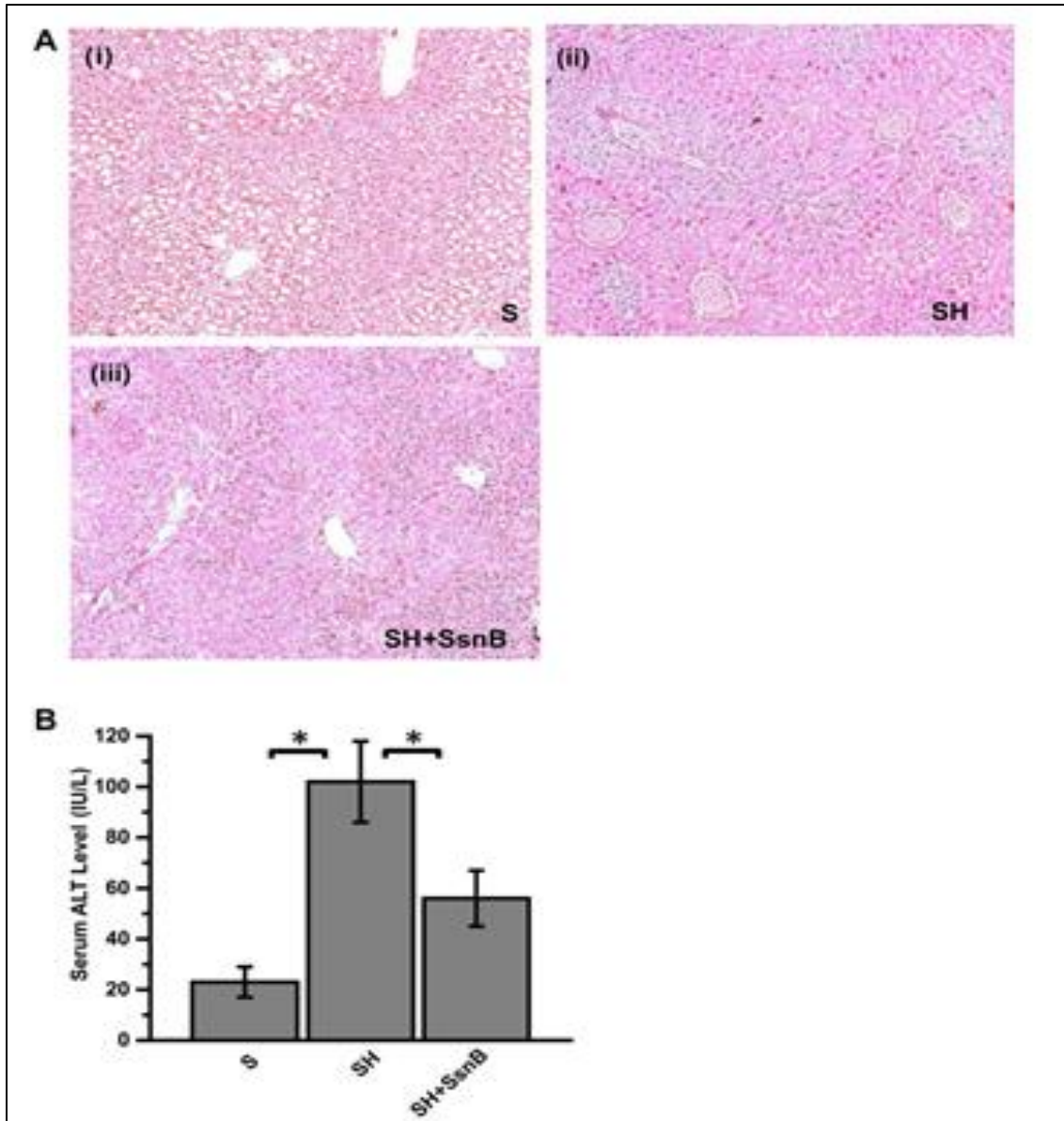
Figure 3.1 Sparstolonin B (SsnB) administration attenuates early steatohepatitic injury in obese mice. A: hematoxylin and eosin-stained paraffin-embedded liver tissue sections of steatosis (S; i), steatohepatitic injury (SH; ii), and SH+SsnB (iii) mice. Images were taken at ×10 magnification. B: serum levels of alanine aminotransferase (ALT) from S, SH, and SH+SsnB groups. *P < 0.05.
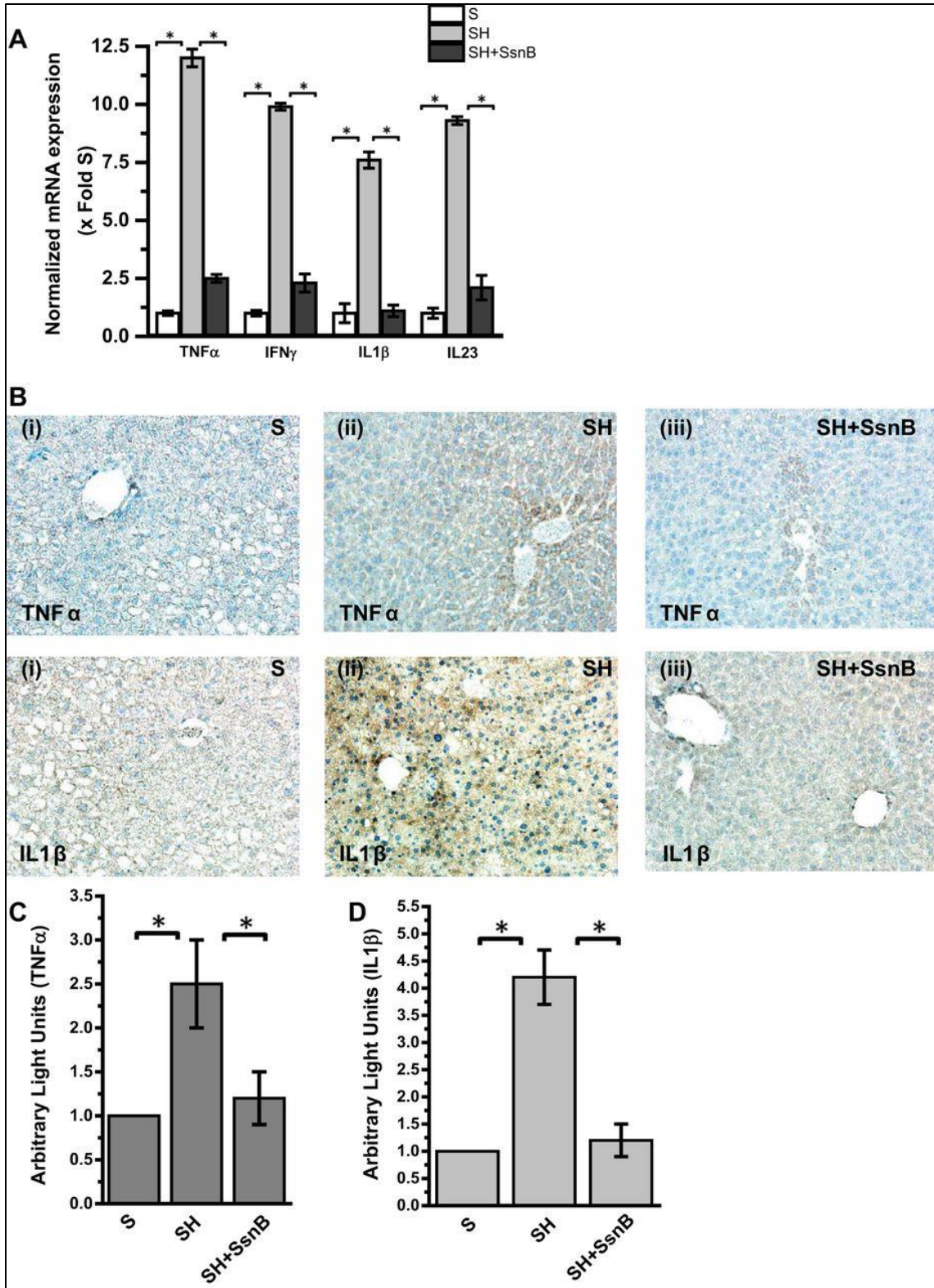
Figure 3.2 SsnB administration to SH mice ameliorates proinflammatory cytokines and decreases M1 polarization. A: qRT-PCR analysis of mRNA expression of TNF-α, IFN-γ, IL-1β, and IL-23 from liver homogenates of S, SH, and SH+SsnB mice, normalized

against S (*P < 0.05). B: TNF-α (top) and IL-1β (bottom) immunoreactivity as shown by immunohistochemistry in liver slices from S (i), SH (ii), and SH+SsnB (iii) mouse samples. Images were taken at ×20 magnification. C: morphometric analysis of TNF-α immunoreactivity in S, SH, and SsnB groups (*P < 0.05). D: morphometric analysis of IL-1β immunoreactivity in S, SH, and SH+SsnB groups (*P < 0.05).
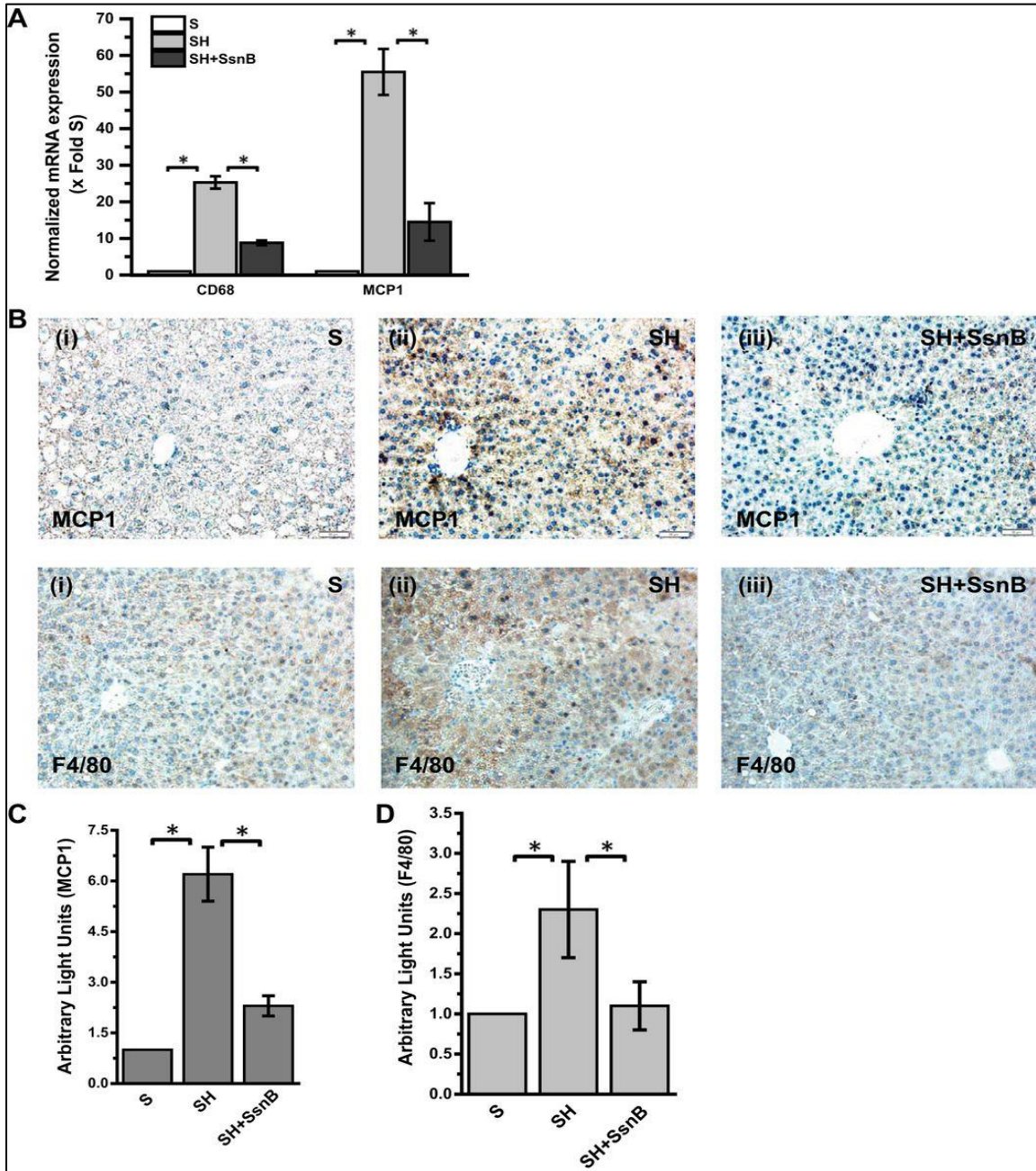
Figure 3.3 SsnB administration modulates Kupffer cell activation in early steatohepatitic injury. A:qRT-PCR analysis of mRNA expression of CD68 and monocyte

chemoattractant protein-1 (MCP1) from liver homogenates of S, SH, and SH+SsnB mice, normalized against S (*P < 0.05). B: MCP1 (top) and F4/80 (bottom) immunoreactivity as shown by immunohistochemistry in liver slices from S (i), SH (ii), and SH+SsnB (iii) mouse samples. Images were taken at ×20 magnification. C: morphometric analysis of MCP1 immunoreactivity in S, SH, and SH+SsnB groups (*P < 0.05). D: morphometric analysis of F4/80 immunoreactivity in S, SH, and SH+SsnB groups (*P < 0.05).
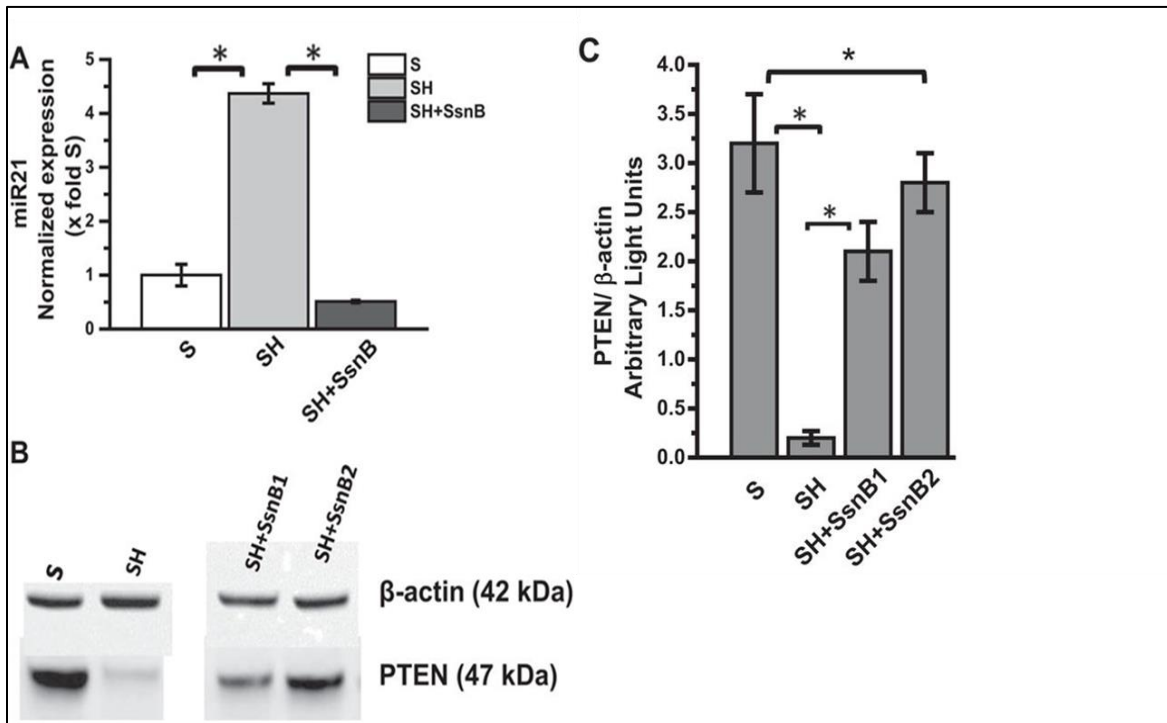
Figure 3.4. SsnB administration attenuates miR21 expression and repression of phosphatase and Tensin homologue (PTEN). A: qRTPCR analysis of miR21 expression of S, SH, SH+SsnB mice samples normalized against S (*P<0.05). B: Western blot analysis of β-actin and PTEN protein levels of S, SH, SH+SsnB sample1 and SH+SsnB sample2 respectively. C: Immunoreactive band analysis of PTEN normalized against β-actin. Y-axis depicts the PTEN/actin ratio from S, SH, SH+SsnB sample1 and SH+SsnB sample2(*P<0.05).
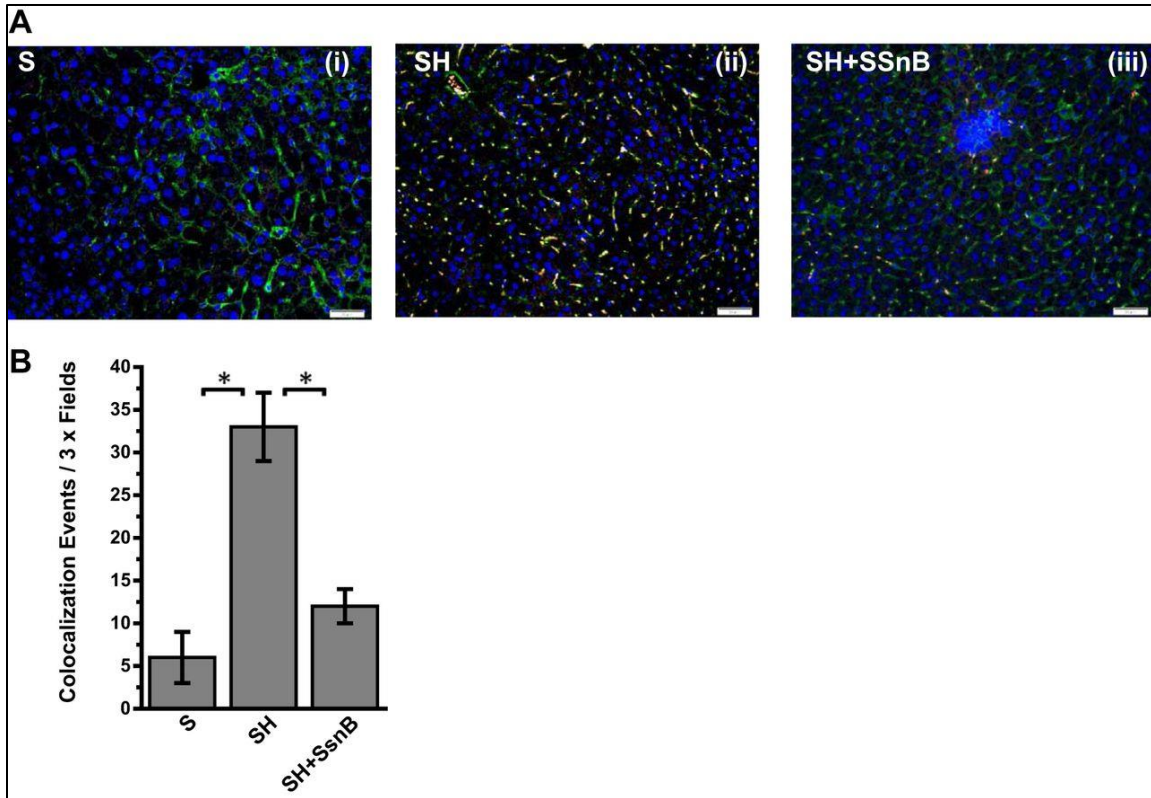
Figure 3.5 SsnB targets TLR4 trafficking to lipid rafts. A: immunofluorescence dual labeling depicting TLR4 (red)-flottilin1 (green) colocalization (yellow) in S (i) SH (ii), and SH+SsnB (iii) liver samples, taken at ×20 magnification. B: morphometric analysis of colocalization events in A, shown as colocalization events per 3× field (*P < 0.05).
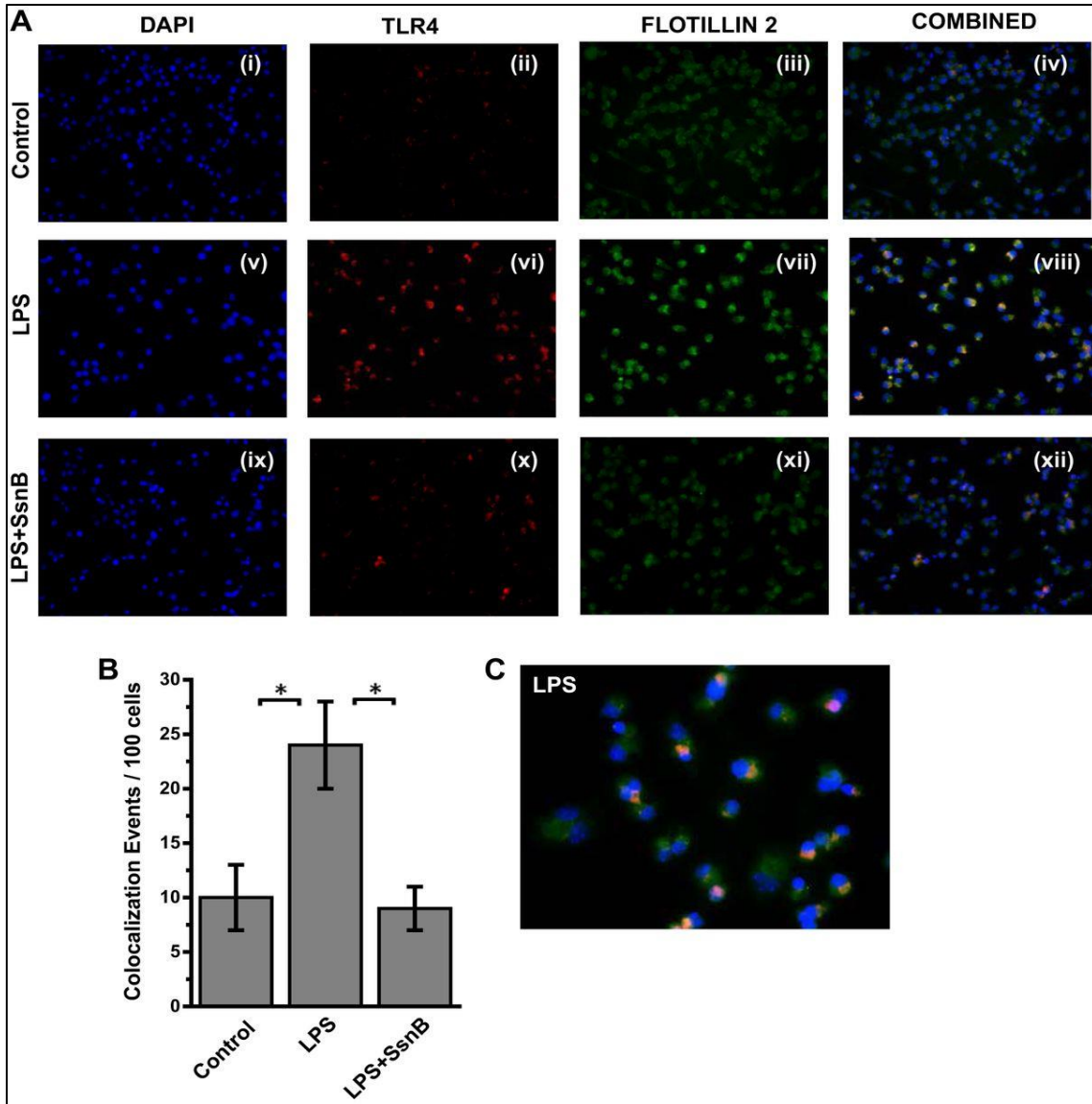
Figure 3.6 SsnB targets LPS-induced TLR4 trafficking in Kupffer cells. A: immunofluorescence laser scanning images for colocalization of TLR4 (red) and flottilin2 (green) in rat Kupffer cells of the control (i–iv), LPS-treated (v–viii), and LPS+SsnB-treated (ix–xii) groups. Images in overlay panels on right depict colocalizations of TLR4-flottilin2, as revealed by the yellow regions. Images were taken at ×40 magnification. B: morphometric analysis of colocalization events in A, shown as colocalization events per 100 cells (*P < 0.05). C: immunofluorescence dual labeling of LPS-treated rat Kupffer cell sample depicting TLR4 (red)-flottilin2 (green) colocalization (yellow) at ×60(oil) magnification.
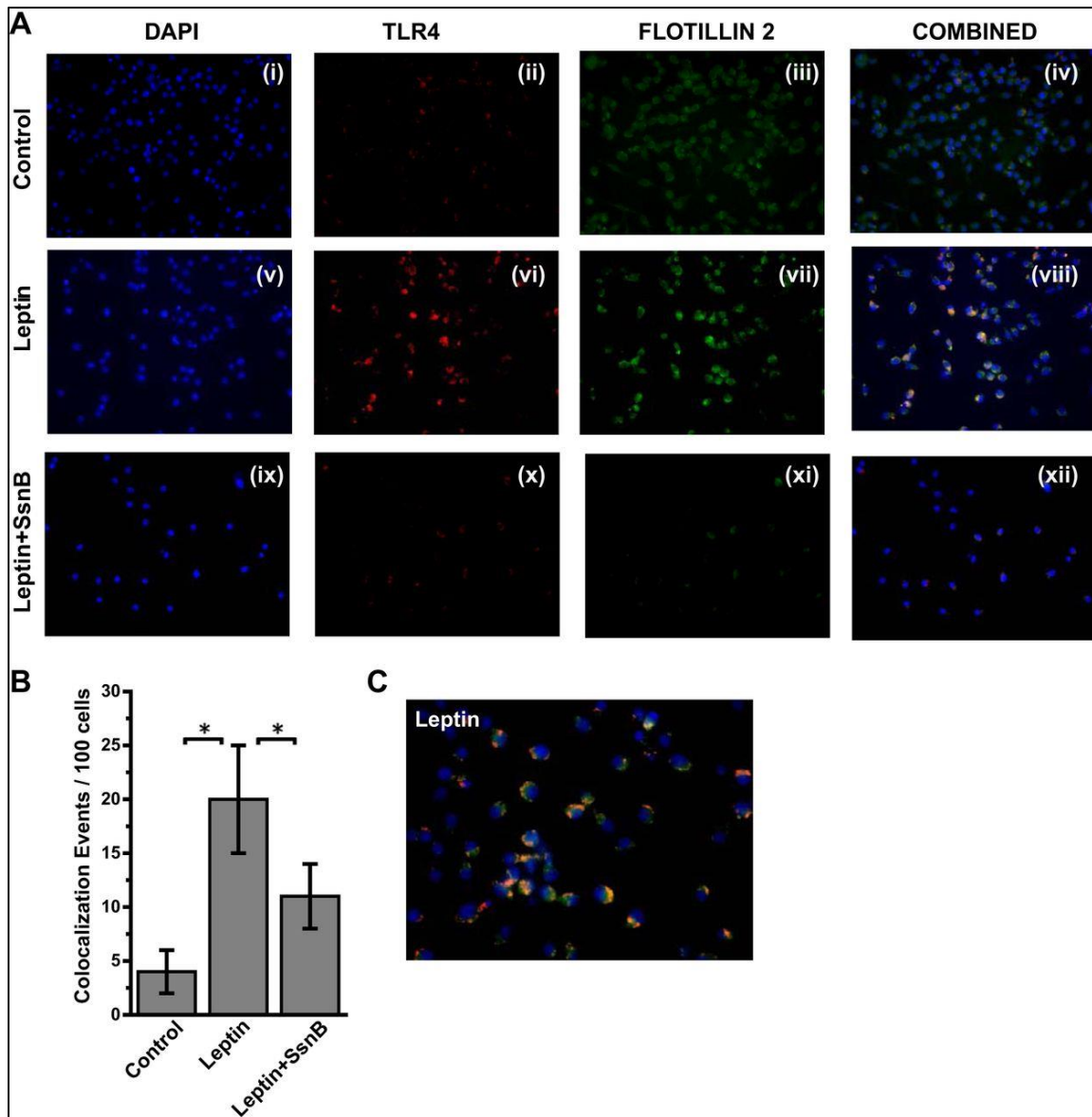
Figure 3.7 SsnB targets leptin-induced TLR4 trafficking in Kupffer cells. A: immunofluorescence laser scanning images for colocalization of TLR4 (red) and flottilin2 (green) in rat Kupffer cells of the Control (i–iv), leptin-treated (v–viii), and leptin+SsnB-treated (ix–xii) groups. Images in overlay panels on right depict colocalizations of TLR4-flottilin2, as revealed by the yellow regions. Images were taken at ×40 magnification. B: morphometric analysis of colocalization events in A, shown as colocalization events per 100 cells (*P < 0.05). C: immunofluorescence dual labeling of leptin-treated rat Kupffer cell sample depicting TLR4 (red)-flottilin2 (green) colocalization (yellow) taken at ×60(oil) magnification.
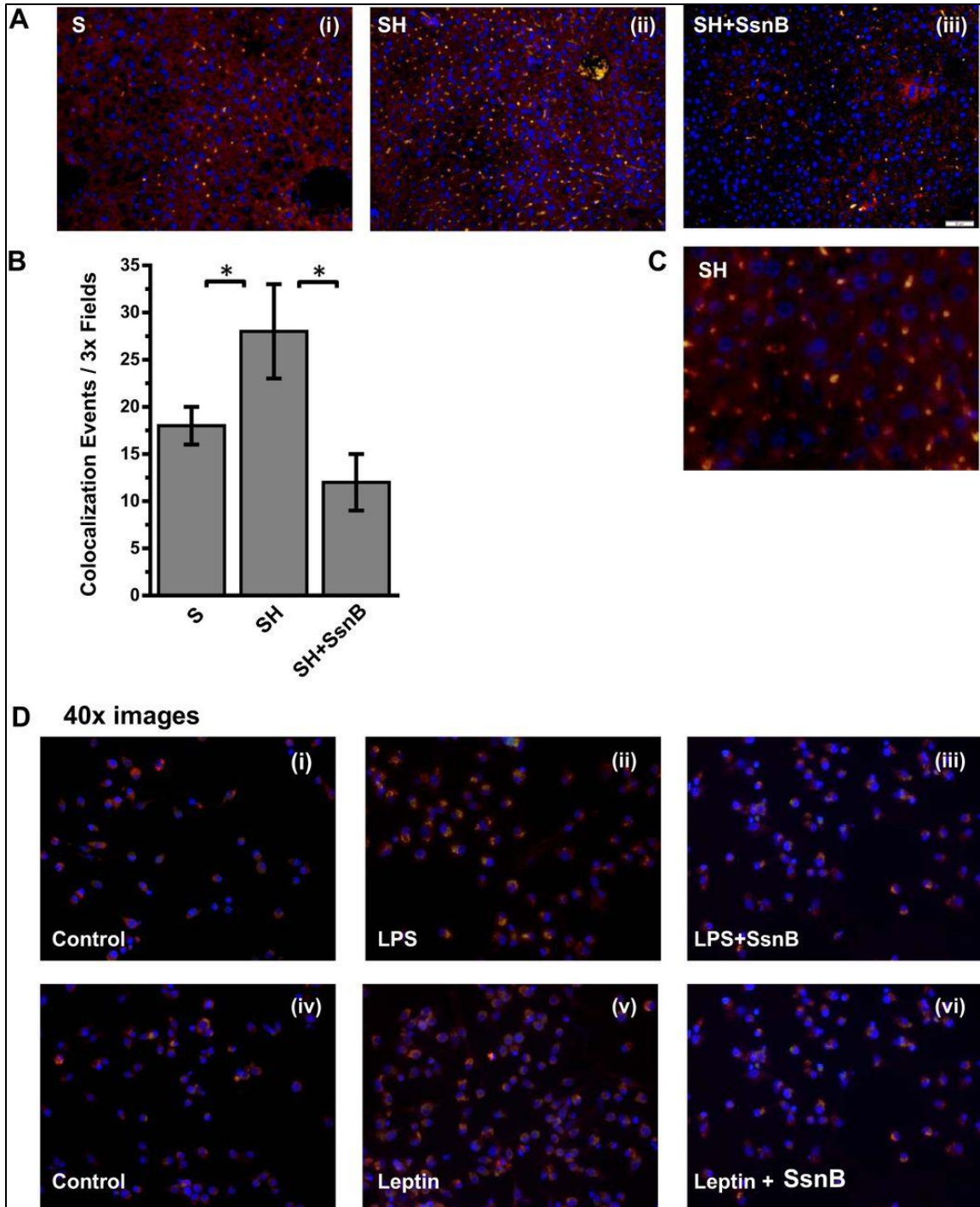
Figure 3.8 SsnB attenuates NADPH oxidase activation. A: immunofluorescence dual labeling depicting gp91phox (red)-p47phox (green) colocalization (yellow) in S (i), SH (ii), and SH+SsnB (iii) liver samples, taken at ×20 magnification. B: morphometric analysis of colocalization events in A, shown as colocalization events per 3× field (*P < 0.05). C: immunofluorescence dual labeling of SH liver sample depicting gp91phox (red)-p47phox (green) colocalization (yellow) taken at ×60 (oil) magnification. D: immunofluorescence dual labeling of control (i), LPS (ii), LPS+SsnB (iii), control (iv),

leptin (v), and leptin+SsnB (vi) rat Kupffer cell samples depicting gp91phox (red)-p47phox (green) colocalization (yellow), taken at ×40 magnification.
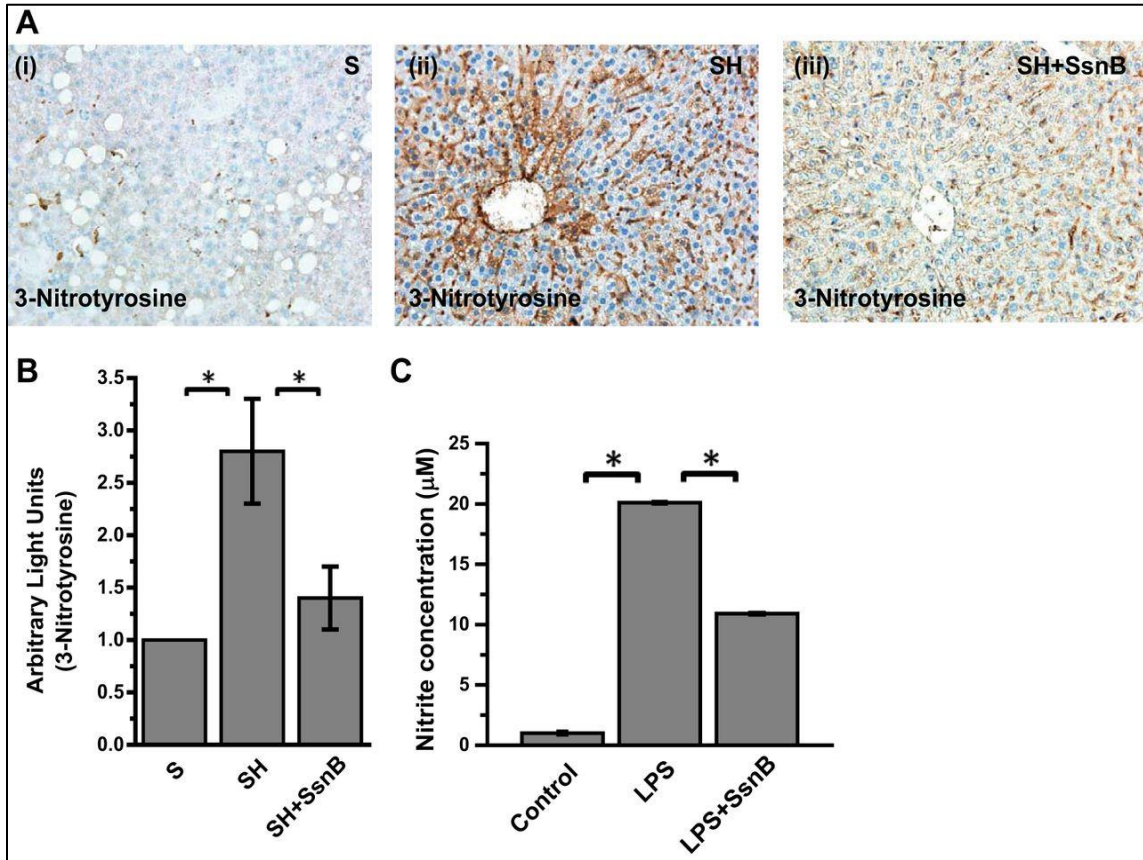
Figure 3.9 SsnB attenuates NADPH oxidase activation and peroxynitrite generation. A: 3-nitrotyrosine immunoreactivity as shown by immunohistochemistry in liver slices from S (i), SH (ii), and SH+SsnB (iii) mouse samples. Images were taken at ×20 magnification. B: morphometric analysis of 3-nitrotyrosine immunoreactivity in S, SH, and SH+SsnB groups (*$P < 0.05$). C: nitric oxide (nitrite) concentration measured by nitric oxide colorimetric assay in the supernatant collected from control, LPS-treated, and LPS+SsnB-treated rat Kupffer cells (*$P < 0.05$).
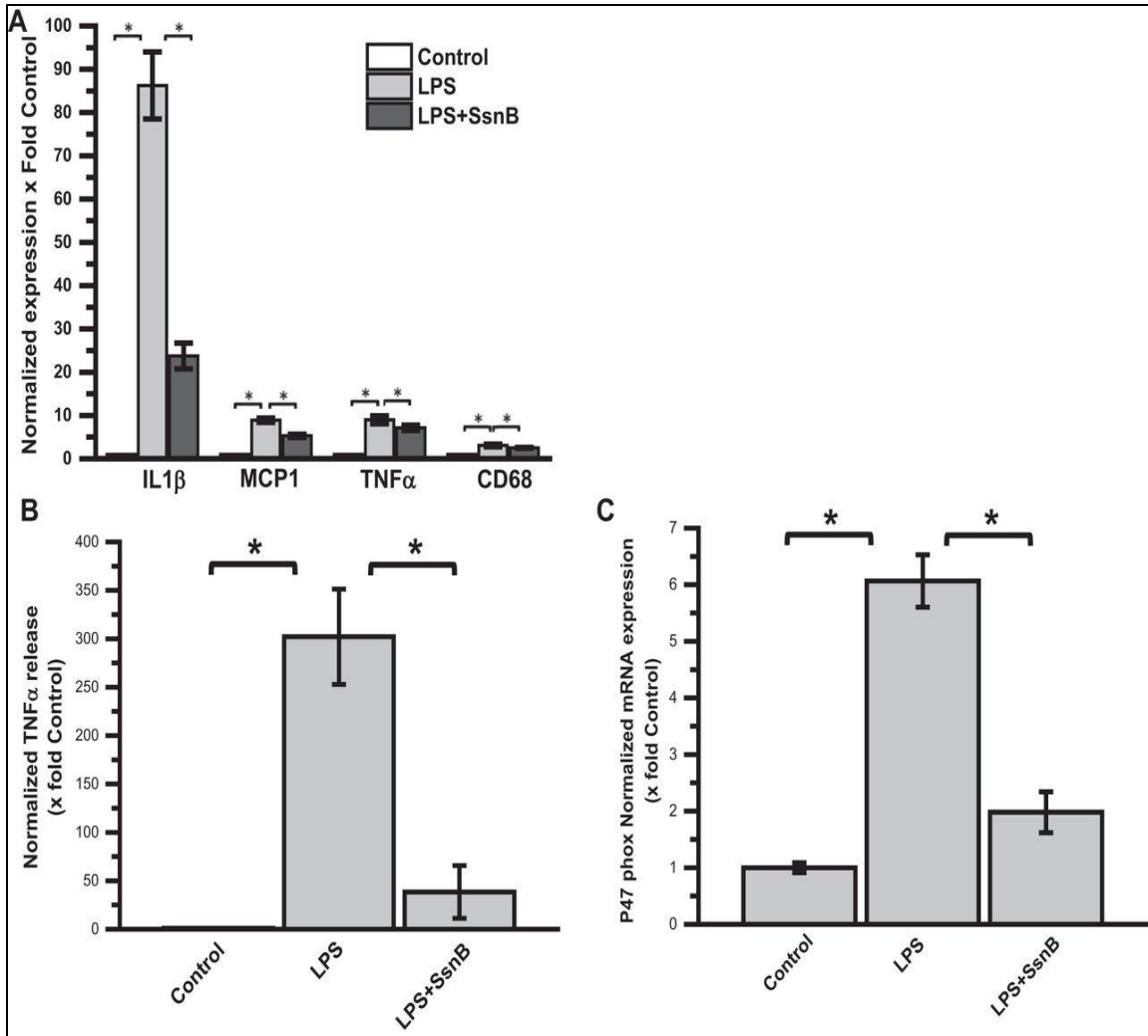
Figure 3.10 SsnB attenuates TLR ligand-induced macrophage activation, gene expression of P47phox, and gene expression and release of inflammatory cytokines in mouse primary hepatic macrophages. A: qRT-PCR analysis of mRNA expression of IL-1β, MCP1, and TNF-α from control (untreated), LPS-treated, and LPS+SsnB-treated mouse primary hepatic macrophages, normalized against control (*P < 0.05). B: TNF-α cytokine levels measured by ELISA from the supernatant collected from control, LPS-treated, and LPS+SsnB-treated mouse primary hepatic macrophages, normalized against control (*P < 0.05). C: qRT-PCR analysis of mRNA expression of p47phox from control (untreated), LPS-treated, and LPS+SsnB-treated mouse primary hepatic macrophages, normalized against control (*P < 0.05).
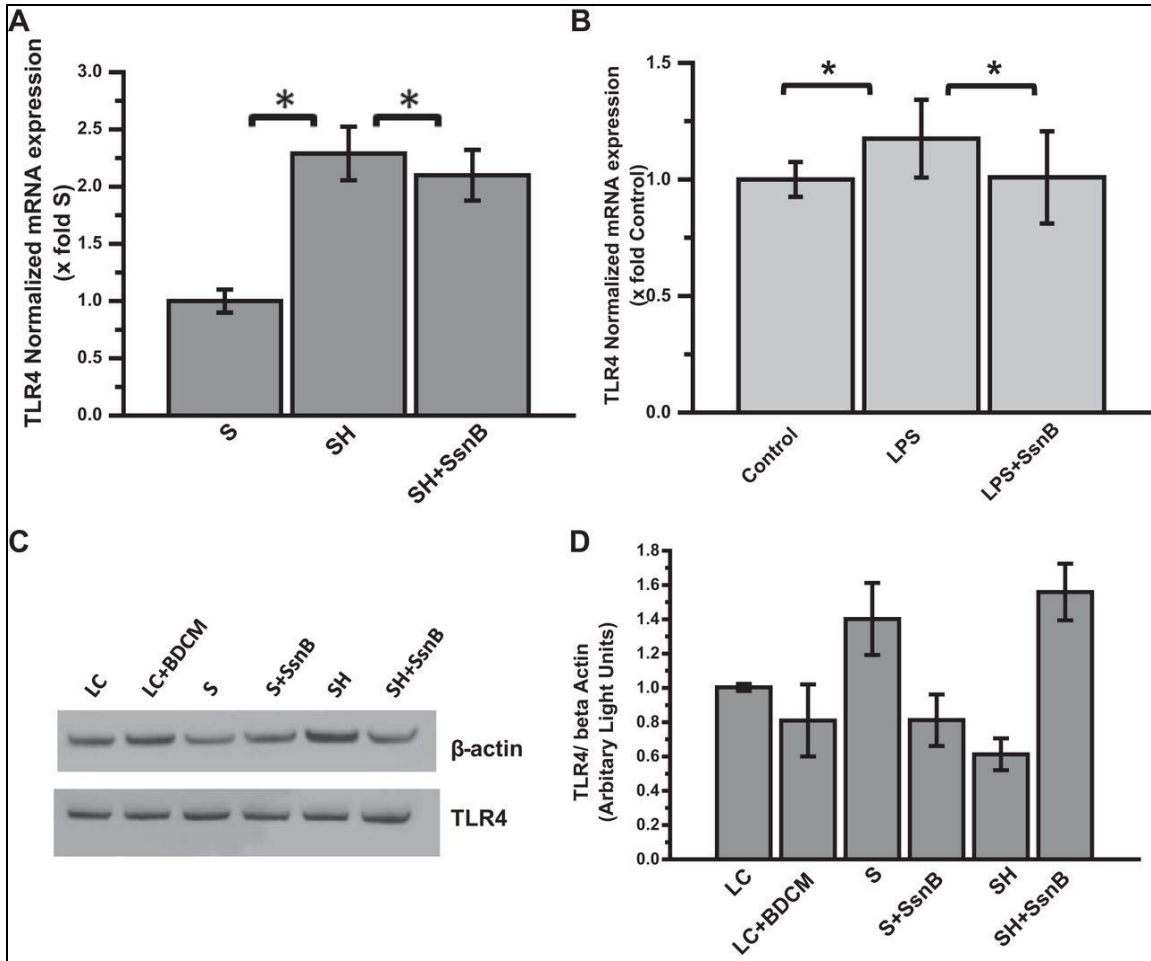
Figure 3.11 SsnB treatment does not reduce TLR4 gene expression or protein concentration. A: qRT-PCR analysis of mRNA expression of TLR4 from liver homogenates of S, SH, and SH+SsnB mice, normalized against S (*P < 0.05). B: qRT-PCR analysis of mRNA expression of TLR4 from control (untreated), LPS-treated, and LPS+SsnB-treated mouse primary hepatic macrophages, normalized against control (*P < 0.05). C: Western blot analysis of β-actin and TLR4 protein levels in the liver homogenates of lean control (LC), LC+bromodichloromethane (BDCM), S, S+SsnB, SH, and SH+SsnB groups. D: immunoreactive band analysis of TLR4 normalized against β-actin. y-Axis depicts the TLR4-to-β-actin ratio for LC, LC+BDCM, S, S+SsnB, SH, and SH+SsnB groups.

CHAPTER 4

ADMINISTRATION OF SPARSTOLONIN B ATTENUATES HEPATIC FIBROSIS BY INHIBITING PROLIFERATION AND INDUCING APOPTOSIS IN HEPATIC STELLATE CELLS.[3]

Abstract:

This research unravels anti-fibrotic and anti-proliferative mechanisms of a plant derived TLR4 antagonist, Sparstolonin B (SsnB) in a Bromodichloromechane (BDCM) induced murine model of NASH and hepatic stellate cell culture. SsnB showed a promising role to lessen liver fibrosis by upregulating cell cycle inhibitory proteins and inhibiting fibrogenic cell proliferation. Mechanistically, SsnB, a TLR4 antagonist, decreased TLR4-PI3k akt signaling by upregulating PTEN protein expression. It also decreased MDM2 protein activation and increased p53 and p21 gene and protein expression. SsnB also downregulated pro-fibrogenic hedgehog signaling pathway, inhibited hepatic stellate cell proliferation and induced apoptosis in hepatic stellate cells. This anti-proliferative and pro-apoptotic properties of SsnB can be instrumental to ameliorate fibrotic lesions in liver when administered to murine model of NASH.

4.1 INTRODUCTION

Nonalcoholic steatohepatitis (NASH) is manifestation of metabolic syndrome in liver which arises from hepatic fat accumulation (73). NASH is characterized by steatosis (fat deposition) in liver along with increased liver inflammation, fibrosis and progressive endothelial dysfunction, which can lead to cirrhosis and hepatocellular carcinoma (125,

126). NASH is a silent liver disease and patients generally feel well until they develop irreversible excessive liver damage. As there is almost no medication available to treat NASH related excessive liver damage, liver transplant can bring the only hope for survival-given that there is always a short supply of liver and liver transplant has been a challenge due to graft rejection, graft steatosis, infection during the transplantation etc. (127). The mortality of NASH affected patients can also increase by cardio-vascular damage (128). As obesity is becoming a worldwide epidemic, the prevalence of Non Alcoholic Fatty Liver Disease (NAFLD) is increasing globally. NAFLD affected liver can progress into NASH like irreversible liver injury due to hepatic toxicity and imposes a major public health threat (127). Toll like receptors (TLRs) have been shown to play a major role in the pathogenesis of NASH and clinical studies show that endotoxemia as a result of leaky gut in NASH condition, can lead to TLR4 activation (24, 90). Increased oxidative stress, peroxinitrite formation, HMGB1 protein, Fibrinogen or other DAMPs (damage associated molecular patterns) associated with liver injury, can also act as ligands for TLR4 signaling (90). TLR4 activation can lead to increased JNK activation, which leads to inflammation, fibrosis, insulin resistance and other metabolic dysregulation during NASH (25). Abrogation of TLR4 trafficking to lipid rafts helps to decrease inflammation in murine NASH models and had better histological outcomes (90). As TLR4 activation is a major event that leads to several inflammatory pathway activations and fibrogenesis, a potent TLR4 antagonist can be useful to treat such condition. Therefore, development of a novel therapeutic strategy to combat this disease is needed. In this research, we study the therapeutic role of a novel plant derived compound, Sparstolonin B (SsnB), on a toxin induced model of nonalcoholic

81

steatohepatitis. The purpose of the present study was to investigate the impact of SsnB on hepatic fibrosis *in vivo* and *in vitro* through assessment of the effects of SsnB on the proliferation of hepatic stellate cells, extracellular matrix deposition and pro-fibrogenic signaling pathways. We also wanted to find out the effect of SsnB on anti- proliferative proteins and hedgehog signaling pathway.

4.2 MATERIALS AND METHODS

Cell culture: Human immortalized stellate cell line (LX2) (kindly gifted by Dr. Ana Mae Diehl, Duke University) was grown in complete Dulbecco's Modified Eagle's Medium (DMEM, Corning, VA) with 10% fetal bovine serum (FBS, Atlas Biologicals, CO) and 1x Penicillin-Streptomycin solution (Gibco, Life Technologies, NY) at 37°C in a humidified incubator with 5% CO_2. Tissue culture plastic wares, HBSS buffer were purchased from Corning (Corning, VA). Sparstolonin B (SsnB) compound was kindly gifted by our collaborator Dr. Daping Fan (Cell Biology and Anatomy, University of South Carolina School of Medicine). Stock solution of SsnB was prepared in 100% dimethyl sulfoxide (DMSO). The final concentrations of SsnB on cells were 10μg/ml, 0.1% DMSO and 100μg/ml, 0.1% DMSO respectively. The cells were plated on 6 well/12 well plates using DMEM medium supplemented with 10% FBS. Before treating the cells with LPS (100ng/ml) and SsnB (10μM, 100μM), cells were cultured in DMEM with 2% FBS (overnight). All treatments are given for 24 hours in 2% FBS containing DMEM medium. Cells treated with 0.1% DMSO were used as control. Primary rat hepatic stellate cells (ScienCell Research Lab, Carlsbad, CA) were cultured in specific medium as instructed by the manufacturer, on poly-l-lysine (ScienCell Research Lab)-coated 6well/ 12-well plates and incubated at 37°C in a humidified incubator with 5%

CO2 to initiate the culture. Treatments of LPS and SsnB were given as discussed above. All treated cells were subjected to mRNA and protein extraction. Maintaining aforementioned conditions, cells were plated on coverslips by putting coverslips on each well of 12 well plates and the cells adhered on coverslips were used for immune-fluorescence dual labelling staining after the treatment.

Mouse Models: Pathogen-free, male mice with C57BL/6J background (Jackson Laboratories, Bar Harbor, ME) were housed one per cage at 23-24°C with a 12-h/12-h light/dark cycle at libitum access to food and water. They were fed with 60% kcal high fat diet (Research Diets, New Brunswick, NJ) from 6 weeks until 16 weeks to generate a model of steatosis. We refer to this group as Control. A similar group of high fat fed mice were administered Bromodichloromethane BDCM (1mmol/kg, diluted in corn oil) though intraperitoneal injection, twice a week for 1 month to generate BDCM induced Non-alcoholic steatohepatitis model of mice (NASH). BDCM and corn oil were purchased from Sigma-Aldrich (St. Louis, MO). A group of NASH mice were administered with SsnB (3mg/kg) intraperitoneally twice for 4 weeks (NASH+SsnB). NIH guideline for Humane Care and Use of Laboratory Animals and local IACUC standards were followed during animal handling. Animal experiments were approved by the University of South Carolina at Columbia. Upon completion of the treatment, all mice were sacrificed for liver tissues and serum samples for further experiments.

Laboratory analysis

Picrosirius red staining: Picrosirius red staining of formalin-fixed, paraffin embedded liver tissue sections (5-µm-thick) was done using a Nova ultra-sirius red stain kit

83

following manufacturer's instructions (IHC-World). Liver sections were observed under a ×20 objective of a light microscope. Morphometric analysis of the stained regions of the tissue sections was performed using cellSens software (Olympus). The degree of fibrosis was evaluated by following the METAVIR scoring system (F0: no fibrosis, F1: portal fibrosis without septum formation, F2: portal fibrosis with few septum formation, F3: portal fibrosis with several septum formations but no cirrhosis and F4: cirrhosis) on the basis of histological observation of the slides.

Immunohistochemistry: Formalin-fixed, paraffin embedded liver tissue sections (5-μm-thick) were subjected to de-paraffinization and antigen retrieval using standard protocol. Immunohistochemistry was performed on neutral buffer formalin (NBF) fixed liver tissues according to the protocol described in our early publication (19). Mouse monoclonal p53 (Cell Signaling Technology, MA) and p21 antibody (Santa cruz Biotechnology, TX) were used in recommended dilution. Rest of the experiment was processed as described in our previous publication (19).

Immunofluorescence Microscopy

In vivo: De-paraffinization and antigen retrieval was performed on formalin-fixed; paraffin embedded liver tissue sections (5-μm-thick) were done by using standard protocol. The primary antibodies MDM2 (Santa cruz Biotechnology, TX), Gli1 (Abcam, MA) were used in recommended dilutions. Species-specific secondary antibodies conjugated with Alexa Fluor 633 (Invitrogen, CA) were used against the appropriate primary antibodies. Rest of the experiment was processed as described in our previous publication (19).

In vitro: After completion of the treatments as previously stated, the cell attached coverslips were fixed and processed according to our previous publication (19). Cells were incubated with αSMA (Abcam, MA), p53 (CST, Danvers MA), and p21 (Santa cruz Biotechnology, TX) primary antibodies followed by species-specific Alexa Fluor 633 and 488 (described above), for immunofluorescence dual-labeling staining. Alexa Fluor 633 was used against p53 and p21 antibodies. Alexa Fluor 488 was used against αSMA antibody. ProLong Gold antifade reagent with DAPI (Life Technologies) was used to mount the stained cells attached on the coverslips and viewed under ×20 objective with an Olympus BX51 microscope.

Quantitative Real-Time Polymerase Chain Reaction: Gene expression (mRNA) levels of rat hepatic stellate cell samples were measured by quantitative real-time reverse transcription-polymerase chain reaction (qRT-PCR) by following our routine lab protocol. The primers used for Real time PCR in 5'to 3' orientations are rat p53 (Forward: GCACGGCCTTTGTGGTAAAA,Reverse: TTTGCCAGGGCTGAGTAACC) ratp21(Forward:TGCCTTAGCCTTCATTCAGTGT,Reverse:TATCGAATTGCACGAG GGGAG).The primers used for Real time PCR in 5'to 3' orientations for LX2 cells are humanGli1(Forward:GGCTCGCCATAGCTACTGAT,Reverse:CCAGCGCCCAGACA GAG),humanGli2(Forward:AGTTAATGAGAACCTGGGCAGT,Reverse:TTGGCAAA GGCGGGATAGTC),humanIHH(Forward:CAGCCTGCTCTCACTACGAG,   Reverse: CCCAAAGGGGCCTAAGATGG),humanPtc(Forward:GGGTGGCACAGTCAAGAAC AG, Reverse: TACCCCTTGAAGTGCTCGTACA). miR21 levels in tissues were measured as described in chapter2.

Western Blotting: Protein extraction and western blot from *in vivo* and *in vitro* samples were performed according to our lab protocol described elsewhere (129). Primary antibodies PTEN, β actin (Abcam, MA), p53 (Cell Signaling Technology, MA), Cyclin E, cleaved caspase3, total caspase3 and cleaved PARP1(Santa cruz Biotechnology, TX) were used at recommended dilutions, and compatible horseradish peroxidase-conjugated secondary antibodies were used.

TUNEL assay: TUNEL based ApopTag® technology (EMD Millipore, MO) was used to detect apoptotic cells according to the manufacturer's instructions. ProLong Gold Antifade Reagent (Life Technologies, Carlsbad, CA) with DAPI was used to mount the coverslips. The cells were imaged using immunofluorescence microscopy under ×20 objective.

Cell cycle analysis: After treating LX2 cells with LPS and/ SsnB (as described previously), the cells harvested and centrifuged for 10 minutes at 1000 rpm at 25°C in the medium. After aspirating the medium, cells were washed with PBS and again centrifuged for 10 minutes at 1000 rpm at 25°C. This step was repeated again and the cells were fixed with 70% ice cold ethanol (dropwise) for 30 minutes on ice. After fixing the cells, they were centrifuged again at 1000rpm for 5 minutes. Ethanol was aspirated and 1 ml of propidium iodide solution (containing RNase A and 0.1%Triton X) was added to the pellets and incubated in ice for 30 minutes on ice. The samples were analyzed by Beckman Coulter FC500 Flow Cytometer at Institutional Resource Facility at the University Of South Carolina School of Medicine.

Statistics: Data were represented as mean ± S.E. Statistical significance was calculated by Student's t test and the graphs were plotted using Origin (OriginLab Corporation, MA). $p \leq 0.05$ was considered statistically significant.

4.3 RESULTS:

SsnB treatment ameliorates liver fibrosis in NASH mice. Picrosirius red stain is widely used to stain extracellular collagen matrix to detect fibrotic scar deposition in tissues. This staining is based on the firm binding of this stain's sulfonic acid groups with the basic moieties of collagen fibers. Histological evaluation of mice liver tissues in NASH group shows increase deposition of collagen matrix and fibrosis compared to Control group. SsnB treated group (NASH+SsnB) showed significant reduction of fibrosis (Figure 4.1A, B). In Control group fibrosis scoring was F_0 (no fibrosis), NASH group the fibrosis grade was F_2 to F_3 (periportal and septal fibrosis). Interestingly, fibrosis scoring in NASH+SsnB group was F_0 to F_1 (no fibrosis to mild fibrosis without septa) (Figure 4.1C).

SsnB treatment decreased microRNA21 expression and upregulated PTEN protein expression in NASH liver. MicroRNA21 (miR21) is known to downregulate tumor suppressor protein PTEN (130). We have previously shown that SsnB administration decreases miR21 expression and induces PTEN expression in an early NASH model where diet induced obese mice were subjected to BDCM treatment for 1 week (19). Interestingly, we observed similar characteristics of SsnB when it was administered in our full-blown NASH model where diet induced obese mice were subjected to BDCM treatment for 4 weeks. We found that, SsnB treatment (NASH+SsnB group) significantly

87

reduces miR21 expression compared to NASH group (Figure 4.2 A). PTEN protein expression was decreased in NASH group compared to Control. However, SsnB treatment (NASH+SsnB) augmented PTEN expression (Figure 4.2 B) which complemented the reduced expression of miR21 in that group.

SsnB treatment induced PTEN expression increases p53, p21 upregulation and decreases hedgehog signaling in liver. To detect the possible mechanism of PTEN induced expression of p53, we measured the immunoreactivity of MDM2 in paraffin embedded liver tissue sections though immunofluorescence microscopy. We observed significantly increased immunoreactivity of MDM2 in NASH liver section compared to Control liver. SsnB treated (NASH+SsnB) liver showed considerable decrease in MDM2 immunoreactivity compared to NASH liver (Figure 4.3A). MDM2 is a known inhibitor of p53. Interestingly, Immunohistochemistry against p53 revealed decreased p53 protein expression in NASH mice liver in the sinusoidal area which was augmented with SsnB treatment (NASH+SsnB) (Figure 4.3B). Immunohistochemistry against p21 also reveals significant decrease in p21 immunoreactivity in NASH liver compared to Control. SsnB treatment significantly increased p21 immunoreactivity in the sinusoidal area of liver in NASH+SsnB group compared to NASH group (Figure 4.3C). Moreover, immunoreactivity against Gli1, a pro-fibrogenic nuclear transcription factor, was significantly increased in NASH liver section compared to Control liver. SsnB treated (NASH+SsnB) liver showed remarkable decrease in Gli1 immunoreactivity compared to NASH liver –as observed by immunofluorescence microscopy (Figure 4.3D).

SsnB treatment decreased p53, p21 expression in vitro. To see whether SsnB can reduce expression of p53 and p21 *in vitro* as it does *in vivo*, we measured gene expression

of p53 and p21 through qRT PCR experiments in primary rat hepatic stellate cells. LPS treatment increased the gene expression of p53 and p21 compared to untreated or control cells. However, SsnB treatment was able to repress LPS induced upregulation of those genes (Figure 4.4A). Immunofluorescence microscopy also revealed increased immunoreactivity of p53 and p21 in SsnB treated primary rat hepatic stellate cells (LPS+SsnB) compared to only LPS treatment (Figure 4.4B, C respectively).

SsnB treatment decreased gene expression of hedgehog signaling markers and reduces Cyclin E protein expression in vitro. To correlate SsnB induced repression of Gli1 (a hedgehog transcription factor) in vivo in an in vitro model, we measured gene expression of hedgehog signaling specific markers through qRT PCR experiments. LPS treatment increased the gene expression of Gli1, Gli2, Indian hedgehog (IHH) and Patched (Ptc) compared to untreated or control cells. However, SsnB treatment was able to repress LPS induced upregulation of those genes (Figure 4.5A). To see whether SsnB upregulation of PTEN, p53, p21 and repression of Gli1 alters proliferation of activated HSCs, we measured Cyclin E protein level from cell homogenates. LPS treatment had increased Cyclin E level compared to Control which decreased upon SsnB treatment (Figure 4.5B).

SsnB treatment decreases proliferation and induces apoptosis in hepatic stellate cells. We performed flow cytometry to evaluate the effect of SsnB on hepatic stellate cell cycle progression. After treating the LX2 cells with vehicle, LPS and/ SsnB for 24 hours (as described previously), the cells were collected and stained with propidium iodide and then analyzed by Beckman Coulter FC500 Flow Cytometer. The resulting data clearly demonstrates that treatment of LX2 cells with SsnB (both 10 and 100μM concentrations)

induced accumulation of cells in G2/M phase (38.14% and 36.75% in SsnB 10μM and 100μM respectively) compared to LPS treated group (27.55%) accompanied by a decreased number of cells in the G0-G1 phase (Figure 4.6 A). We also observed higher number of apoptotic nuclei in SsnB treated cells (LPS+SsnB) (Figure 4.6B). Western blot data clearly reveals increased p53 accumulation, increased cleaved caspase3 and cleaved PARP1 proteins in SsnB treated LX2 cells compared to LPS treated and control cells (Figure 4.6C), further establishing the pro-apoptotic role of SsnB.

4.4 DISCUSSION:

This study shows the anti-fibrotic and anti-proliferative mechanisms of plant derived TLR4 antagonist, Sparstolonin B (SsnB). Mechanistically, SsnB reduces TLR signaling by inhibiting MyD88 recruitment to TLR4 (28). Our initial histochemical data from picrosirius red stained liver slices proved that SsnB prevents NASH induced fibrotic scars. We wanted to explore whether SsnB inhibits fibrosis through inhibiting TLR4 dependent pro-fibrogenic pathways. It is known that TLR4 signaling pathway activation can upregulate miR21 (131) which was reversed by SsnB, a TLR4 antagonist. PTEN (phosphatase and tensin homolog deleted on chromosome ten) is known to be a tumor suppressor. It can also inhibit PI3K/Akt signaling by dephosphorylating phosphatidylInositol (3,4,5) -trisphosphate (PIP3) at position 3 and also known to be involved in cell motility, proliferation, survival, metabolism and cellular architecture. It is known that PTEN can down regulate TLR4 induced pro-inflammatory pathways (132). Micro-RNA 21 is a known inhibitor of PTEN. Our study shows that PTEN expression is augmented in SsnB treated samples where miR21 was also downregulated. This proves that, SsnB can upregulate PTEN expression by inhibiting TLR4 induced miR21

expression in our NASH model. It is known that activated TLR4-PI3K pathway can induce p53 degradation by upregulating MDM2 (133). Recent research shows that senescence induction in fibrogenic cells by increasing p21, p53 can help to reduce excessive fibroblast proliferation and suppress hepatic tumor (134). However, no research has focused on the possible route of repressing hepatic stellate cell proliferation by antagonizing TLR4-PI3K/Akt-MDM2 signaling pathway by SsnB. We found that SsnB, a TLR4 antagonist can possibly affect TLR4-PI3K/Akt signaling by upregulating PTEN protein expression. Our data suggested that SsnB treatment downregulated MDM2 which was otherwise activated in NASH liver. Interestingly, we found that, p53 was upregulated in SsnB treatment, which proves that SsnB induced p53 activation by suppressing MDM2 in a PTEN dependent mechanism (135). We also found upregulated p21 protein expression in SsnB treated liver (NASH+SsnB) compared to NASH liver. It is known that increased p53 induces p21 expression (136) which further supports our findings. Induction of p53 and p21 in fibrotic liver can be instrumental to decrease uncontrolled proliferation of fibroblasts. As uncontrolled HSC (a hepatic fibroblast) proliferation plays a major factor in hepatic fibrogenesis, we wanted to see whether SsnB induced activation of p53, p21 and decreased the proliferation of activated stellate cells. In vitro results showed that SsnB treatment increases mRNA and protein levels of p53 and p21 in HSC which was otherwise repressed by LPS-proving the anti-proliferative effect of SsnB. Hedgehog signaling plays a key role in liver fibrosis and is an important therapeutic target of anti-fibrotic drugs (137). Glioma-associated oncogene homolog1 (Gli1) is a transcription factor which is a downstream target of hedgehog signaling pathway (138). Previous research has shown that increased p53 expression is known to inhibit Gli1

91

(139).We found that SsnB treated mice liver tissue (NASH+SsnB) having upregulated p53 protein expression also had reduced expression of Gli1 compared to NASH mice liver. Activation of hepatic stellate cells (HSC) induces fibrosis in the liver and suppression of Hedgehog signaling in these cells is known to inhibit HSC activation (140).We found that SsnB treatment in HSC culture downregulates LPS induced activation of Hedgehog signal specific gene expression.

Hedgehog signaling pathway is known to induce proliferation by upregulating Cyclin D and Cyclin E. Shh proliferative signaling stimulates or maintain cyclin gene expression and activity of the G1cyclin-Rb axis in proliferating cells (141, 142). Gli1 inhibition is also known to inhibit cell growth and cell cycle progression at G2/M phase and induced apoptosis (143). Several researchers have already shown that SsnB can inhibit angiogenesis and proliferation of cancer cells by inhibiting mitotic cyclins (104, 136). Similarly, our study found that SsnB treatment decreased Cyclin E activation in hepatic stellate cells. We also observed SsnB induced suppression of stellate cell proliferation at G2/M phase of cell cycle and apoptosis of hepatic stellate cells. Apoptosis induction in activated HSCs is one important therapeutic target to decrease HSC proliferation and hepatic fibrosis (144). Anti-apoptotic role of SsnB has previously been shown in different cell types (103). We observed significant number of apoptotic cells in SsnB treated group (LPS+SsnB) compared to untreated cells and LPS treated cells. Inhibition of hepatic stellate cell proliferation can reduce liver fibrosis and is a major therapeutic target of anti-fibrotic drugs (145, 146). Anti-proliferative and pro-apoptotic properties of SsnB make it a potential antifibrotic molecule. As In future, it will be interesting to see therapeutic role of SsnB in other *in vivo* models of liver fibrosis. Apart

from HSCs, portal fibroblasts and mesothelial cells are also known to be precursors of myofibroblasts. Hepatic cholangiocytes and hepatocytes can also acquire phenotype of myofibroblasts through a process of epithelial to mesenchymal transition in the liver (147, 148). It is important to elucidate the cell specific anti-fibrotic mechanisms of SsnB in future studies.

In conclusion, SsnB inhibited liver fibrosis in murine NASH model and in HSC culture by modulating the expression of cell cycle related proteins and by downregulating the Hedgehog signaling pathway. These results suggest that SsnB is a promising compound to attenuate liver fibrogenesis.
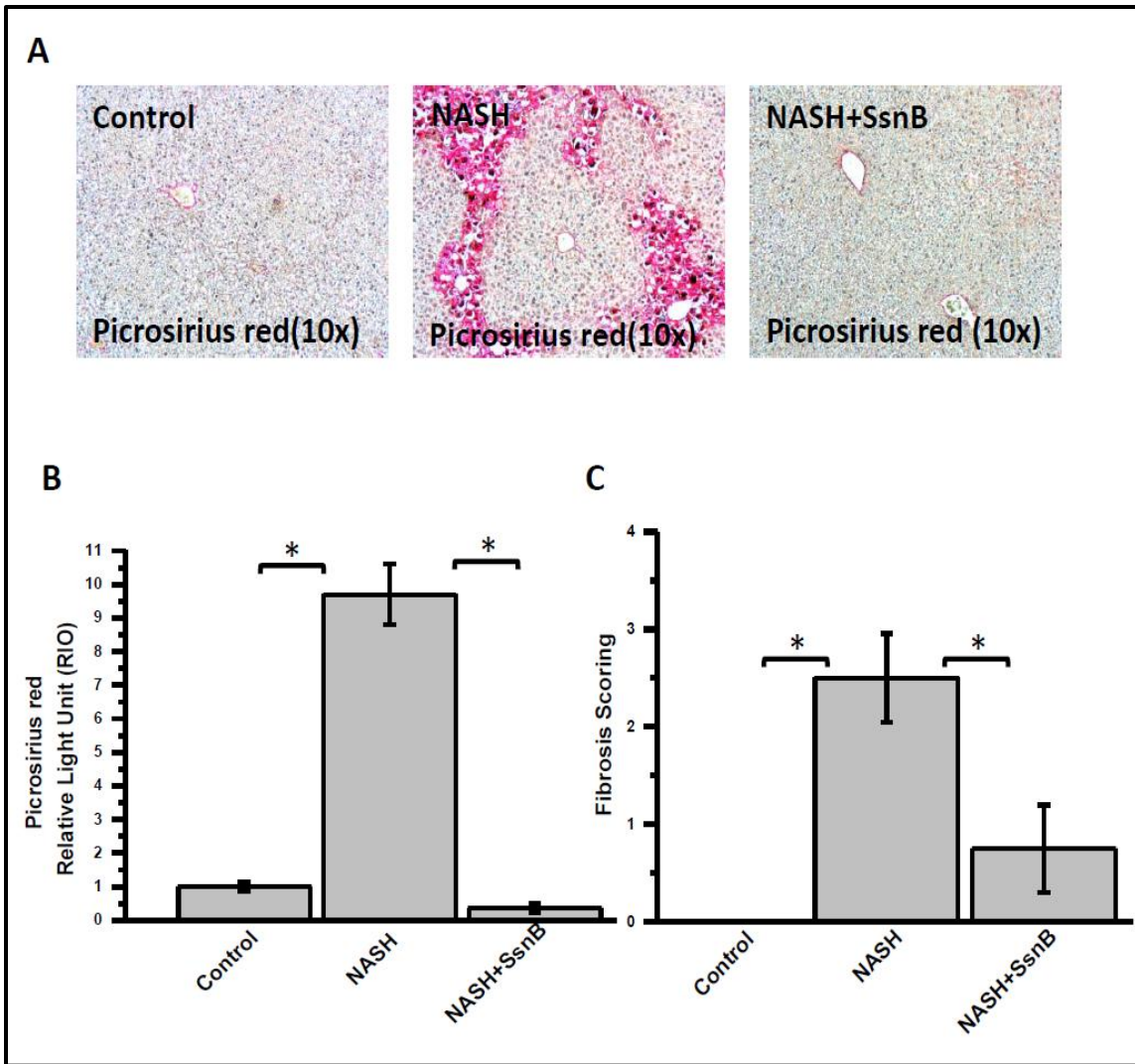
Figure 4.1 SsnB treatment ameliorates liver fibrosis in NASH mice. A: Representative images of picrisirius red stain of Control, NASH and NASH+SsnB mice. Images were taken at ×20 magnification. (*P < 0.05). B: Morphometric analysis of picrosirius red immunohistochemistry in liver slices from Control, NASH and NASH+SsnB mice groups. (*P < 0.05). C: The degree of fibrosis by METAVIR scoring system. (*p<0.05).
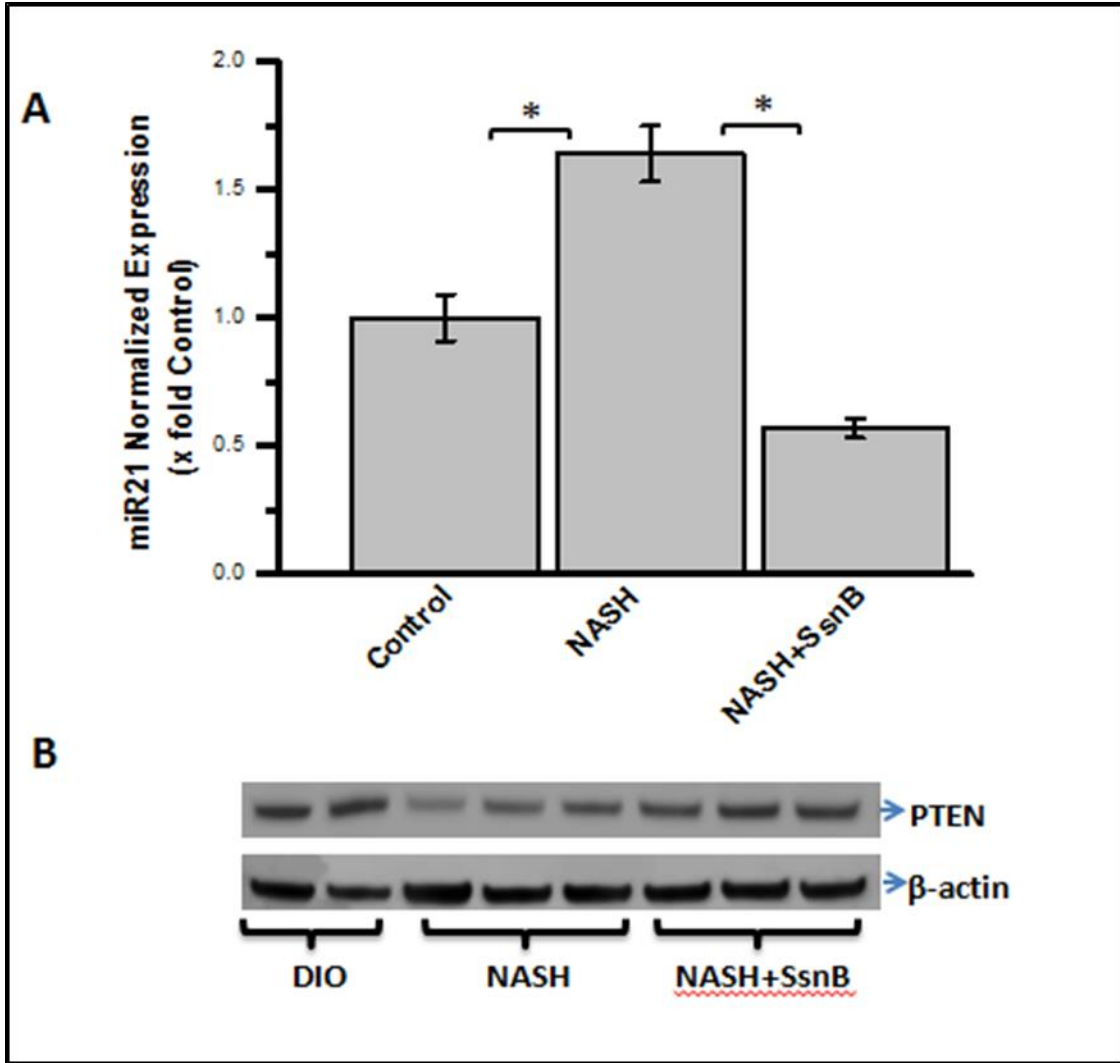
Figure 4.2 SsnB treatment decreased microRNA21 expression and upregulated PTEN protein expression in NASH liver. A: qRT-PCR analysis of miR21 expression of Control, NASH, and NASH+SsnB mouse liver samples normalized against Control (*P < 0.05). B: Western blot analysis of β-actin and PTEN protein levels of Control, NASH, and NASH+SsnB liver homogenates.
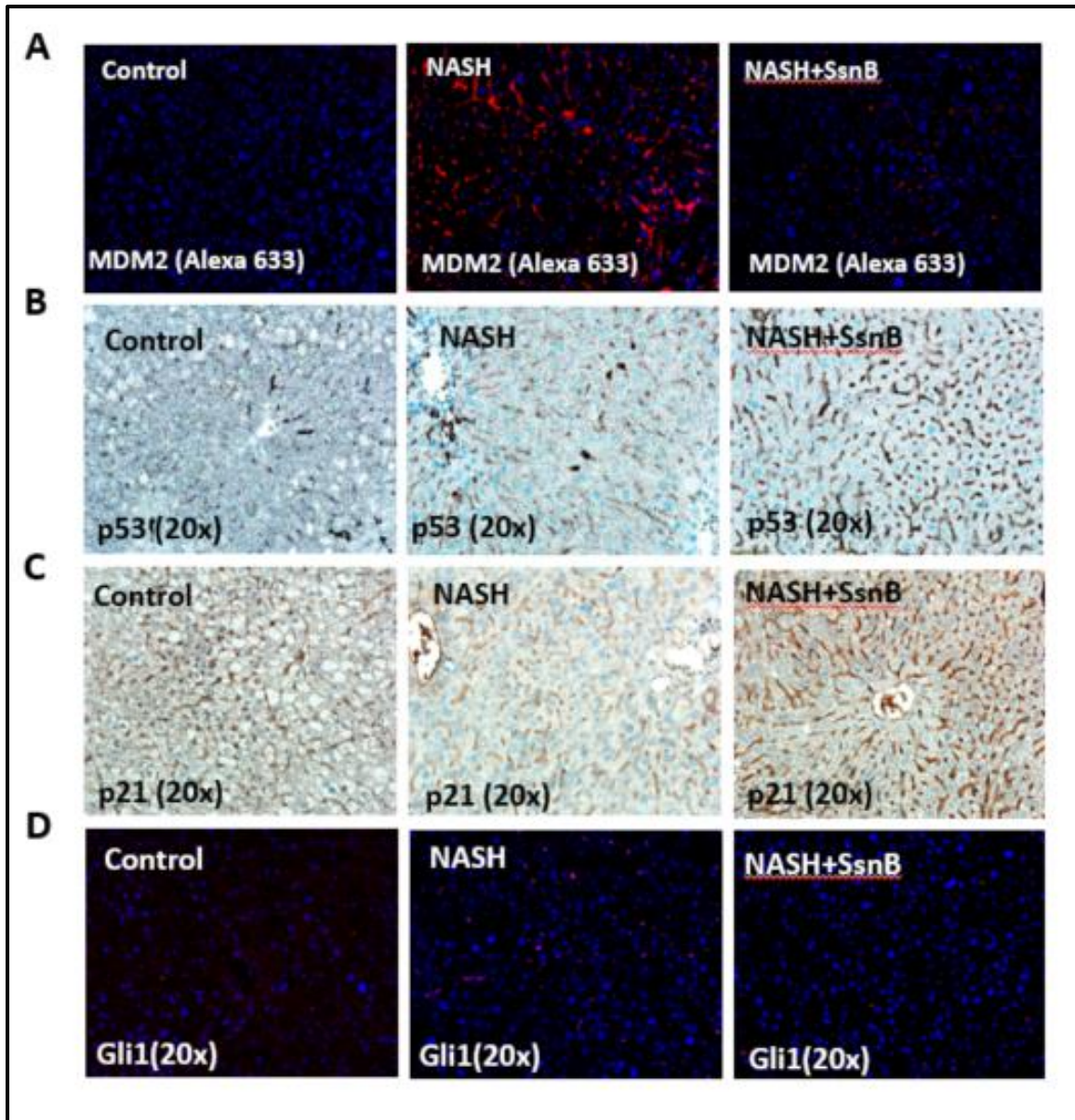
Figure 4.3 SsnB treatment induced PTEN expression increases p53, p21 upregulation and decreases hedgehog signaling in liver. A: Representative images of MDM2 immunoreactivity as shown by immunofluorescence microscopy on liver slices of Control, NASH and NASH+SsnB mice, taken at ×20 magnification using immunofluorescence microscopy. B: Representative images of p53 immunoreactivity as shown by immunohistochemistry on liver slices of Control, NASH and NASH+SsnB mice, taken at ×20 magnification. C: Representative images of p21 immunohistochemistry on liver slices of Control, NASH and NASH+SsnB mice, taken at ×20 magnification. D: Representative images of Gli1 immunoreactivity as shown by immunofluorescence microscopy on liver slices of Control, NASH and NASH+SsnB mice, taken at ×20 magnification using immunofluorescence microscopy.

96
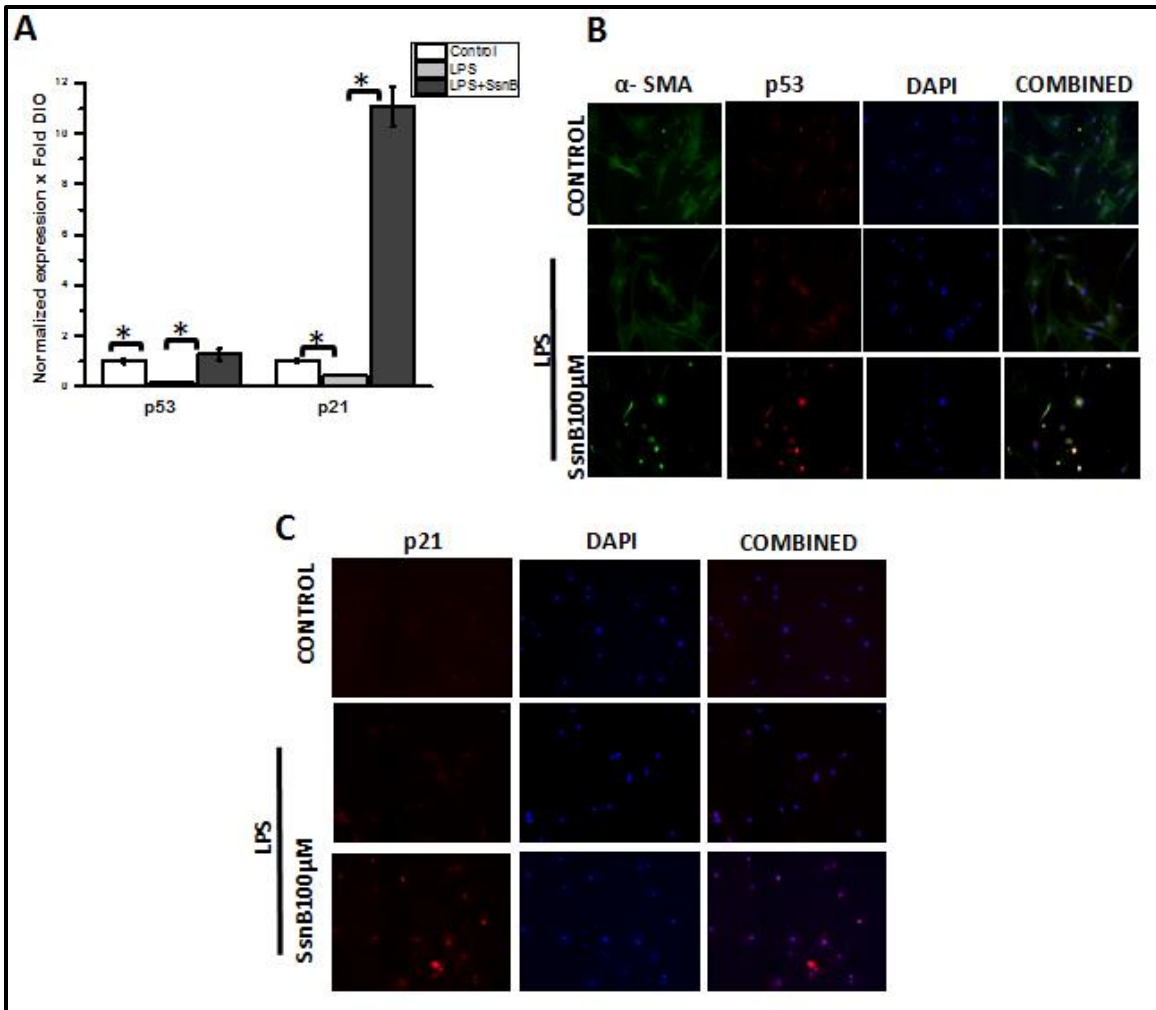
Figure 4.4 SsnB treatment decreased p53, p21 expression in vitro. A: qRT-PCR analysis of mRNA expression of p53 and p21 from control (untreated), LPS-treated, and LPS+SsnB(100μM) treated rat primary hepatic stellate cells, normalized against control (*P < 0.05). B. Immunofluorescence dual labeling of Control (untreated), LPS-treated, and LPS+SsnB(100μM) treated rat primary hepatic stellate cells depicting α-SMA(green)-p53 (red) co-localization (yellow), taken at ×20 magnification. C. Immunoreactivity of p21 (red) in control (untreated), LPS-treated, and LPS+SsnB(100μM) treated rat primary hepatic stellate as shown by immunofluorescence microscopy at ×20 magnification.
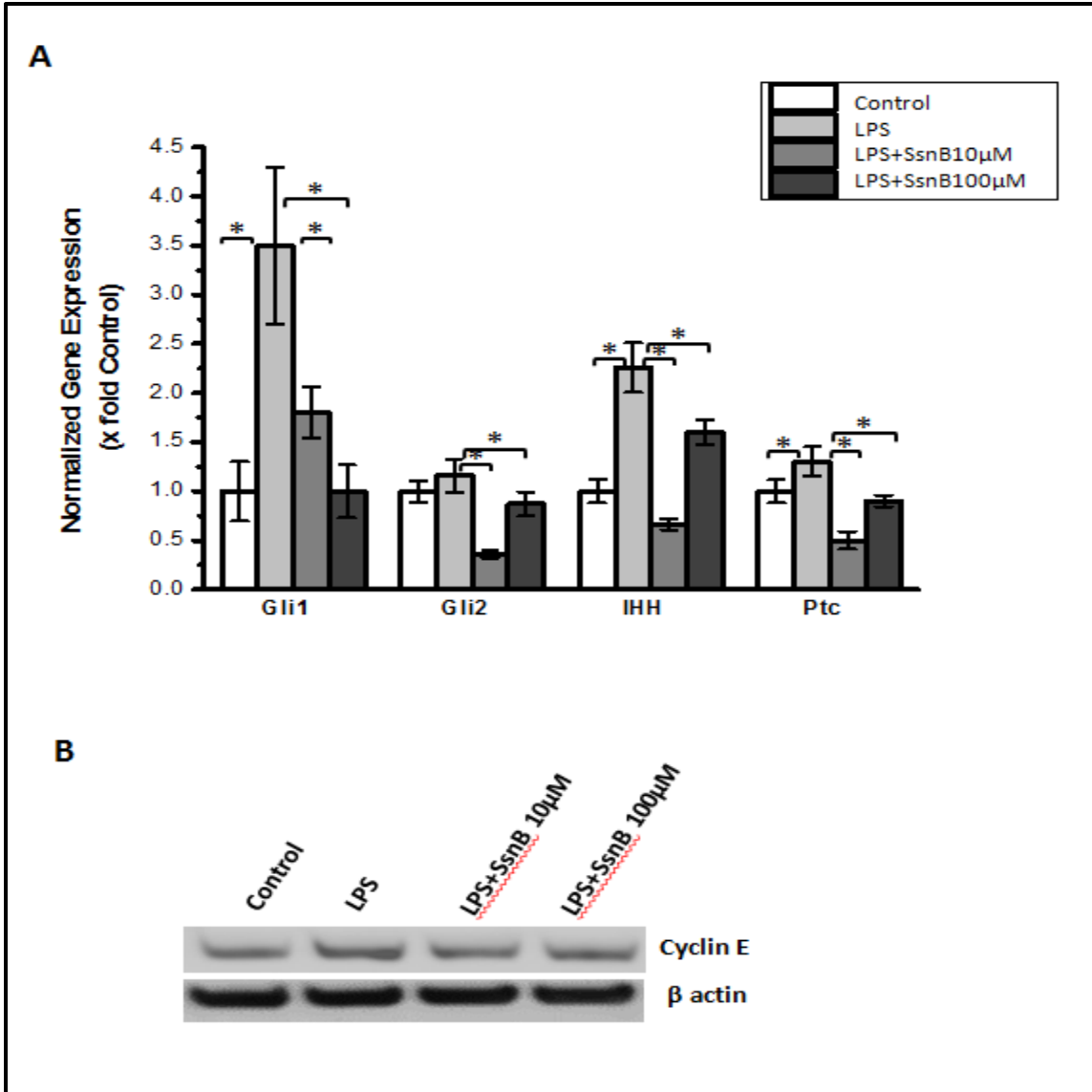
Figure 4.5 SsnB treatment decreased gene expression of hedgehog signaling markers and reduces Cyclin E protein expression in vitro. A: qRT-PCR analysis of mRNA expression of Gli1, Gli2, IHH, Ptc from Control (untreated), LPS-treated, and LPS+SsnB(10μM /100μM) treated human immortalized hepatic stellate cells (LX2), normalized against control (*$P < 0.05$). B: Western blot analysis of Cyclin E and β-actin protein levels of Control (untreated), LPS-treated, and LPS+SsnB(100μM) treated human immortalized hepatic stellate cells (LX2).
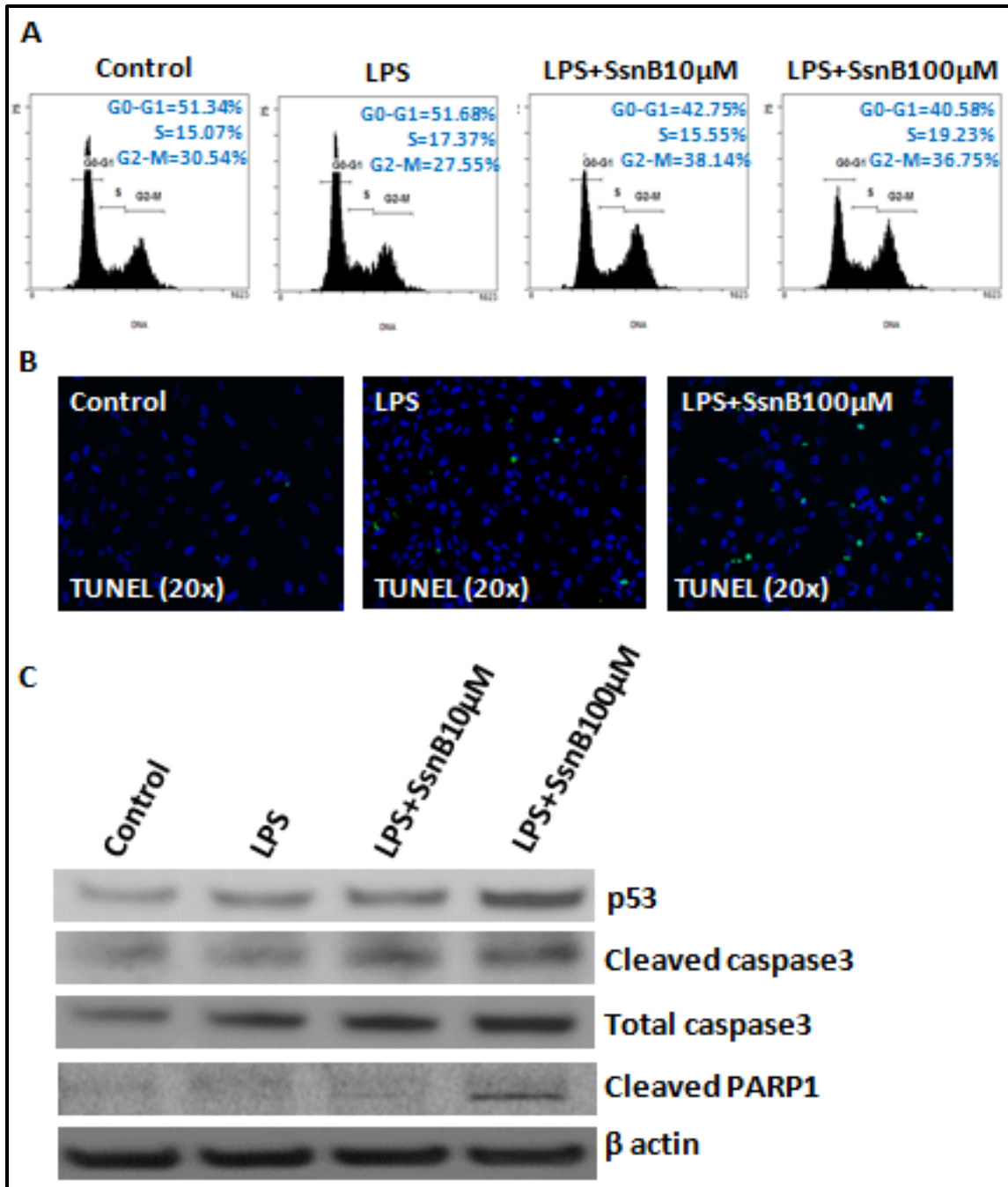
Figure 4.6 SsnB treatment decreases proliferation and induces apoptosis in hepatic stellate cells. A: Cell cycle analysis of untreated cells (control), cells treated with LPS and LPS+SsnB (10/100µM) Quantitation of the PI staining data is presented as the cell cycle distribution percentages. B: Apoptosis is indicated by TUNEL based ApopTag® technology (EMD Millipore, MO) which labels 3'-OH ends of DNA fragments by fluorescent antibody as detected by immunofluorescence microscopy in Control (untreated), LPS-treated, and LPS+SsnB(100µM) treated LX2 cells. C: Western blot analysis of p53,cleaved caspase3, total caspase3, cleaved PARP1 and β-actin protein levels of Control (untreated), LPS-treated, and LPS+SsnB(10/100µM) treated LX2 cells.

CHAPTER 5

ADMINISTRATION OF SPARSTOLONIN B ATTENUATES HEPATIC

FIBROSIS BY INHIBITING TGFβ SIGNALING, STAT3 ACTIVATION

AND BY MODULATING HEPATIC STELLATE CELL MORPHOLOGY

IN NASH.[4]

---

[4] Dattaroy D, Chandrashekaran V, Seth RK, Alhasson F, Fan D, Nagarkatti M, Nagarkatti Chatterjee S. To be submitted to Journal of Pharmacology and Experimental Therapeutics.

Abstract:

Chronic hepatic inflammation can induce hepatic fibrosis and anti-fibrotic drug discovery is one of the major focuses to treat the pathogenesis of nonalcoholic steatohepatitis (NASH). We have previously shown that TLR4 activation increases inflammation and fibrosis in NASH. We have also observed anti-fibrotic and anti-proliferative activity of Sparstolonin B (SsnB). By using Bromodichloromethane (BDCM) induced model of NASH and a preventive model where mice having NASH were treated with SsnB, we aim to explore an alternative molecular mechanism through which SsnB can decrease fibrosis by antagonizing TLR4 induced TGFβ signaling pathway. Mechanistically, SsnB augmented BAMBI (a TGFβ pseudo-receptor) expression in mice liver by inhibiting TLR4 signaling pathway and thus reduced TGFβ signaling, resulting in decreased hepatic stellate cell activation and extracellular matrix deposition. In vitro experiments on hepatic stellate cells showed that SsnB increased gene and protein expression of BAMBI. It also decreased nuclear co-localization of phospho SMAD2/3 and SMAD4 protein and thus attenuated TGFβ signaling in vitro. We also observed a significant decrease in phosphorylation of SMAD2/3 protein, decreased STAT3 activation, alteration of focal adhesion protein and stress fiber disassembly upon SsnB administration in hepatic stellate cells which further confirms the antagonistic effect of SsnB on fibrogenesis.

5.1 INTRODUCTION:

Nonalcoholic steatohepatitis (NASH) is a significant cause of mortality as it can cause liver fibrosis, cirrhosis, portal hypertension, and hepatocellular carcinoma (149-151). During NASH associated chronic liver inflammation, activated hepatic stellate cells (HSCs) deposits excessive extracellular matrix proteins in the liver resulting in fibrotic scars (152). However, there is no therapy available to treat liver fibrosis in the patients with NASH except some life style modifications (153). Thus it is important to understand the molecular mechanisms of hepatic fibrosis to design therapeutic strategies to prevent and treat liver fibrosis. Different inflammatory signaling pathways are pivotal mediators of liver fibrogenesis and control the transition of quiescent hepatic stellate cells (HSC) to collagen-secreting myofibroblasts (154). Systemic levels of endotoxins have been detected in patients with liver cirrhosis (lipopolysaccharide, LPS) (155). Systemic endotoxins can be recognized by Toll like receptor 4 (TLR4) present in hepatocytes, kupffer cells, stellate cells, sinusoidal endothelial cells, biliary epithelial cells in the liver (156). Upon detecting the LPS or pathogen associated molecular patterns (PAMPS), the TLR4 receptors give rise to a myriad of inflammatory signaling pathways and increase the production of inflammatory cytokines, induce macrophage infiltration and increase oxidative stress (156-158). Recent studies have indicated that tissue injury and matrix degradation can release some endogenous ligands also referred to as damaged associated molecular patterns (DAMPS) which can activate TLR4 signaling. Injured liver has augmented expression of TLR4 and its co-receptors which makes it more sensitive to the cascade of inflammatory cell signaling pathway mediated by TLR4 signaling in the damaged tissue (27). Induced TLR4 signaling can give rise to different downstream

factors like pro-inflammatory cytokines, chemotactic cytokines, reactive oxygen species (ROS), adhesion molecules, cell cycle regulating proteins, TGF-β1 pseudoreceptor BAMBI-which can give rise to pro-fibrogenic signals. Hepatic stellate cells along with kupffer cells, may be a target for TLR4 ligand induced liver injury and offer a direct connection between inflammatory and fibrotic liver damage (27). In our Bromodichloromethane (BDCM) induced model of NASH, we have previously shown that, activation of NADPH oxidase induces Toll like receptor 4 (TLR4) recruitment to the lipid rafts and thus potentiates inflammation (24). We have also shown that environmentally relevant doses of Bromodichloromethane (BDCM), induces fibrogenesis by a NADPH oxidase dependent pathway which increases microRNA21 activation, hepatic stellate cell activation and accelerates TGFβ signaling (20).

Our collaborators have characterized a plant derived compound Sparstolonin B (SsnB) as a TLR4 antagonist. SsnB has also been shown to have anti-inflammatory, anti-angiogenic, anti-proliferative and anti-oxidant properties (99, 102-104). We have already shown that SsnB decreases oxidative stress, kupffer cell activation, cytokine production and macrophage infiltration in an early model of NASH (19).

In this study we test the hypothesis that administration of SsnB in NASH, abrogates TGFβ signaling and fibrogenesis by upregulating BAMBI in hepatic stellate cells. As TGFβ signaling activation can also induce JAK-STAT pathway and upregulates stress fiber assembly in myofibroblasts, we investigated the role of SsnB in alteration of those pathways (159, 160). In this study, we used a rodent model of NASH in Bromodichloromethane induced oxidative stress, lipotoxicity, and inflammation were used as "second/multiple hits" to cause NASH. We also used rat primary hepatic stellate

103

cells and human transformed hepatic stellate cells (LX2) as our in vitro models. Our data shows that SsnB can decrease myofibroblast proliferation through modulating multiple signaling pathways.

5.2 MATERIALS AND METHODS:

Cell culture: Human immortalized stellate cell line (LX2) and rat primary hepatic stellate cells were cultured as described in the previous chapter.

Mouse Models: Pathogen-free, male mice with C57BL/6J background were treated as described in the previous chapter.

Laboratory analysis

Immunohistochemistry: Immunohistochemistry on formalin-fixed, paraffin embedded liver tissue sections (5-μm-thick) was performed as described in the previous chapter. Antibodies against fibronectin, BAMBI (Abcam, MA) were used in recommended dilution. Morphometric analysis of the immunoreactivity of tissue sections was performed using cellSens software (Olympus).

Immunofluorescence

In vivo: Formalin-fixed; paraffin embedded liver tissue sections (5-μm-thick) were processed as mentioned in the previous chapter. The primary antibodies against SMAD4 (Santa cruz Biotechnology, TX), SMAD2/3, αSMA (Abcam, MA) were used in recommended dilutions. Species-specific secondary antibodies conjugated with Alexa Fluor 488 (Invitrogen, CA) were used against α-SMA and SMAD4 antibodies and secondary antibody conjugated with Alexa Fluor 633 was used against SMAD2/3 in

recommended dilutions. Rest of the experiments was performed as described elsewhere (17).

In vitro: Cells were incubated with p-SMAD2/3 (Abcam, MA) and SMAD4 (Santa cruz Biotechnology, TX) primary antibodies followed by species-specific Alexa Fluor 633 and 488 (described above), for immunofluorescence dual-labeling staining. Alexa Fluor 633 was used against anti-p-SMAD2/3 antibody. Alexa Fluor 488 was used against anti-SMAD4 antibody. Paxillin, αSMA and vinculin primary antibodies (Santa Cruz biotechnology, Inc. Santa Cruz, CA) were used in 1:250 dilutions. Species specific alexa Fluor 488 was used against αSMA antibody.Species specific alexa Fluor 633 was used against αSMA antibody. Rest of the experiment was performed as described in the previous chapter.

Quantitative real-time polymerase chain reaction: Gene expression (mRNA) levels from mice liver tissue and hepatic stellate cell samples were measured by quantitative real-time reverse transcription-polymerase chain reaction (qRT-PCR) as described in previous chapter. The primers used for real time PCR in 5'to 3' orientations are rat BAMBI (Forward: GCGGGGCGTCAATGGATCGC, Reverse: GAACTCAGAAGGCCTTCAAGG).

Western blot: Western blot from in vivo and in vitro samples were performed according to our previous publication (18). Primary antibodies BAMBI, β actin, αSMA, CTGF (Abcam, MA), phospho SMAD2/4, total SMAD2/3 (Cell Signaling Technology, MA), phospho STAT3 (Santa Cruz biotechnology, Inc. Santa Cruz, CA) were used at

recommended dilutions, and compatible horseradish peroxidase-conjugated secondary antibodies were used.

Statistics: As described previously.

5.3 RESULTS:

SsnB treatment decreases hepatic stellate cell activation in murine NASH: Hepatic stellate cells reside in the sinusoidal endothelium space of the liver and play a key role to induce fibrosis in the liver. Upon activation in NASH, the quiescent hepatic stellate cells transform into fibrogenic myofibroblasts and produce alpha smooth muscle actin protein (αSMA). αSMA is a reliable marker to detect hepatic stellate cell activation in the liver. We have already shown in the previous chapter that SsnB administration ameliorates fibrotic scars in NASH liver. Our immunofluorescence data showed that SsnB administration significantly decreased αSMA expression compared to NASH mouse liver (Figure 5.1 A, B).

SsnB treatment in NASH mice upregulates BAMBI in liver: Studies have shown than TLR4 signaling activation can induce increased hepatic fibrosis by downregulating TGFβ pseudo receptor BAMBI. BAMBI is TGF-β type I receptor lacking an intracellular kinase domain. So it blocks signal transduction even after stimulation with TGF-beta superfamily ligands (161-163). Interestingly, immunohistochemistry of BAMBI on mouse liver sections showed that, BAMBI immunoreactivity was significantly decreased in NASH group compared to the Control group. However, NASH mice treated with SsnB (NASH+SsnB group) showed considerably increased immunoreactivity of BAMBI compared to NASH liver tissues (Figure 5.2 A, B).

SsnB treatment decreases fibronectin deposition in NASH liver: Fibronectin is an extracellular matrix (ECM) protein and its expression is stimulated by TGFβ signaling pathway (164). It is also known to play an important role in liver fibrosis (20). Interestingly, immunohistochemistry of fibronectin on mouse liver sections showed that, fibronectin immunoreactivity was significantly increased in NASH group in the sinusoidal area compared to the Control group. However, NASH mice treated with SsnB (NASH+SsnB group) showed considerably decreased immunoreactivity of fibronectin compared to NASH liver tissues (Figure 5.3A, B).

SsnB upregulates BAMBI and decreases TGFβ signaling in vitro: Upon activated by TGFβ ligands and PAMPS, quiescent hepatic stellate cells (HSC) become profibrogenic myofibroblasts and are primarily responsible to induce hepatic fibrogenesis in NASH by producing excessive extracellular matrix proteins (165, 166). Interestingly, our in vitro data from rat primary hepatic stellate cells show that LPS treatment decreases BAMBI mRNA and protein expression compared to untreated or control cells. However, LPS+SsnB treated cells augmented BAMBI mRNA and protein expression compared to only LPS treated cells (Figure.5.4 A, B). SsnB treatment also decreased SMAD2/3, SMAD4 co-localization compared to only LPS treated LX2 cells (transformed human hepatic stellate cells) (Figure.5.4 C). Phosphorylation of SMAD2/3 protein was also decreased upon SsnB treatment compared to the LPS treated cells (Figure.5.4 D).

SsnB downregulates STAT3 phosphorylation, decreases stellate cell activation and connective tissue growth factor in vitro: STAT3 inhibition is known to suppress hepatic stellate cell mediated fibrogenesis (167). STAT3 also cooperates with TGFβ1 in activation and anti-apoptosis of hepatic stellate cells (168). TGFβ is also known to

107

activate JAK1-STAT3 axis to augment liver fibrosis in coordination of SMAD mediated signaling pathway (159). We wanted to see whether SsnB modulates STAT3 activation in LX2 cells. Western blot experiment showed that SsnB treatment decreases STAT3 phosphorylation, αSMA and CTGF protein expression compared to LPS treated LX2 cells (Figure.5.5).

SsnB treatment decreases focal adhesion associated adaptor protein expression and inhibits stress fiber formation in vitro: Paxillin is a multi-domain focal-adhesion adaptor protein located at the edge between the plasma membrane and cytoskeleton. It helps in the process of cell adhesion and acts as a scaffold to bind many signaling proteins to the cell membrane (169). Immunofluorescent imaging of paxillin (Figure 5.6 A, B) shows that Control and LPS stimulated LX2 cells displayed heterogeneous adhesions which are large and elongated at the periphery of the cells. However, SsnB treatment on LX2 cells significantly decreases paxillin immunoreactivity at the periphery. The focal adhesion regions in SsnB treated cells are smaller than Control or LPS treated cells. While lower concentration of SsnB (10µM) decreased paxillin expression at the periphery of LX2 cells, higher concentration of SsnB further abrogated this focal adhesion adaptor protein expression and altered the cell morphology (Figure 5.6A,B). Maturation of focal adhesions fuels the assemblage of adhesion-associated actin bundles known as radial stress fibers (170). We have already seen in Figure5.5 that LPS treatment in LX2 cells increased αSMA protein expression compared to untreated or control cells. SsnB treatment decreased αSMA protein expression in LPS stimulated LX2 cells. In Figure 5.6C, immunofluorescent staining of αSMA specifically depicts the stress fiber morphology on LX2 cells. We observed that, SsnB treatment bocks the stress fiber

108

formation compared to LPS treated cells as indicated by immunoreactivity of αSMA (red) and vinculin (green). The cell morphology also changed upon SsnB treatment. They have smaller cell body, extended cell processes and they also lose stress fibers-similar to the quiescent stellate cells (171).

.5.4 DISCUSSION:

Intestinal microflora and a functional TLR4 (but not TLR2) are essential for hepatic fibrogenesis. TLR4 activation can induce hepatic stellate cell proliferation and extracellular matrix deposition in the liver, resulting in liver scarring in chronic liver diseases. Increased TLR4 signaling in hepatic stellate cells induces chemokine secretion and chemotaxis of macrophages but downregulates TGFβ pseudoreceptor bone morphogenetic protein and activin membrane bound inhibitor (BAMBI) and thus sensitizes the HSCs to TGFβ induced activation and myofibroblastic differentiation (161). We observed that SsnB treatment decreased hepatic stellate cell activation in vivo as indicated by αSMA immunoreactivity. TLR4 activation induces NF-κBp50:HDAC1 interaction which represses transcription of BAMBI promoter (163). BAMBI is TGFβ type I receptor lacking an intracellular kinase domain. It blocks signal transduction even after stimulation with TGFβ superfamily ligands. Thus, decrease of BAMBI on hepatic stellate cells can increase TGFβ signaling and fibrogenesis (161, 163). As abrogation of TLR4 signaling induces BAMBI mediated inhibition of pro-fibrogenic TGFβ signaling pathway, a TLR4 antagonist like SsnB have the potency to decrease TLR4 mediated hepatic fibrosis. Here we found that SsnB treated NASH mice had upregulated BAMBI expression in liver which corresponds to decreased fibrogenesis. Fibronectin, a multifunctional glycoprotein and extracellular matrix (ECM) component is produced by

hepatic stellate cells and is required to support other extracellular matrix protein assembly (65, 172). We have previously shown that, BDCM induced TGFβ signaling induces fibronectin protein expression in the NASH liver (20). Here we have observed that SsnB induced decreased stellate cell activation and TGFβ signaling through BAMBI upregulation which resulted in decreased fibronectin expression. From the histological data of picrosirius red stained liver slices in the previous chapter, we saw that SsnB treatment significantly decreased fibrotic scar deposition compared to NASH liver. Decreased fibronectin deposition upon SsnB treatment might be responsible in decreased collagen matrix accumulation in the liver. As hepatic stellate cells are the major fibrogenic cells in the liver, we wanted to see if SsnB mediated repression of TGFβ signaling by BAMBI upregulation is stellate cell dependent. Interestingly, we found that SsnB upregulates BAMBI in vitro. TGFβ signals by binding to TGFβRI an TGFβRII transmembrane proteins, each having serine/threonine kinase Ligand binding to this receptor protein complex, phosphorylates and activates TGFβRI by the cytoplasmic kinase domains of TGFβRII Activated TGFβRI phosphorylates SMAD2 and SMAD3 which can form a complex with SMAD4 and assemble in the nucleus to initiate target gene expression in a SMAD dependent pathway (173). We found that SsnB decreased LPS induced TGFβ signaling by decreasing SMAD2/3 phosphorylation. SsnB induced reduction of TGFβ signaling was further confirmed by decreased co-localization of SMAD4 and phosphorylated SMAD2/3 in the nucleus in vitro. TGFβRI can also signal through non-SMAD pathways (174). It has been recently discovered that activated TGFβ signaling can also phosphorylate STAT3 and thus activates JAK1-STAT3 axis in coordination with SMAD pathway to induce TGFβ mediated fibrotic response in hepatic

stellate cells (159). Our in vitro data shows that SsnB decreased STAT3 phosphorylation in hepatic stellate cells and also downregulates αSMA and CTGF (connective tissue growth factor) protein levels. Both of these proteins are key players in fibrotic proliferation of myofibroblasts and are downstream mediators of TGFβ signaling (175). SsnB mediated downregulation of both αSMA and CTGF in hepatic stellate cells can be instrumental to decrease pro-fibrogenic cell proliferation. It is known that phosphorylated STAT3 localization to the focal adhesions increases the aggressive clinical behavior of proliferative cells. STAT3 is known to be required for cell motility (176). Focal adhesion plays an important role in liver fibrosis through activating hepatic stellate cells and induces TGFβ driven pro-fibrotic responses (144). αSMA is vital for focal adhesion maturation in myofibroblasts Activated myofibroblasts incorporate αSMA in stress fibers. αSMA has been found to decrease the intracellular mechanical stress on focal adhesions and induces their supermaturation (177).We found that, SsnB treatment changes the cell morphology of hepatic stellate cells. SsnB (100μM) treated LX2 cells became smaller, possessed less stress fibers and acquired a dendritic morphology. SsnB also induced αSMA filament disassembly and abolished focal adhesions. Inhibition focal adhesions and stress fibers of hepatic stellate cells by higher concentrations of SsnB can be crucial to inhibit stellate cell migration and it can also stop the stellate cells from acquiring a fibrogenic phenotype.

To our knowledge, this is the first study reported to show the effects of SsnB on suppression of hepatic fibrogenesis through downregulation of a myriad of cell signaling pathways. In future, due to the strong anti-angiogenic and anti-proliferative properties of

SsnB, it will be interesting test the therapeutic effect of SsnB to improve the

pathophysiological conditions in liver cancer and other fibrotic diseases.
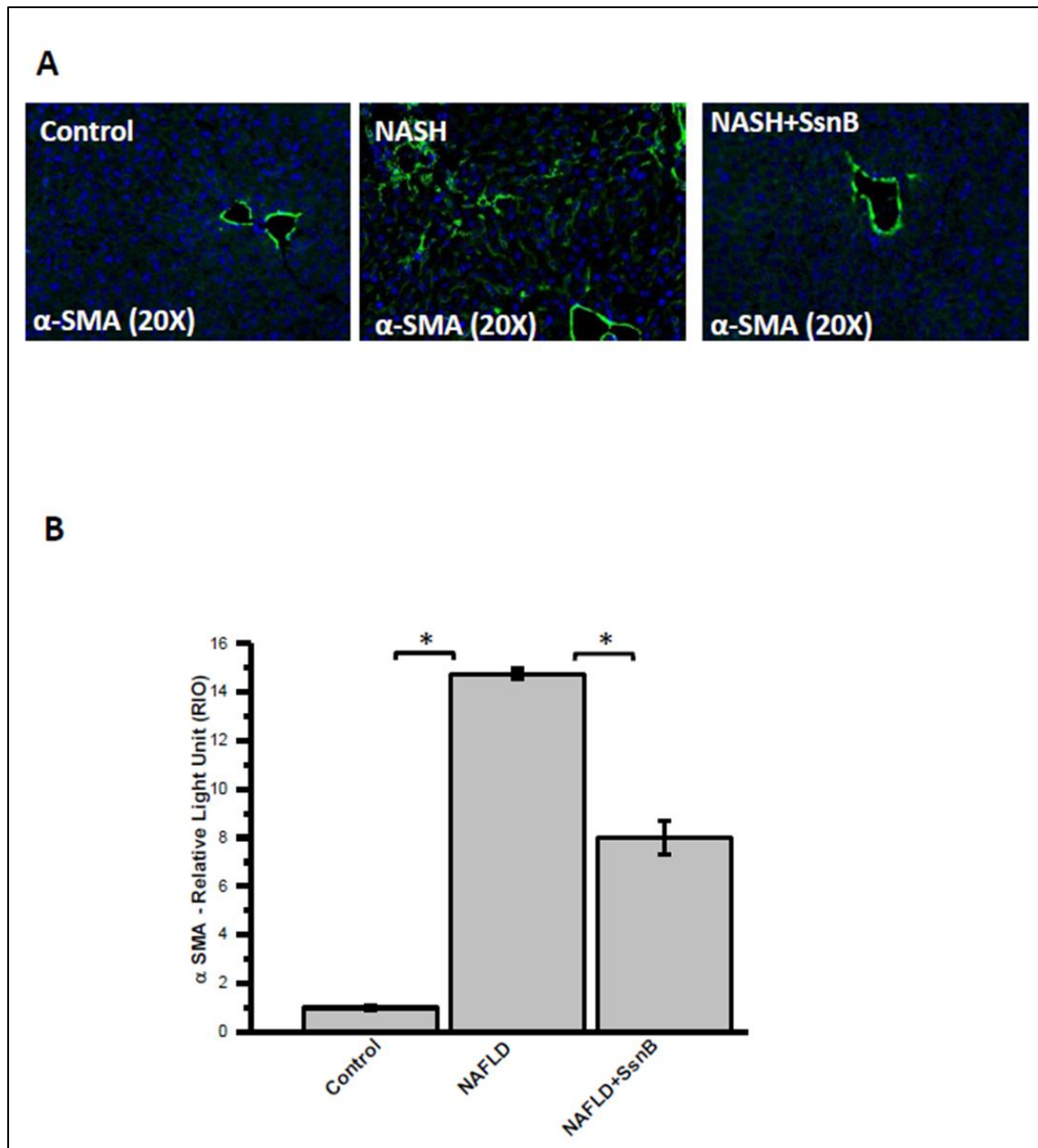
Figure 5.1 SsnB treatment decreases hepatic stellate cell activation in murine NASH. A: Representative images of αSMA immunoreactivity as shown by immunofluorescence microscopy on liver slices of Control, NASH and NASH+SsnB mice, taken at ×20 magnification using immunofluorescence microscopy. B: Morphometric analysis of αSMA immunoreactivity in A. (*P < 0.05).
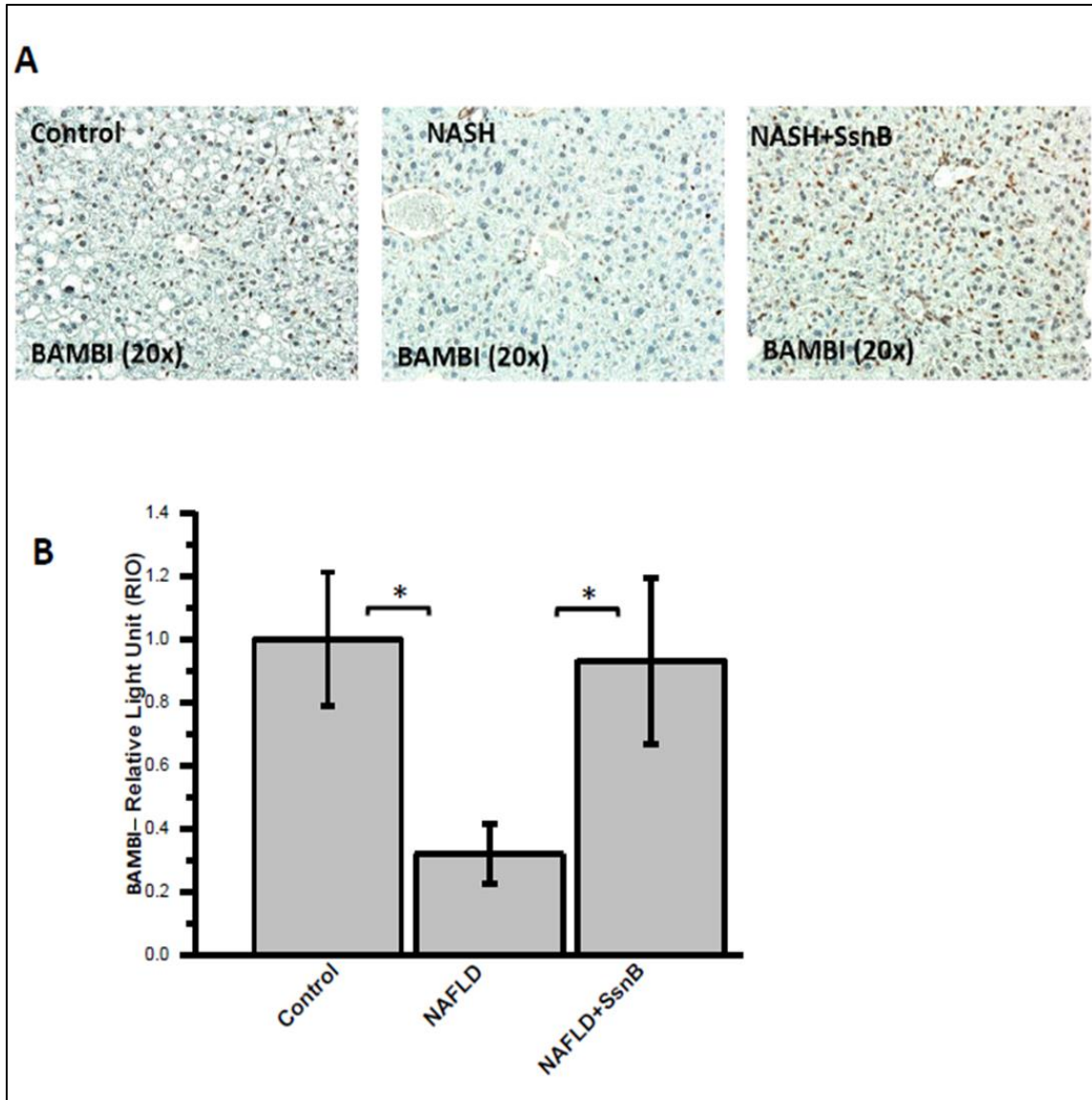
Figure 5.2 SsnB treatment in NASH mice upregulates BAMBI in liver. A: Representative images of BAMBI immunoreactivity as shown by immunohistochemistry on liver slices of Control, NASH and NASH+SsnB mice, taken at ×20 magnification. B: Morphometric analysis of BAMBI immunoreactivity in A. (*P < 0.05).
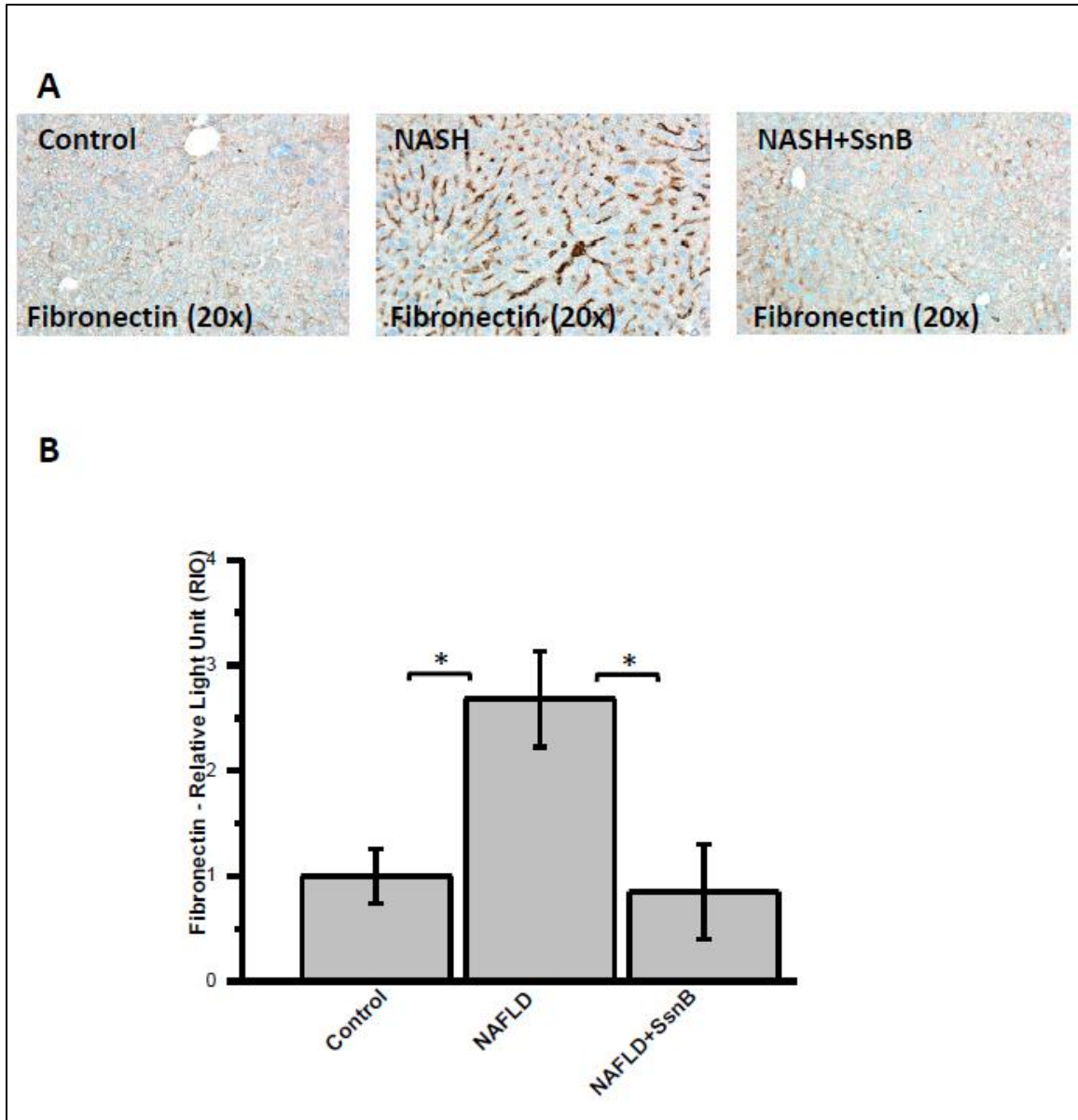
Figure 5.3 SsnB treatment decreases fibronectin deposition in NASH liver. A: Representative images of fibronectin immunoreactivity as shown by immunohistochemistry on liver slices of Control, NASH and NASH+SsnB mice, taken at ×20 magnification. B: Morphometric analysis of fibronectin immunoreactivity in A. (*P < 0.05).
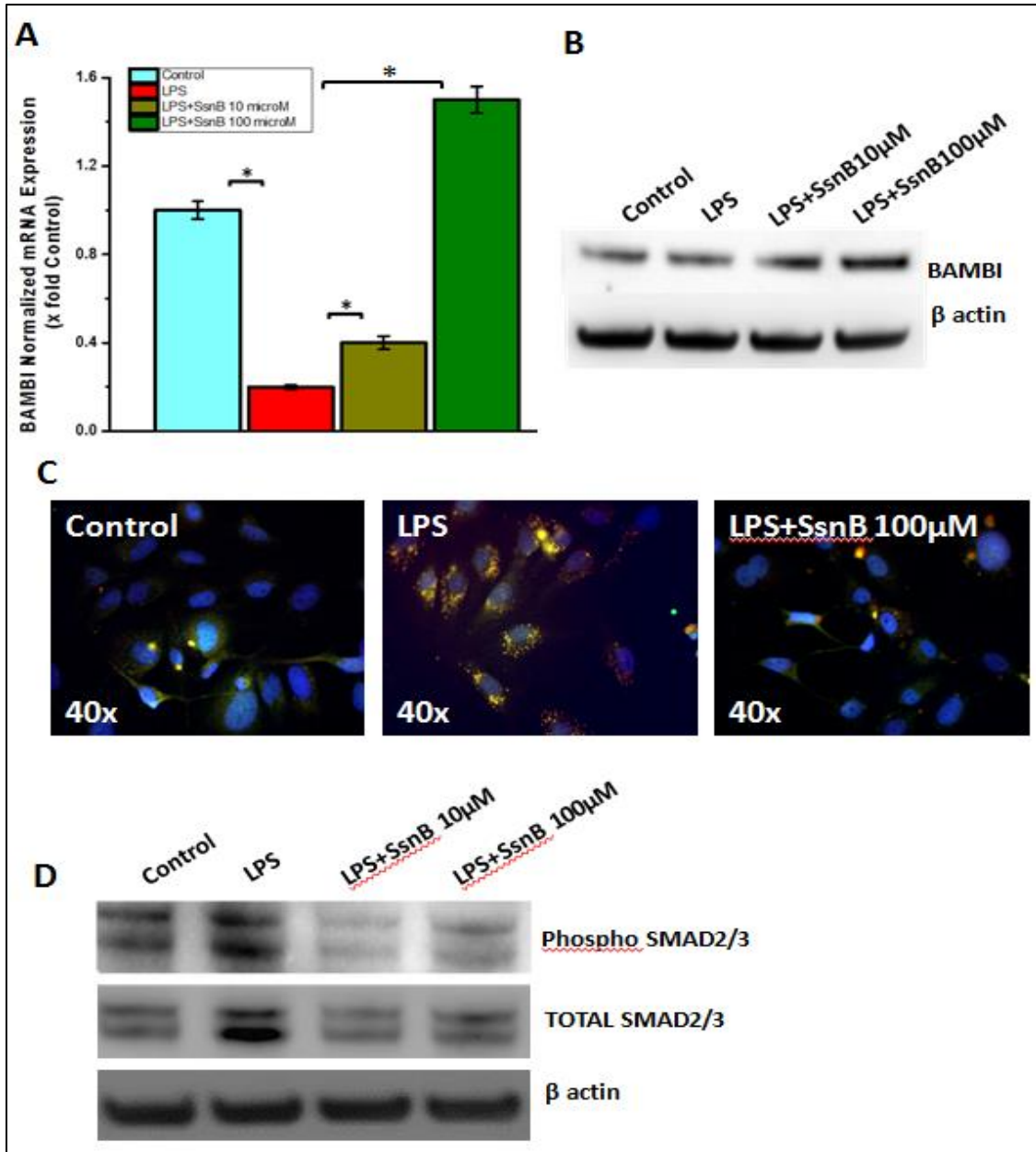
Figure 5.4 SsnB upregulates BAMBI and decreases TGFβ signaling in vitro. A: qRT-PCR analysis of mRNA expression of BAMBI from control (untreated), LPS-treated, and LPS+SsnB treated rat primary hepatic stellate cells, normalized against control (*P < 0.05). B. Western blot analysis of β-actin and BAMBI protein levels of Control (untreated), LPS-treated, and LPS+SsnB treated rat primary hepatic stellate cells. C. Immunofluorescence dual labeling depicting SMAD2/3 (red)-SMAD4 (green) co-localization (yellow) on Control (untreated), LPS-treated, and LPS+SsnB treated human immortalized hepatic stellate cells (LX2) taken at ×40 magnification. D. Western blot analysis of phospho SMAD2/3, total SMAD2/3 and β actin protein levels of Control (untreated), LPS-treated, and LPS+SsnB (10/100µM) treated human immortalized hepatic stellate cells (LX2).
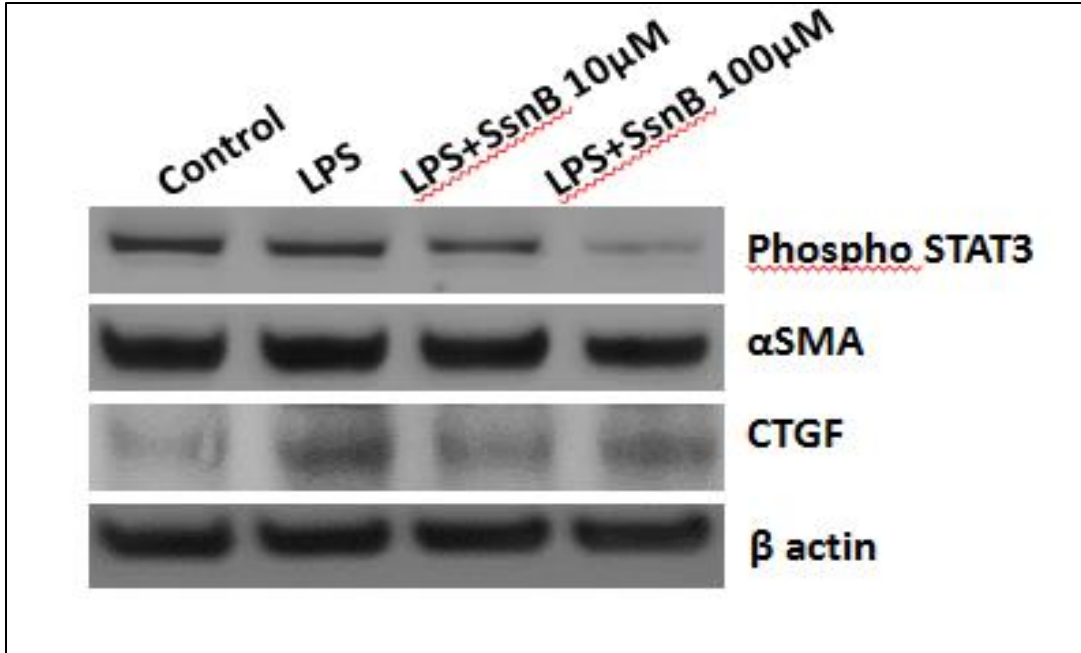
Figure 5.5 SsnB downregulates STAT3 phosphorylation, decreases stellate cell activation and connective tissue growth factor in vitro. A: Western blot analysis of phospho STAT3, αSMA, CTGF and β actin protein levels of Control (untreated), LPS-treated, and LPS+SsnB (10/100μM) treated human immortalized hepatic stellate cells (LX2).
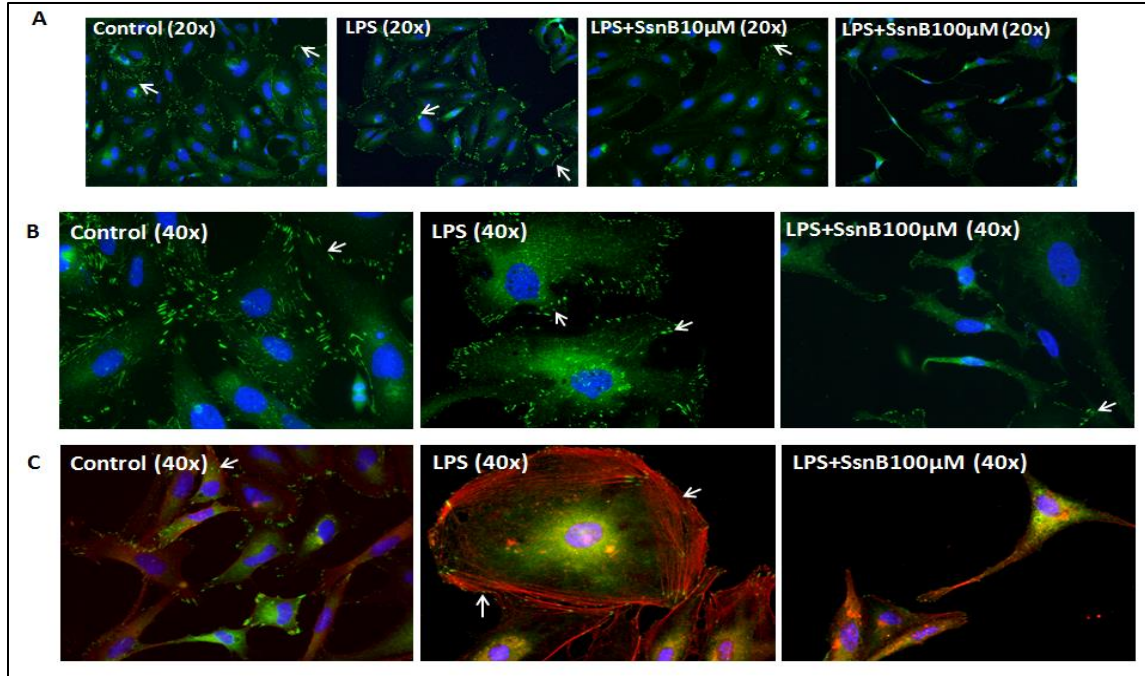
Figure 5.6 SsnB treatment decreases focal adhesion protein expression and inhibits stress fiber formation in vitro. A: Immunofluorescence microscopy depicting paxillin (green) immunoreactivity in Control (untreated), LPS-treated, and LPS+SsnB(10/100µM) treated human immortalized hepatic stellate cells (LX2) taken at ×20 magnification B: Immunofluorescence microscopy depicting paxillin (green) immunoreactivity at ×40 magnification in Control (untreated), LPS-treated, and LPS+SsnB(100µM) treated human immortalized hepatic stellate cells (LX2). Paxillin immunoreactivity (on the edges of the cells) is pointed by white arrows. C: Immunofluorescence dual labeling depicting αSMA(red)-Vinculin(green) on Control (untreated), LPS-treated, and LPS+SsnB(100µM) treated human immortalized hepatic stellate cells (LX2) taken at ×40 magnification. αSMA immunoreactivity (as stress fibers) is pointed by white arrows. Nucleus is stained with DAPI (blue).

CHAPTER 6

CONCLUSION

Nonalcoholic steatohepatitis (NASH) is a hepatic manifestation of metabolic syndrome which arises due to fat accumulation in liver. According to the most recognized model of "two-hits" or "multiple-hits" hypothesis of NASH, the primary hit comes from steatosis or lipid accumulation in the liver. The primary hit makes the liver more vulnerable to the secondary hits- like oxidative stress, subsequent lipid peroxidation, proinflamatory cytokines, adipokines and mitochondrial dysfunction. Together they are able to induce hepatic injury, severe inflammation and fibrosis in the liver (105, 178). Our lab has previously established that chronic low exposure to Bromodichloromethane (BDCM), a drinking water disinfection byproduct, causes nonalcoholic steatohepatitis (NASH) in a diet induced obese mice model where CYP2E1 mediated oxidative stress plays an important pathogenic role as a "second hit" (17) of NASH progression. I have studied molecular mechanisms by which BDCM induces hepatic inflammation and fibrosis. I have also looked at the anti-inflammatory and anti-fibrotic effects of a plant derived compound called Sparstolonin B, in vivo and in vitro models of hepatic injury.

It is known that upregulation of NADPH oxidase (NOX), plays a major role in the activation process of hepatic myofibroblasts (179). However, the molecular mechanisms that link NADPH oxidase activation and upregulation of transforming growth factor

(TGFβ) signaling have been indistinct. Here, I have investigated the role of leptin-mediated upregulation of NADPH oxidase and increased expression of microRNA 21 (miR21) in hepatic fibrogenesis. Human NASH liver samples and a high-fat (60% kcal) diet-fed BDCM induced mouse NASH model were used for this study. Mice lacking in genes for p47phox, leptin and miR21 were used to prove the role of the leptin-NADPH oxidase-miR21 axis. Our results showed that oxidative stress was significantly increased in wild-type (C57BL/6 background) mice NASH model and human NASH liver samples. These samples also showed increased p47phox expression, induced NF-κB activation and increased miR21. Both wild type mice NASH model and human NASH liver samples showed increased TGFβ signaling, increased SMAD2/3 and SMAD4 co-localizations in the nucleus, increased immunoreactivity against extracellular matrix markers with an associated decrease in protein concentration of SMAD7, an antagonist of TGFβ signaling pathway. NADPH oxidase activation has been shown in fibrogenesis, however, there are no known studies linking NADPH oxidase-based oxidative stress signaling through pro-fibrogenic miRNA expression and TGFβ signaling. This was the first study that elucidates the role of leptin mediated NADPH oxidase in the induction of miR21 in a murine NASH model as well as in human NASH liver samples (20). This research revealed some interesting mechanisms by which leptin-mir21 axis can induce hepatic injury by increasing inflammation, oxidative stress and fibrogenesis in NASH liver. Thus, mir21 can be considered as an important therapeutic target to mitigate NASH pathogenesis.

Apart from exploring the basic mechanisms of hepatic injury in NASH, I have also investigated the hepatoprotective effects of Sparstolonin B (SsnB), an isocoumarin

120

isolated from *Sparganium stoloniferum*. This herb has historically been used in traditional Chinese herbal medicine as an anti-inflammatory, anti-cancer drug. SsnB has been shown to disrupt TLR4 and TLR2 dependent downstream signaling pathways, including NfkB and MAPK (102). We are the first group to test the therapeutic effect of this compound in NASH. Interestingly, I observed that SsnB administration attenuated hepatic inflammation and serum alanine aminotransferase (ALT) in a BDCM induced mice model of early NASH. SsnB also showed decreased gene and protein expression of proinflammatory cytokines in vivo and in vitro. Kupffer cell activation was also significantly decreased by SsnB as evidenced by reduction in CD68 and monocyte chemoattractant protein 1 (MCP1) mRNA and protein levels with associated inhibition of macrophage infiltration in liver. Mechanistically, SsnB abrogated TLR4 trafficking to the lipid rafts, as evidenced by the co-localization of TLR4 and lipid raft marker flotillin in liver tissues and immortalized kupffer cells. As we have shown previously that NADPH oxidase drives TLR4 trafficking in NASH, we studied the role of SsnB in modulating this pathway. SsnB also seems to inhibit peroxynitrite mediated oxidative stress by deactivating NADPH oxidase (19).

SsnB has also been characterized as anti-proliferative drug which induced cell cycle arrest in neuroblastoma cells. It could also induce apoptosis and promote cell death in cancer cells (103). I have established anti-fibrotic and anti-proliferative mechanisms of SsnB in a BDCM induced murine model of NASH and in hepatic stellate cell (HSC) culture. I have found that SsnB shows a promising role to decrease liver fibrosis by reducing TLR4-PI3K mediated pro-inflammatory signaling pathway. It is known that activated TLR4-PI3K pathway can induce p53 degradation by upregulating MDM2

(133). Recent research shows that senescence induction in fibrogenic cells by the increase of p21, p53 can help to reduce excessive fibroblast proliferation and suppress hepatic tumor (134). However, no research has focused on the possible mechanism of senescence induction by antagonizing TLR4-PI3k -MDM2 signaling. My work shows that SsnB antagonizes TLR4-PI3k signaling by upregulating PTEN protein expression. It further lowers MDM2 activation and thus increases p53 and p21 gene and protein expression. SsnB also decreased TGFβ signaling by upregulating TGFβ pseudo-receptor BAMBI in vivo. As HSCs are the major fibrogenic cells in the liver, I wanted to see the therapeutic effect of SsnB on these cells. SsnB treatment also downregulated gene expression of pro-fibrogenic hedgehog signaling pathway markers (Ihh, Shh, Gli1, Gli2) in HSCs. SsnB also arrested cell cycle at G2-M phase and induced apoptosis in HSCs. In vitro experiments on rat and human HSCs showed that SsnB treatment increased gene and protein expression of BAMBI and decreased nuclear co-localization of phospho SMAD2/3 and SMAD4 protein. A decrease in phosphorylated SMAD2/3 protein upon SsnB administration in HSCs further confirms the inhibitory effects of SsnB on TGFβ signaling. SsnB decreased STAT3 phosphorylation, downregulated hepatic stellate cell activation and extracellular matrix protein synthesis. We also found that SsnB diminishes the fibroblastic morphology of hepatic stellate cells by downregulating focal adhesion associated adaptor protein and attenuating the stress fiber formation. this research unravels a novel mechanistic approach to diminish fibrogenesis in NASH through inhibiting a myriad of pro-fibrogenic signaling pathways by SsnB.

Although our research has shown promising anti-inflammatory and anti-fibrotic potential of SsnB, our results are constrained within limited scope of experiments. It will

122

be interesting to establish a therapeutic model of NASH where mice with full blown NASH will be administered with SsnB after the disease development. To increase absorption and bioavailability of SsnB, it will be interesting if SsnB can be coupled with nanoparticle to facilitate targeted delivery and controlled release. SsnB mediated alteration of metabolic pathways and steatosis regulation will be worth exploring. As SsnB has shown itself to be a strong anti-angiogenic and anti-proliferative molecule, it will be interesting to see the therapeutic effect of SsnB on liver cancer and other fibrotic diseases.

REFERENCES

1.   Neuschwander-Tetri BA. Non-alcoholic fatty liver disease. BMC medicine. 2017;15(1):45. Epub 2017/03/01. doi: 10.1186/s12916-017-0806-8. PubMed PMID: 28241825; PubMed Central PMCID: PMCPMC5330146.

2.   Bellentani S, Scaglioni F, Marino M, Bedogni G. Epidemiology of non-alcoholic fatty liver disease. Digestive diseases (Basel, Switzerland). 2010;28(1):155-61. Epub 2010/05/13. doi: 10.1159/000282080. PubMed PMID: 20460905.

3.   Musso G, Cassader M, Gambino R. Non-alcoholic steatohepatitis: emerging molecular targets and therapeutic strategies. Nature reviews Drug discovery. 2016;15(4):249-74. Epub 2016/01/23. doi: 10.1038/nrd.2015.3. PubMed PMID: 26794269.

4.   Yu J, Marsh S, Hu J, Feng W, Wu C. The Pathogenesis of Nonalcoholic Fatty Liver Disease: Interplay between Diet, Gut Microbiota, and Genetic Background. Gastroenterology research and practice. 2016;2016:2862173. Epub 2016/06/02. doi: 10.1155/2016/2862173. PubMed PMID: 27247565; PubMed Central PMCID: PMCPMC4876215.

5.   Johnson AR, Milner JJ, Makowski L. The inflammation highway: metabolism accelerates inflammatory traffic in obesity. Immunological reviews. 2012;249(1):218-38. Epub 2012/08/15. doi: 10.1111/j.1600-065X.2012.01151.x. PubMed PMID: 22889225; PubMed Central PMCID: PMCPMC3422768.

6.   Tilg H. The role of cytokines in non-alcoholic fatty liver disease. Digestive diseases (Basel, Switzerland). 2010;28(1):179-85. Epub 2010/05/13. doi: 10.1159/000282083. PubMed PMID: 20460908.

7.   Stern JH, Rutkowski JM, Scherer PE. Adiponectin, Leptin, and Fatty Acids in the Maintenance of Metabolic Homeostasis through Adipose Tissue Crosstalk. Cell metabolism. 2016;23(5):770-84. Epub 2016/05/12. doi: 10.1016/j.cmet.2016.04.011. PubMed PMID: 27166942; PubMed Central PMCID: PMCPMC4864949.

8.   Polyzos SA, Kountouras J, Zavos C, Deretzi G. The potential adverse role of leptin resistance in nonalcoholic fatty liver disease: a hypothesis based on critical review of the literature. Journal of clinical gastroenterology. 2011;45(1):50-4. Epub 2010/08/19. doi: 10.1097/MCG.0b013e3181ec5c66. PubMed PMID: 20717042.

9.   Tsochatzis E, Papatheodoridis GV, Archimandritis AJ. The evolving role of leptin and adiponectin in chronic liver diseases. The American journal of gastroenterology. 2006;101(11):2629-40. Epub 2006/09/06. doi: 10.1111/j.1572-0241.2006.00848.x. PubMed PMID: 16952281.

10.   Tomaru M, Takano H, Inoue K, Yanagisawa R, Osakabe N, Yasuda A, et al. Pulmonary exposure to diesel exhaust particles enhances fatty change of the liver in obese diabetic mice. International journal of molecular medicine. 2007;19(1):17-22. Epub 2006/12/05. PubMed PMID: 17143543.

11.   Arciello M, Gori M, Maggio R, Barbaro B, Tarocchi M, Galli A, et al. Environmental pollution: a tangible risk for NAFLD pathogenesis. International journal of molecular sciences. 2013;14(11):22052-66. Epub 2013/11/12. doi:

10.3390/ijms141122052. PubMed PMID: 24213605; PubMed Central PMCID: PMCPMC3856051.

12. Liggi M, Murgia D, Civolani A, Demelia E, Sorbello O, Demelia L. The relationship between copper and steatosis in Wilson's disease. Clinics and research in hepatology and gastroenterology. 2013;37(1):36-40. Epub 2012/05/11. doi: 10.1016/j.clinre.2012.03.038. PubMed PMID: 22572525.

13. Matsubara T, Tanaka N, Krausz KW, Manna SK, Kang DW, Anderson ER, et al. Metabolomics identifies an inflammatory cascade involved in dioxin- and diet-induced steatohepatitis. Cell metabolism. 2012;16(5):634-44. Epub 2012/11/13. doi: 10.1016/j.cmet.2012.10.006. PubMed PMID: 23140643; PubMed Central PMCID: PMCPMC3496181.

14. Makris KC, Andrianou XD, Charisiadis P, Burch JB, Seth RK, Ioannou A, et al. Association between exposures to brominated trihalomethanes, hepatic injury and type II diabetes mellitus. Environment international. 2016;92-93:486-93. Epub 2016/05/14. doi: 10.1016/j.envint.2016.04.012. PubMed PMID: 27173514.

15. Burch JB, Everson TM, Seth RK, Wirth MD, Chatterjee S. Trihalomethane exposure and biomonitoring for the liver injury indicator, alanine aminotransferase, in the United States population (NHANES 1999-2006). The Science of the total environment. 2015;521-522:226-34. Epub 2015/04/08. doi: 10.1016/j.scitotenv.2015.03.050. PubMed PMID: 25847167; PubMed Central PMCID: PMCPMC4462191.

16. Seth RK, Kumar A, Das S, Kadiiska MB, Michelotti G, Diehl AM, et al. Environmental toxin-linked nonalcoholic steatohepatitis and hepatic metabolic reprogramming in obese mice. Toxicological sciences : an official journal of the Society

of Toxicology. 2013;134(2):291-303. Epub 2013/05/04. doi: 10.1093/toxsci/kft104. PubMed PMID: 23640861; PubMed Central PMCID: PMCPMC3707434.

17.   Seth RK, Das S, Kumar A, Chanda A, Kadiiska MB, Michelotti G, et al. CYP2E1-dependent and leptin-mediated hepatic CD57 expression on CD8+ T cells aid progression of environment-linked nonalcoholic steatohepatitis. Toxicology and applied pharmacology. 2014;274(1):42-54. Epub 2013/11/12. doi: 10.1016/j.taap.2013.10.029. PubMed PMID: 24211274; PubMed Central PMCID: PMCPMC3874401.

18.   Das S, Kumar A, Seth RK, Tokar EJ, Kadiiska MB, Waalkes MP, et al. Proinflammatory adipokine leptin mediates disinfection byproduct bromodichloromethane-induced early steatohepatitic injury in obesity. Toxicology and applied pharmacology. 2013;269(3):297-306. Epub 2013/02/27. doi: 10.1016/j.taap.2013.02.003. PubMed PMID: 23438451; PubMed Central PMCID: PMCPMC3654077.

19.   Dattaroy D, Seth RK, Das S, Alhasson F, Chandrashekaran V, Michelotti G, et al. Sparstolonin B attenuates early liver inflammation in experimental NASH by modulating TLR4 trafficking in lipid rafts via NADPH oxidase activation. American journal of physiology Gastrointestinal and liver physiology. 2016;310(7):G510-25. Epub 2016/01/01. doi: 10.1152/ajpgi.00259.2015. PubMed PMID: 26718771; PubMed Central PMCID: PMCPMC4824178.

20.   Dattaroy D, Pourhoseini S, Das S, Alhasson F, Seth RK, Nagarkatti M, et al. Micro-RNA 21 inhibition of SMAD7 enhances fibrogenesis via leptin-mediated NADPH oxidase in experimental and human nonalcoholic steatohepatitis. American journal of physiology Gastrointestinal and liver physiology. 2015;308(4):G298-312. Epub

2014/12/17. doi: 10.1152/ajpgi.00346.2014. PubMed PMID: 25501551; PubMed Central PMCID: PMCPMC4329476.

21.   Yang SQ, Lin HZ, Lane MD, Clemens M, Diehl AM. Obesity increases sensitivity to endotoxin liver injury: implications for the pathogenesis of steatohepatitis. Proceedings of the National Academy of Sciences of the United States of America. 1997;94(6):2557-62. Epub 1997/03/18. PubMed PMID: 9122234; PubMed Central PMCID: PMCPMC20127.

22.   Lau E, Carvalho D, Freitas P. Gut Microbiota: Association with NAFLD and Metabolic Disturbances. BioMed research international. 2015;2015:979515. Epub 2015/06/20. doi: 10.1155/2015/979515. PubMed PMID: 26090468; PubMed Central PMCID: PMCPMC4452311.

23.   Gill R, Tsung A, Billiar T. Linking oxidative stress to inflammation: Toll-like receptors. Free radical biology & medicine. 2010;48(9):1121-32. Epub 2010/01/20. doi: 10.1016/j.freeradbiomed.2010.01.006. PubMed PMID: 20083193; PubMed Central PMCID: PMCPMC3423196.

24.   Das S, Alhasson F, Dattaroy D, Pourhoseini S, Seth RK, Nagarkatti M, et al. NADPH Oxidase-Derived Peroxynitrite Drives Inflammation in Mice and Human Nonalcoholic Steatohepatitis via TLR4-Lipid Raft Recruitment. The American journal of pathology. 2015;185(7):1944-57. Epub 2015/05/20. doi: 10.1016/j.ajpath.2015.03.024. PubMed PMID: 25989356; PubMed Central PMCID: PMCPMC4483465.

25.   Nace GW, Huang H, Klune JR, Eid RE, Rosborough BR, Korff S, et al. Cellular-specific role of toll-like receptor 4 in hepatic ischemia-reperfusion injury in mice. Hepatology (Baltimore, Md). 2013;58(1):374-87. Epub 2013/03/06. doi:

10.1002/hep.26346. PubMed PMID: 23460269; PubMed Central PMCID: PMCPMC3688695.

26. Jia L, Vianna CR, Fukuda M, Berglund ED, Liu C, Tao C, et al. Hepatocyte Toll-like receptor 4 regulates obesity-induced inflammation and insulin resistance. Nature communications. 2014;5:3878. Epub 2014/05/13. doi: 10.1038/ncomms4878. PubMed PMID: 24815961; PubMed Central PMCID: PMCPMC4080408.

27. Guo J, Friedman SL. Toll-like receptor 4 signaling in liver injury and hepatic fibrogenesis. Fibrogenesis & tissue repair. 2010;3:21. Epub 2010/10/23. doi: 10.1186/1755-1536-3-21. PubMed PMID: 20964825; PubMed Central PMCID: PMCPMC2984459.

28. Liang Q, Wu Q, Jiang J, Duan J, Wang C, Smith MD, et al. Characterization of sparstolonin B, a Chinese herb-derived compound, as a selective Toll-like receptor antagonist with potent anti-inflammatory properties. The Journal of biological chemistry. 2011;286(30):26470-9. Epub 2011/06/15. doi: 10.1074/jbc.M111.227934. PubMed PMID: 21665946; PubMed Central PMCID: PMCPMC3143611.

29. Ikejima K, Okumura K, Kon K, Takei Y, Sato N. Role of adipocytokines in hepatic fibrogenesis. Journal of gastroenterology and hepatology. 2007;22 Suppl 1:S87-92. Epub 2007/08/25. doi: 10.1111/j.1440-1746.2007.04961.x. PubMed PMID: 17567476.

30. Singh S, Allen AM, Wang Z, Prokop LJ, Murad MH, Loomba R. Fibrosis Progression in Nonalcoholic Fatty Liver vs Nonalcoholic Steatohepatitis: A Systematic Review and Meta-analysis of Paired-Biopsy Studies. Clinical gastroenterology and hepatology : the official clinical practice journal of the American Gastroenterological

Association. 2014. Epub 2014/04/29. doi: 10.1016/j.cgh.2014.04.014. PubMed PMID: 24768810.

31.   Schuppan D, Schattenberg JM. Non-alcoholic steatohepatitis: pathogenesis and novel therapeutic approaches. Journal of gastroenterology and hepatology. 2013;28 Suppl 1:68-76. Epub 2013/07/24. doi: 10.1111/jgh.12212. PubMed PMID: 23855299.

32.   Yilmaz Y, Younossi ZM. Obesity-associated nonalcoholic fatty liver disease. Clinics in liver disease. 2014;18(1):19-31. Epub 2013/11/28. doi: 10.1016/j.cld.2013.09.018. PubMed PMID: 24274862.

33.   Paik YH, Kim J, Aoyama T, De Minicis S, Bataller R, Brenner DA. Role of NADPH oxidases in liver fibrosis. Antioxid Redox Signal. 2014;20(17):2854-72. Epub 2013/09/18. doi: 10.1089/ars.2013.5619. PubMed PMID: 24040957; PubMed Central PMCID: PMCPMC4026397.

34.   De Minicis S, Svegliati-Baroni G. Fibrogenesis in nonalcoholic steatohepatitis. Expert review of gastroenterology & hepatology. 2011;5(2):179-87. Epub 2011/04/12. doi: 10.1586/egh.11.28. PubMed PMID: 21476913.

35.   Kamada Y, Takehara T, Hayashi N. Adipocytokines and liver disease. Journal of gastroenterology. 2008;43(11):811-22. Epub 2008/11/18. doi: 10.1007/s00535-008-2213-6. PubMed PMID: 19012034.

36.   Marra F, Aleffi S, Bertolani C, Petrai I, Vizzutti F. Adipokines and liver fibrosis. European review for medical and pharmacological sciences. 2005;9(5):279-84. Epub 2005/10/20. PubMed PMID: 16231590.

37.   Copaci I, Micu L, Voiculescu M. The role of cytokines in non-alcoholic steatohepatitis. A review. Journal of gastrointestinal and liver diseases : JGLD. 2006;15(4):363-73. Epub 2007/01/06. PubMed PMID: 17205149.

38.   Seth RK, Kumar A, Das S, Kadiiska MB, Michelotti G, Diehl AM, et al. Environmental toxin-linked nonalcoholic steatohepatitis and hepatic metabolic reprogramming in obese mice. Toxicological sciences : an official journal of the Society of Toxicology. 2013. Epub 2013/05/04. doi: 10.1093/toxsci/kft104. PubMed PMID: 23640861.

39.   Procaccini C, Galgani M, De Rosa V, Carbone F, La Rocca C, Ranucci G, et al. Leptin: the prototypic adipocytokine and its role in NAFLD. Current pharmaceutical design. 2010;16(17):1902-12. Epub 2010/04/08. PubMed PMID: 20370676.

40.   Chatterjee S, Ganini D, Tokar EJ, Kumar A, Das S, Corbett J, et al. Leptin is key to peroxynitrite-mediated oxidative stress and Kupffer cell activation in experimental nonalcoholic steatohepatitis. J Hepatol. 2012. Epub 2012/12/05. doi: 10.1016/j.jhep.2012.11.035. PubMed PMID: 23207144.

41.   De Minicis S, Seki E, Oesterreicher C, Schnabl B, Schwabe RF, Brenner DA. Reduced nicotinamide adenine dinucleotide phosphate oxidase mediates fibrotic and inflammatory effects of leptin on hepatic stellate cells. Hepatology. 2008;48(6):2016-26. Epub 2008/11/26. doi: 10.1002/hep.22560. PubMed PMID: 19025999.

42.   Honda H, Ikejima K, Hirose M, Yoshikawa M, Lang T, Enomoto N, et al. Leptin is required for fibrogenic responses induced by thioacetamide in the murine liver. Hepatology. 2002;36(1):12-21. Epub 2002/06/27. doi: 10.1053/jhep.2002.33684. PubMed PMID: 12085344.

43.   Tang M, Potter JJ, Mezey E. Leptin enhances the effect of transforming growth factor beta in increasing type I collagen formation. Biochem Biophys Res Commun. 2002;297(4):906-11. Epub 2002/10/03. PubMed PMID: 12359239.

44.   Wang J, Leclercq I, Brymora JM, Xu N, Ramezani-Moghadam M, London RM, et al. Kupffer cells mediate leptin-induced liver fibrosis. Gastroenterology. 2009;137(2):713-23. Epub 2009/04/21. doi: 10.1053/j.gastro.2009.04.011. PubMed PMID: 19375424; PubMed Central PMCID: PMC2757122.

45.   Saxena NK, Saliba G, Floyd JJ, Anania FA. Leptin induces increased alpha2(I) collagen gene expression in cultured rat hepatic stellate cells. Journal of cellular biochemistry. 2003;89(2):311-20. Epub 2003/04/22. doi: 10.1002/jcb.10494. PubMed PMID: 12704794; PubMed Central PMCID: PMCPMC2925439.

46.   Paik YH, Brenner DA. NADPH oxidase mediated oxidative stress in hepatic fibrogenesis. Korean J Hepatol. 2011;17(4):251-7. Epub 2012/02/09. doi: 10.3350/kjhep.2011.17.4.251. PubMed PMID: 22310788; PubMed Central PMCID: PMCPMC3304665.

47.   Medici V, Ali MR, Seo S, Aoki CA, Rossaro L, Kim K, et al. Increased soluble leptin receptor levels in morbidly obese patients with insulin resistance and nonalcoholic fatty liver disease. Obesity (Silver Spring, Md). 2010;18(12):2268-73. Epub 2010/05/08. doi: 10.1038/oby.2010.95. PubMed PMID: 20448542.

48.   Bataller R, Schwabe RF, Choi YH, Yang L, Paik YH, Lindquist J, et al. NADPH oxidase signal transduces angiotensin II in hepatic stellate cells and is critical in hepatic fibrosis. The Journal of clinical investigation. 2003;112(9):1383-94. Epub 2003/11/05.

doi: 10.1172/jci18212. PubMed PMID: 14597764; PubMed Central PMCID: PMCPMC228420.

49.   Yao H, Yang SR, Kode A, Rajendrasozhan S, Caito S, Adenuga D, et al. Redox regulation of lung inflammation: role of NADPH oxidase and NF-kappaB signalling. Biochem Soc Trans. 2007;35(Pt 5):1151-5. Epub 2007/10/25. doi: 10.1042/BST0351151. PubMed PMID: 17956299.

50.   Zhang Z, Gao Z, Hu W, Yin S, Wang C, Zang Y, et al. 3,3'-Diindolylmethane ameliorates experimental hepatic fibrosis via inhibiting miR-21 expression. Br J Pharmacol. 2013;170(3):649-60. Epub 2013/08/02. doi: 10.1111/bph.12323. PubMed PMID: 23902531; PubMed Central PMCID: PMCPMC3792002.

51.   Noetel A, Kwiecinski M, Elfimova N, Huang J, Odenthal M. microRNA are Central Players in Anti- and Profibrotic Gene Regulation during Liver Fibrosis. Frontiers in physiology. 2012;3:49. Epub 2012/03/30. doi: 10.3389/fphys.2012.00049. PubMed PMID: 22457651; PubMed Central PMCID: PMCPMC3307137.

52.   Patel V, Noureddine L. MicroRNAs and fibrosis. Current opinion in nephrology and hypertension. 2012;21(4):410-6. Epub 2012/05/25. doi: 10.1097/MNH.0b013e328354e559. PubMed PMID: 22622653; PubMed Central PMCID: PMCPMC3399722.

53.   Liu G, Friggeri A, Yang Y, Milosevic J, Ding Q, Thannickal VJ, et al. miR-21 mediates fibrogenic activation of pulmonary fibroblasts and lung fibrosis. The Journal of experimental medicine. 2010;207(8):1589-97. Epub 2010/07/21. doi: 10.1084/jem.20100035. PubMed PMID: 20643828; PubMed Central PMCID: PMCPMC2916139.

54.   Chung AC, Dong Y, Yang W, Zhong X, Li R, Lan HY. Smad7 suppresses renal fibrosis via altering expression of TGF-beta/Smad3-regulated microRNAs. Mol Ther. 2013;21(2):388-98. Epub 2012/12/05. doi: 10.1038/mt.2012.251. PubMed PMID: 23207693; PubMed Central PMCID: PMCPMC3594008.

55.   Ikejima K, Okumura K, Lang T, Honda H, Abe W, Yamashina S, et al. The role of leptin in progression of non-alcoholic fatty liver disease. Hepatology research : the official journal of the Japan Society of Hepatology. 2005;33(2):151-4. Epub 2005/10/04. doi: 10.1016/j.hepres.2005.09.024. PubMed PMID: 16198623.

56.   Yang L, Roh YS, Song J, Zhang B, Liu C, Loomba R, et al. Transforming growth factor beta signaling in hepatocytes participates in steatohepatitis through regulation of cell death and lipid metabolism in mice. Hepatology. 2014;59(2):483-95. Epub 2013/09/03. doi: 10.1002/hep.26698. PubMed PMID: 23996730; PubMed Central PMCID: PMCPMC3946696.

57.   Chatterjee S, Ganini D, Tokar EJ, Kumar A, Das S, Corbett J, et al. Leptin is key to peroxynitrite-mediated oxidative stress and Kupffer cell activation in experimental non-alcoholic steatohepatitis. J Hepatol. 2013;58(4):778-84. Epub 2012/12/05. doi: 10.1016/j.jhep.2012.11.035. PubMed PMID: 23207144; PubMed Central PMCID: PMCPMC3596459.

58.   Sheedy FJ, Palsson-McDermott E, Hennessy EJ, Martin C, O'Leary JJ, Ruan Q, et al. Negative regulation of TLR4 via targeting of the proinflammatory tumor suppressor PDCD4 by the microRNA miR-21. Nat Immunol. 2010;11(2):141-7. Epub 2009/12/01. doi: 10.1038/ni.1828. PubMed PMID: 19946272.

59.   Quinn SR, O'Neill LA. A trio of microRNAs that control Toll-like receptor signalling. Int Immunol. 2011;23(7):421-5. Epub 2011/06/10. doi: 10.1093/intimm/dxr034. PubMed PMID: 21652514.

60.   Dooley S, ten Dijke P. TGF-beta in progression of liver disease. Cell Tissue Res. 2012;347(1):245-56. Epub 2011/10/19. doi: 10.1007/s00441-011-1246-y. PubMed PMID: 22006249; PubMed Central PMCID: PMCPMC3250614.

61.   Nakao A, Roijer E, Imamura T, Souchelnytskyi S, Stenman G, Heldin CH, et al. Identification of Smad2, a human Mad-related protein in the transforming growth factor beta signaling pathway. The Journal of biological chemistry. 1997;272(5):2896-900. Epub 1997/01/31. PubMed PMID: 9006934.

62.   Nakao A, Imamura T, Souchelnytskyi S, Kawabata M, Ishisaki A, Oeda E, et al. TGF-beta receptor-mediated signalling through Smad2, Smad3 and Smad4. EMBO J. 1997;16(17):5353-62. Epub 1997/10/06. doi: 10.1093/emboj/16.17.5353. PubMed PMID: 9311995; PubMed Central PMCID: PMCPMC1170167.

63.   Nakao A, Afrakhte M, Moren A, Nakayama T, Christian JL, Heuchel R, et al. Identification of Smad7, a TGFbeta-inducible antagonist of TGF-beta signalling. Nature. 1997;389(6651):631-5. Epub 1997/10/23 22:33. doi: 10.1038/39369. PubMed PMID: 9335507.

64.   Liu Y, Liu H, Meyer C, Li J, Nadalin S, Konigsrainer A, et al. Transforming growth factor-beta (TGF-beta)-mediated connective tissue growth factor (CTGF) expression in hepatic stellate cells requires Stat3 signaling activation. The Journal of biological chemistry. 2013;288(42):30708-19. Epub 2013/09/06. doi:

10.1074/jbc.M113.478685. PubMed PMID: 24005672; PubMed Central PMCID: PMCPMC3798541.

65.   Kohan M, Muro AF, White ES, Berkman N. EDA-containing cellular fibronectin induces fibroblast differentiation through binding to alpha4beta7 integrin receptor and MAPK/Erk 1/2-dependent signaling. FASEB J. 2010;24(11):4503-12. Epub 2010/07/21. doi: 10.1096/fj.10-154435. PubMed PMID: 20643910.

66.   Aschner Y, Khalifah AP, Briones N, Yamashita C, Dolgonos L, Young SK, et al. Protein tyrosine phosphatase alpha mediates profibrotic signaling in lung fibroblasts through TGF-beta responsiveness. The American journal of pathology. 2014;184(5):1489-502. Epub 2014/03/22. doi: 10.1016/j.ajpath.2014.01.016. PubMed PMID: 24650563; PubMed Central PMCID: PMCPMC4005983.

67.   Choi SS, Syn WK, Karaca GF, Omenetti A, Moylan CA, Witek RP, et al. Leptin promotes the myofibroblastic phenotype in hepatic stellate cells by activating the hedgehog pathway. The Journal of biological chemistry. 2010;285(47):36551-60. Epub 2010/09/17. doi: 10.1074/jbc.M110.168542. PubMed PMID: 20843817; PubMed Central PMCID: PMCPMC2978583.

68.   Lin Y, Liu X, Cheng Y, Yang J, Huo Y, Zhang C. Involvement of MicroRNAs in hydrogen peroxide-mediated gene regulation and cellular injury response in vascular smooth muscle cells. The Journal of biological chemistry. 2009;284(12):7903-13. Epub 2009/01/23. doi: 10.1074/jbc.M806920200. PubMed PMID: 19158092; PubMed Central PMCID: PMCPMC2658083.

69.   Pirola CJ, Fernandez Gianotti T, Castano GO, Mallardi P, San Martino J, Mora Gonzalez Lopez Ledesma M, et al. Circulating microRNA signature in non-alcoholic

fatty liver disease: from serum non-coding RNAs to liver histology and disease pathogenesis. Gut. 2015;64(5):800-12. Epub 2014/06/29. doi: 10.1136/gutjnl-2014-306996. PubMed PMID: 24973316; PubMed Central PMCID: PMCPMC4277726.

70.   Michelotti GA, Machado MV, Diehl AM. NAFLD, NASH and liver cancer. Nat Rev Gastroenterol Hepatol. 2013;10(11):656-65. Epub 2013/10/02. doi: 10.1038/nrgastro.2013.183. PubMed PMID: 24080776.

71.   Cheung O, Sanyal AJ. Role of microRNAs in non-alcoholic steatohepatitis. Curr Pharm Des. 2010;16(17):1952-7. Epub 2010/04/08. PubMed PMID: 20370674.

72.   Ruan Q, Wang T, Kameswaran V, Wei Q, Johnson DS, Matschinsky F, et al. The microRNA-21-PDCD4 axis prevents type 1 diabetes by blocking pancreatic beta cell death. Proceedings of the National Academy of Sciences of the United States of America. 2011;108(29):12030-5. Epub 2011/07/07. doi: 10.1073/pnas.1101450108. PubMed PMID: 21730150; PubMed Central PMCID: PMCPMC3141944.

73.   Kim CH, Younossi ZM. Nonalcoholic fatty liver disease: a manifestation of the metabolic syndrome. Cleve Clin J Med. 2008;75(10):721-8. Epub 2008/10/23. PubMed PMID: 18939388.

74.   Day CP. Clinical spectrum and therapy of non-alcoholic steatohepatitis. Digestive diseases (Basel, Switzerland). 2012;30 Suppl 1:69-73. Epub 2012/10/25. doi: 10.1159/000341128. PubMed PMID: 23075871.

75.   Durazzo M, Belci P, Collo A, Grisoglio E, Bo S. Focus on therapeutic strategies of nonalcoholic Fatty liver disease. Int J Hepatol. 2012;2012:464706. Epub 2012/12/05. doi: 10.1155/2012/464706. PubMed PMID: 23209914; PubMed Central PMCID: PMCPMC3502854.

76.   Rodriguez B, Torres DM, Harrison SA. Physical activity: an essential component of lifestyle modification in NAFLD. Nat Rev Gastroenterol Hepatol. 2012;9(12):726-31. Epub 2012/10/24. doi: 10.1038/nrgastro.2012.200. PubMed PMID: 23090329.

77.   Pacana T, Sanyal AJ. Vitamin E and nonalcoholic fatty liver disease. Curr Opin Clin Nutr Metab Care. 2012;15(6):641-8. Epub 2012/10/19. doi: 10.1097/MCO.0b013e328357f747. PubMed PMID: 23075940; PubMed Central PMCID: PMCPMC4984672.

78.   Ma YY, Li L, Yu CH, Shen Z, Chen LH, Li YM. Effects of probiotics on nonalcoholic fatty liver disease: a meta-analysis. World journal of gastroenterology. 2013;19(40):6911-8. Epub 2013/11/05. doi: 10.3748/wjg.v19.i40.6911. PubMed PMID: 24187469; PubMed Central PMCID: PMCPMC3812493.

79.   Roh YS, Seki E. Toll-like receptors in alcoholic liver disease, non-alcoholic steatohepatitis and carcinogenesis. J Gastroenterol Hepatol. 2013;28 Suppl 1:38-42. Epub 2013/07/24. doi: 10.1111/jgh.12019. PubMed PMID: 23855294; PubMed Central PMCID: PMCPMC3721430.

80.   Miura K, Ohnishi H. Role of gut microbiota and Toll-like receptors in nonalcoholic fatty liver disease. World journal of gastroenterology : WJG. 2014;20(23):7381-91. Epub 2014/06/27. doi: 10.3748/wjg.v20.i23.7381. PubMed PMID: 24966608; PubMed Central PMCID: PMCPMC4064083.

81.   Farhadi A, Gundlapalli S, Shaikh M, Frantzides C, Harrell L, Kwasny MM, et al. Susceptibility to gut leakiness: a possible mechanism for endotoxaemia in non-alcoholic steatohepatitis. Liver Int. 2008;28(7):1026-33. Epub 2008/04/10. doi: 10.1111/j.1478-

138

3231.2008.01723.x. PubMed PMID: 18397235; PubMed Central PMCID: PMCPMC4303249.

82.   Zheng Z, Xu X, Zhang X, Wang A, Zhang C, Huttemann M, et al. Exposure to ambient particulate matter induces a NASH-like phenotype and impairs hepatic glucose metabolism in an animal model. J Hepatol. 2013;58(1):148-54. Epub 2012/08/21. doi: 10.1016/j.jhep.2012.08.009. PubMed PMID: 22902548; PubMed Central PMCID: PMCPMC3527686.

83.   Ye D, Li FY, Lam KS, Li H, Jia W, Wang Y, et al. Toll-like receptor-4 mediates obesity-induced non-alcoholic steatohepatitis through activation of X-box binding protein-1 in mice. Gut. 2012;61(7):1058-67. Epub 2012/01/19. doi: 10.1136/gutjnl-2011-300269. PubMed PMID: 22253482.

84.   Velayudham A, Dolganiuc A, Ellis M, Petrasek J, Kodys K, Mandrekar P, et al. VSL#3 probiotic treatment attenuates fibrosis without changes in steatohepatitis in a diet-induced nonalcoholic steatohepatitis model in mice. Hepatology (Baltimore, Md). 2009;49(3):989-97. Epub 2008/12/31. doi: 10.1002/hep.22711. PubMed PMID: 19115316; PubMed Central PMCID: PMCPMC3756672.

85.   Tsujimoto T, Kawaratani H, Kitazawa T, Uemura M, Fukui H. Innate immune reactivity of the ileum-liver axis in nonalcoholic steatohepatitis. Dig Dis Sci. 2012;57(5):1144-51. Epub 2012/03/01. doi: 10.1007/s10620-012-2073-z. PubMed PMID: 22367065.

86.   Singh R, Bullard J, Kalra M, Assefa S, Kaul AK, Vonfeldt K, et al. Status of bacterial colonization, Toll-like receptor expression and nuclear factor-kappa B activation

in normal and diseased human livers. Clin Immunol. 2011;138(1):41-9. Epub 2010/10/14. doi: 10.1016/j.clim.2010.09.006. PubMed PMID: 20940109.

87.   Siebler J, Galle PR, Weber MM. The gut-liver-axis: endotoxemia, inflammation, insulin resistance and NASH. J Hepatol. 2008;48(6):1032-4. Epub 2008/05/13. doi: 10.1016/j.jhep.2008.03.007. PubMed PMID: 18468548.

88.   Shanab AA, Scully P, Crosbie O, Buckley M, O'Mahony L, Shanahan F, et al. Small intestinal bacterial overgrowth in nonalcoholic steatohepatitis: association with toll-like receptor 4 expression and plasma levels of interleukin 8. Dig Dis Sci. 2011;56(5):1524-34. Epub 2010/11/04. doi: 10.1007/s10620-010-1447-3. PubMed PMID: 21046243.

89.   Sakaguchi S, Takahashi S, Sasaki T, Kumagai T, Nagata K. Progression of alcoholic and non-alcoholic steatohepatitis: common metabolic aspects of innate immune system and oxidative stress. Drug Metab Pharmacokinet. 2011;26(1):30-46. Epub 2010/12/15. PubMed PMID: 21150132.

90.   Petrasek J, Csak T, Szabo G. Toll-like receptors in liver disease. Adv Clin Chem. 2013;59:155-201. Epub 2013/03/07. PubMed PMID: 23461136.

91.   Imajo K, Fujita K, Yoneda M, Nozaki Y, Ogawa Y, Shinohara Y, et al. Hyperresponsivity to low-dose endotoxin during progression to nonalcoholic steatohepatitis is regulated by leptin-mediated signaling. Cell metabolism. 2012;16(1):44-54. Epub 2012/07/10. doi: 10.1016/j.cmet.2012.05.012. PubMed PMID: 22768838.

92.   Ilan Y. Leaky gut and the liver: a role for bacterial translocation in nonalcoholic steatohepatitis. World journal of gastroenterology. 2012;18(21):2609-18. Epub

2012/06/13. doi: 10.3748/wjg.v18.i21.2609. PubMed PMID: 22690069; PubMed Central PMCID: PMCPMC3369997.

93.   Henao-Mejia J, Elinav E, Jin C, Hao L, Mehal WZ, Strowig T, et al. Inflammasome-mediated dysbiosis regulates progression of NAFLD and obesity. Nature. 2012;482(7384):179-85. Epub 2012/02/03. doi: 10.1038/nature10809. PubMed PMID: 22297845; PubMed Central PMCID: PMCPMC3276682.

94.   Ajamieh H, Farrell G, Wong HJ, Yu J, Chu E, Chen J, et al. Atorvastatin protects obese mice against hepatic ischemia-reperfusion injury by Toll-like receptor-4 suppression and endothelial nitric oxide synthase activation. J Gastroenterol Hepatol. 2012;27(8):1353-61. Epub 2012/03/22. doi: 10.1111/j.1440-1746.2012.07123.x. PubMed PMID: 22432744.

95.   Wong SW, Kwon MJ, Choi AM, Kim HP, Nakahira K, Hwang DH. Fatty acids modulate Toll-like receptor 4 activation through regulation of receptor dimerization and recruitment into lipid rafts in a reactive oxygen species-dependent manner. J Biol Chem. 2009;284(40):27384-92. Epub 2009/08/04. doi: 10.1074/jbc.M109.044065. PubMed PMID: 19648648; PubMed Central PMCID: PMCPMC2785667.

96.   Nakahira K, Kim HP, Geng XH, Nakao A, Wang X, Murase N, et al. Carbon monoxide differentially inhibits TLR signaling pathways by regulating ROS-induced trafficking of TLRs to lipid rafts. J Exp Med. 2006;203(10):2377-89. Epub 2006/09/27. doi: 10.1084/jem.20060845. PubMed PMID: 17000866; PubMed Central PMCID: PMCPMC2118097.

97.   Peri F, Piazza M. Therapeutic targeting of innate immunity with Toll-like receptor 4 (TLR4) antagonists. Biotechnol Adv. 2012;30(1):251-60. Epub 2011/06/15. doi: 10.1016/j.biotechadv.2011.05.014. PubMed PMID: 21664961.

98.   Liu Q, Wang J, Liang Q, Wang D, Luo Y, Li J, et al. Sparstolonin B attenuates hypoxia-reoxygenation-induced cardiomyocyte inflammation. Exp Biol Med (Maywood). 2014;239(3):376-84. Epub 2014/01/31. doi: 10.1177/1535370213517620. PubMed PMID: 24477822.

99.   Liu Q, Li J, Liang Q, Wang D, Luo Y, Yu F, et al. Sparstolonin B suppresses rat vascular smooth muscle cell proliferation, migration, inflammatory response and lipid accumulation. Vascul Pharmacol. 2015;67-69:59-66. Epub 2015/04/15. doi: 10.1016/j.vph.2015.03.015. PubMed PMID: 25869499; PubMed Central PMCID: PMCPMC4433853.

100.   Liu Q, Li J, Jubair S, Wang D, Luo Y, Fan D, et al. Sparstolonin B attenuates hypoxia-induced apoptosis, necrosis and inflammation in cultured rat left ventricular tissue slices. Cardiovasc Drugs Ther. 2014;28(5):433-9. Epub 2014/08/15. doi: 10.1007/s10557-014-6545-6. PubMed PMID: 25117676; PubMed Central PMCID: PMCPMC4164598.

101.   Liang Q, Yu F, Cui X, Duan J, Wu Q, Nagarkatti P, et al. Sparstolonin B suppresses lipopolysaccharide-induced inflammation in human umbilical vein endothelial cells. Archives of pharmacal research. 2013;36(7):890-6. Epub 2013/04/23. doi: 10.1007/s12272-013-0120-8. PubMed PMID: 23604718; PubMed Central PMCID: PMCPMC4145723.

102.	Liang Q, Dong S, Lei L, Liu J, Zhang J, Li J, et al. Protective effects of Sparstolonin B, a selective TLR2 and TLR4 antagonist, on mouse endotoxin shock. Cytokine. 2015;75(2):302-9. Epub 2015/01/13. doi: 10.1016/j.cyto.2014.12.003. PubMed PMID: 25573805; PubMed Central PMCID: PMCPMC4950682.

103.	Kumar A, Fan D, Dipette DJ, Singh US. Sparstolonin B, a novel plant derived compound, arrests cell cycle and induces apoptosis in N-myc amplified and N-myc nonamplified neuroblastoma cells. PloS one. 2014;9(5):e96343. Epub 2014/05/03. doi: 10.1371/journal.pone.0096343. PubMed PMID: 24788776; PubMed Central PMCID: PMCPMC4006872.

104.	Bateman HR, Liang Q, Fan D, Rodriguez V, Lessner SM. Sparstolonin B inhibits pro-angiogenic functions and blocks cell cycle progression in endothelial cells. PloS one. 2013;8(8):e70500. Epub 2013/08/14. doi: 10.1371/journal.pone.0070500. PubMed PMID: 23940584; PubMed Central PMCID: PMCPMC3734268.

105.	Tilg H, Moschen AR. Evolution of inflammation in nonalcoholic fatty liver disease: the multiple parallel hits hypothesis. Hepatology (Baltimore, Md). 2010;52(5):1836-46. Epub 2010/11/03. doi: 10.1002/hep.24001. PubMed PMID: 21038418.

106.	Chatterjee S, Das S. P2X7 receptor as a key player in oxidative stress-driven cell fate in nonalcoholic steatohepatitis. Oxidative medicine and cellular longevity. 2015;2015:172493. Epub 2015/03/31. doi: 10.1155/2015/172493. PubMed PMID: 25815106; PubMed Central PMCID: PMCPMC4359843.

107.	Nebiker CA, Han J, Eppenberger-Castori S, Iezzi G, Hirt C, Amicarella F, et al. GM-CSF Production by Tumor Cells Is Associated with Improved Survival in Colorectal

Cancer. Clinical cancer research : an official journal of the American Association for Cancer Research. 2014;20(12):3094-106. Epub 2014/04/17. doi: 10.1158/1078-0432.ccr-13-2774. PubMed PMID: 24737547.

108.   Seth RK, Das S, Pourhoseini S, Dattaroy D, Igwe S, Ray JB, et al. M1 polarization bias and subsequent nonalcoholic steatohepatitis progression is attenuated by nitric oxide donor DETA NONOate via inhibition of CYP2E1-induced oxidative stress in obese mice. The Journal of pharmacology and experimental therapeutics. 2015;352(1):77-89. Epub 2014/10/29. doi: 10.1124/jpet.114.218131. PubMed PMID: 25347994; PubMed Central PMCID: PMCPMC4279102.

109.   Dattaroy D, Pourhoseini S, Das S, Alhasson F, Seth RK, Nagarkatti M, et al. Micro RNA 21 inhibition of SMAD 7 enhances fibrogenesis via leptin mediated NADPH oxidase in experimental and human nonalcoholic steatohepatitis. American journal of physiology Gastrointestinal and liver physiology. 2014:ajpgi 00346 2014. Epub 2014/12/17. doi: 10.1152/ajpgi.00346.2014. PubMed PMID: 25501551.

110.   Pourhoseini S, Seth RK, Das S, Dattaroy D, Kadiiska MB, Xie G, et al. Upregulation of miR21 and Repression of Grhl3 by Leptin Mediates Sinusoidal Endothelial Injury in Experimental Nonalcoholic Steatohepatitis. PloS one. 2015;10(2):e0116780. Epub 2015/02/07. doi: 10.1371/journal.pone.0116780. PubMed PMID: 25658689.

111.   Das S, Alhasson F, Dattaroy D, Pourhoseini S, Seth RK, Nagarkatti M, et al. NADPH Oxidase-Derived Peroxynitrite Drives Inflammation in Mice and Human Nonalcoholic Steatohepatitis via TLR4-Lipid Raft Recruitment. The American journal of

pathology. 2015. Epub 2015/05/20. doi: 10.1016/j.ajpath.2015.03.024. PubMed PMID: 25989356.

112.   Ding X, Saxena NK, Lin S, Xu A, Srinivasan S, Anania FA. The roles of leptin and adiponectin: a novel paradigm in adipocytokine regulation of liver fibrosis and stellate cell biology. The American journal of pathology. 2005;166(6):1655-69. Epub 2005/05/28. doi: 10.1016/s0002-9440(10)62476-5. PubMed PMID: 15920151; PubMed Central PMCID: PMCPMC1602420.

113.   Konner AC, Bruning JC. Selective insulin and leptin resistance in metabolic disorders. Cell metabolism. 2012;16(2):144-52. Epub 2012/08/14. doi: 10.1016/j.cmet.2012.07.004. PubMed PMID: 22883229.

114.   Rivera CA, Adegboyega P, van Rooijen N, Tagalicud A, Allman M, Wallace M. Toll-like receptor-4 signaling and Kupffer cells play pivotal roles in the pathogenesis of non-alcoholic steatohepatitis. J Hepatol. 2007;47(4):571-9. Epub 2007/07/24. doi: 10.1016/j.jhep.2007.04.019. PubMed PMID: 17644211; PubMed Central PMCID: PMCPMC2094119.

115.   Mathurin P, Deng QG, Keshavarzian A, Choudhary S, Holmes EW, Tsukamoto H. Exacerbation of alcoholic liver injury by enteral endotoxin in rats. Hepatology. 2000;32(5):1008-17. Epub 2000/10/26. doi: 10.1053/jhep.2000.19621. PubMed PMID: 11050051.

116.   Chen M, Huang W, Wang C, Nie H, Li G, Sun T, et al. High-mobility group box 1 exacerbates CCl(4)-induced acute liver injury in mice. Clinical immunology (Orlando, Fla). 2014;153(1):56-63. Epub 2014/04/15. doi: 10.1016/j.clim.2014.03.021. PubMed PMID: 24726765.

117.   Eguchi K, Manabe I, Oishi-Tanaka Y, Ohsugi M, Kono N, Ogata F, et al. Saturated fatty acid and TLR signaling link beta cell dysfunction and islet inflammation. Cell metabolism. 2012;15(4):518-33. Epub 2012/04/03. doi: 10.1016/j.cmet.2012.01.023. PubMed PMID: 22465073.

118.   Fan J, Frey RS, Malik AB. TLR4 signaling induces TLR2 expression in endothelial cells via neutrophil NADPH oxidase. The Journal of clinical investigation. 2003;112(8):1234-43. Epub 2003/10/17. doi: 10.1172/jci18696. PubMed PMID: 14561708; PubMed Central PMCID: PMCPMC213490.

119.   Liang Q, Dong S, Lei L, Liu J, Zhang J, Li J, et al. Protective effects of Sparstolonin B, a selective TLR2 and TLR4 antagonist, on mouse endotoxin shock. Cytokine. 2015. Epub 2015/01/13. doi: 10.1016/j.cyto.2014.12.003. PubMed PMID: 25573805.

120.   Bohinc BN, Diehl AM. Mechanisms of disease progression in NASH: new paradigms. Clinics in liver disease. 2012;16(3):549-65. Epub 2012/07/25. doi: 10.1016/j.cld.2012.05.002. PubMed PMID: 22824480.

121.   El Kasmi KC, Anderson AL, Devereaux MW, Fillon SA, Harris JK, Lovell MA, et al. Toll-like receptor 4-dependent Kupffer cell activation and liver injury in a novel mouse model of parenteral nutrition and intestinal injury. Hepatology. 2012;55(5):1518-28. Epub 2011/11/29. doi: 10.1002/hep.25500. PubMed PMID: 22120983.

122.   Jaedicke KM, Roythorne A, Padget K, Todryk S, Preshaw PM, Taylor JJ. Leptin up-regulates TLR2 in human monocytes. Journal of leukocyte biology. 2013;93(4):561-71. Epub 2013/01/24. doi: 10.1189/jlb.1211606. PubMed PMID: 23341537.

123.	Loukili N, Rosenblatt-Velin N, Li J, Clerc S, Pacher P, Feihl F, et al. Peroxynitrite induces HMGB1 release by cardiac cells in vitro and HMGB1 upregulation in the infarcted myocardium in vivo. Cardiovascular research. 2011;89(3):586-94. Epub 2010/11/30. doi: 10.1093/cvr/cvq373. PubMed PMID: 21113057; PubMed Central PMCID: PMCPMC3028979.

124.	Ogden CL, Carroll MD, Kit BK, Flegal KM. Prevalence of childhood and adult obesity in the United States, 2011-2012. JAMA. 2014;311(8):806-14. doi: 10.1001/jama.2014.732. PubMed PMID: 24570244; PubMed Central PMCID: PMCPMC4770258.

125.	Larrain S, Rinella ME. A myriad of pathways to NASH. Clin Liver Dis. 2012;16(3):525-48. doi: 10.1016/j.cld.2012.05.009. PubMed PMID: 22824479.

126.	Pasarin M, La Mura V, Gracia-Sancho J, Garcia-Caldero H, Rodriguez-Vilarrupla A, Garcia-Pagan JC, et al. Sinusoidal endothelial dysfunction precedes inflammation and fibrosis in a model of NAFLD. PLoS One. 2012;7(4):e32785. doi: 10.1371/journal.pone.0032785. PubMed PMID: 22509248; PubMed Central PMCID: PMCPMC3317918.

127.	Zezos P, Renner EL. Liver transplantation and non-alcoholic fatty liver disease. World J Gastroenterol. 2014;20(42):15532-8. doi: 10.3748/wjg.v20.i42.15532. PubMed PMID: 25400437; PubMed Central PMCID: PMCPMC4229518.

128.	Targher G, Day CP, Bonora E. Risk of cardiovascular disease in patients with nonalcoholic fatty liver disease. N Engl J Med. 2010;363(14):1341-50. doi: 10.1056/NEJMra0912063. PubMed PMID: 20879883.

129.	Chandrashekaran V, Das S, Seth RK, Dattaroy D, Alhasson F, Michelotti G, et al. Purinergic receptor X7 mediates leptin induced GLUT4 function in stellate cells in nonalcoholic steatohepatitis. Biochim Biophys Acta. 2016;1862(1):32-45. doi: 10.1016/j.bbadis.2015.10.009. PubMed PMID: 26474534; PubMed Central PMCID: PMCPMC4988689.

130.	Zhang JG, Wang JJ, Zhao F, Liu Q, Jiang K, Yang GH. MicroRNA-21 (miR-21) represses tumor suppressor PTEN and promotes growth and invasion in non-small cell lung cancer (NSCLC). Clin Chim Acta. 2010;411(11-12):846-52. doi: 10.1016/j.cca.2010.02.074. PubMed PMID: 20223231.

131.	Yang L, Seki E. Toll-like receptors in liver fibrosis: cellular crosstalk and mechanisms. Frontiers in physiology. 2012;3:138. Epub 2012/06/05. doi: 10.3389/fphys.2012.00138. PubMed PMID: 22661952; PubMed Central PMCID: PMCPMC3357552.

132.	Yin H, Tan Y, Wu X, Yan H, Liu F, Yao Y, et al. Association between TLR4 and PTEN Involved in LPS-TLR4 Signaling Response. Biomed Res Int. 2016;2016:6083178. doi: 10.1155/2016/6083178. PubMed PMID: 27563672; PubMed Central PMCID: PMCPMC4985570.

133.	Odkhuu E, Mendjargal A, Koide N, Naiki Y, Komatsu T, Yokochi T. Lipopolysaccharide downregulates the expression of p53 through activation of MDM2 and enhances activation of nuclear factor-kappa B. Immunobiology. 2015;220(1):136-41. Epub 2014/08/31. doi: 10.1016/j.imbio.2014.08.010. PubMed PMID: 25172547.

134.	Krizhanovsky V, Yon M, Dickins RA, Hearn S, Simon J, Miething C, et al. Senescence of activated stellate cells limits liver fibrosis. Cell. 2008;134(4):657-67. Epub

2008/08/30. doi: 10.1016/j.cell.2008.06.049. PubMed PMID: 18724938; PubMed Central PMCID: PMCPMC3073300.

135. Brooks CL, Gu W. p53 ubiquitination: Mdm2 and beyond. Mol Cell. 2006;21(3):307-15. Epub 2006/02/04. doi: 10.1016/j.molcel.2006.01.020. PubMed PMID: 16455486; PubMed Central PMCID: PMCPMC3737769.

136. Benson EK, Mungamuri SK, Attie O, Kracikova M, Sachidanandam R, Manfredi JJ, et al. p53-dependent gene repression through p21 is mediated by recruitment of E2F4 repression complexes. Oncogene. 2014;33(30):3959-69. doi: 10.1038/onc.2013.378. PubMed PMID: 24096481; PubMed Central PMCID: PMCPMC4067464.

137. Yang JJ, Tao H, Li J. Hedgehog signaling pathway as key player in liver fibrosis: new insights and perspectives. Expert Opin Ther Targets. 2014;18(9):1011-21. doi: 10.1517/14728222.2014.927443. PubMed PMID: 24935558.

138. Rimkus TK, Carpenter RL, Qasem S, Chan M, Lo HW. Targeting the Sonic Hedgehog Signaling Pathway: Review of Smoothened and GLI Inhibitors. Cancers (Basel). 2016;8(2). doi: 10.3390/cancers8020022. PubMed PMID: 26891329; PubMed Central PMCID: PMCPMC4773745.

139. Yoon JW, Lamm M, Iannaccone S, Higashiyama N, Leong KF, Iannaccone P, et al. p53 modulates the activity of the GLI1 oncogene through interactions with the shared coactivator TAF9. DNA Repair (Amst). 2015;34:9-17. doi: 10.1016/j.dnarep.2015.06.006. PubMed PMID: 26282181; PubMed Central PMCID: PMCPMC4592456.

140. Li T, Leng XS, Zhu JY, Wang G. Suppression of hedgehog signaling regulates hepatic stellate cell activation and collagen secretion. Int J Clin Exp Pathol.

2015;8(11):14574-9. PubMed PMID: 26823780; PubMed Central PMCID: PMCPMC4713566.

141.   Kenney AM, Rowitch DH. Sonic hedgehog promotes G(1) cyclin expression and sustained cell cycle progression in mammalian neuronal precursors. Molecular and cellular biology. 2000;20(23):9055-67. Epub 2000/11/14. PubMed PMID: 11074003; PubMed Central PMCID: PMCPMC86558.

142.   Duman-Scheel M, Weng L, Xin S, Du W. Hedgehog regulates cell growth and proliferation by inducing Cyclin D and Cyclin E. Nature. 2002;417(6886):299-304. Epub 2002/05/17. doi: 10.1038/417299a. PubMed PMID: 12015606.

143.   Sun Y, Guo W, Ren T, Liang W, Zhou W, Lu Q, et al. Gli1 inhibition suppressed cell growth and cell cycle progression and induced apoptosis as well as autophagy depending on ERK1/2 activity in human chondrosarcoma cells. Cell death & disease. 2014;5:e979. Epub 2014/01/05. doi: 10.1038/cddis.2013.497. PubMed PMID: 24384722; PubMed Central PMCID: PMCPMC4040663.

144.   Zhao XK, Yu L, Cheng ML, Che P, Lu YY, Zhang Q, et al. Focal Adhesion Kinase Regulates Hepatic Stellate Cell Activation and Liver Fibrosis. Scientific reports. 2017;7(1):4032. Epub 2017/06/24. doi: 10.1038/s41598-017-04317-0. PubMed PMID: 28642549; PubMed Central PMCID: PMCPMC5481439.

145.   Pan Q, Li DG, Lu HM, Lu LY, Wang YQ, Xu QF. Antiproliferative and proapoptotic effects of somatostatin on activated hepatic stellate cells. World journal of gastroenterology. 2004;10(7):1015-8. Epub 2004/03/31. PubMed PMID: 15052685; PubMed Central PMCID: PMCPMC4717091.

146. Balta C, Herman H, Boldura OM, Gasca I, Rosu M, Ardelean A, et al. Chrysin attenuates liver fibrosis and hepatic stellate cell activation through TGF-beta/Smad signaling pathway. Chemico-biological interactions. 2015;240:94-101. Epub 2015/08/25. doi: 10.1016/j.cbi.2015.08.013. PubMed PMID: 26297989.

147. Fausther M, Lavoie EG, Dranoff JA. Contribution of Myofibroblasts of Different Origins to Liver Fibrosis. Curr Pathobiol Rep. 2013;1(3):225-30. doi: 10.1007/s40139-013-0020-0. PubMed PMID: 23997993; PubMed Central PMCID: PMCPMC3755779.

148. Forbes SJ, Parola M. Liver fibrogenic cells. Best Pract Res Clin Gastroenterol. 2011;25(2):207-17. doi: 10.1016/j.bpg.2011.02.006. PubMed PMID: 21497739.

149. Amarapurka DN, Amarapurkar AD, Patel ND, Agal S, Baigal R, Gupte P, et al. Nonalcoholic steatohepatitis (NASH) with diabetes: predictors of liver fibrosis. Ann Hepatol. 2006;5(1):30-3. PubMed PMID: 16531962.

150. Fierbinteanu-Braticevici C, Bengus A, Neamtu M, Usvat R. The risk factors of fibrosis in nonalcoholic steatohepatitis. Rom J Intern Med. 2002;40(1-4):81-8. PubMed PMID: 15526543.

151. Yoshioka Y, Hashimoto E, Yatsuji S, Kaneda H, Taniai M, Tokushige K, et al. Nonalcoholic steatohepatitis: cirrhosis, hepatocellular carcinoma, and burnt-out NASH. J Gastroenterol. 2004;39(12):1215-8. doi: 10.1007/s00535-004-1475-x. PubMed PMID: 15622489.

152. Higashi T, Friedman SL, Hoshida Y. Hepatic stellate cells as key target in liver fibrosis. Adv Drug Deliv Rev. 2017. doi: 10.1016/j.addr.2017.05.007. PubMed PMID: 28506744.

153.   Blond E, Disse E, Cuerq C, Drai J, Valette PJ, Laville M, et al. EASL-EASD-EASO clinical practice guidelines for the management of non-alcoholic fatty liver disease in severely obese people: do they lead to over-referral? Diabetologia. 2017;60(7):1218-22. doi: 10.1007/s00125-017-4264-9. PubMed PMID: 28352941.

154.   Yi HS, Jeong WI. Interaction of hepatic stellate cells with diverse types of immune cells: foe or friend? J Gastroenterol Hepatol. 2013;28 Suppl 1:99-104. doi: 10.1111/jgh.12017. PubMed PMID: 23855303.

155.   Fukui H, Tsujita S, Matsumoto M, Morimura M, Kitano H, Kinoshita K, et al. Endotoxin inactivating action of plasma in patients with liver cirrhosis. Liver. 1995;15(2):104-9. PubMed PMID: 7791538.

156.   Weber SN, Bohner A, Dapito DH, Schwabe RF, Lammert F. TLR4 Deficiency Protects against Hepatic Fibrosis and Diethylnitrosamine-Induced Pre-Carcinogenic Liver Injury in Fibrotic Liver. PLoS One. 2016;11(7):e0158819. doi: 10.1371/journal.pone.0158819. PubMed PMID: 27391331; PubMed Central PMCID: PMCPMC4938399.

157.   Carrillo-Sepulveda MA, Spitler K, Pandey D, Berkowitz DE, Matsumoto T. Inhibition of TLR4 attenuates vascular dysfunction and oxidative stress in diabetic rats. J Mol Med (Berl). 2015;93(12):1341-54. doi: 10.1007/s00109-015-1318-7. PubMed PMID: 26184970.

158.   Shen XD, Ke B, Zhai Y, Gao F, Tsuchihashi S, Lassman CR, et al. Absence of toll-like receptor 4 (TLR4) signaling in the donor organ reduces ischemia and reperfusion injury in a murine liver transplantation model. Liver Transpl. 2007;13(10):1435-43. doi: 10.1002/lt.21251. PubMed PMID: 17902130.

159. Tang LY, Heller M, Meng Z, Yu LR, Tang Y, Zhou M, et al. Transforming Growth Factor-beta (TGF-beta) Directly Activates the JAK1-STAT3 Axis to Induce Hepatic Fibrosis in Coordination with the SMAD Pathway. The Journal of biological chemistry. 2017;292(10):4302-12. Epub 2017/02/06. doi: 10.1074/jbc.M116.773085. PubMed PMID: 28154170; PubMed Central PMCID: PMCPMC5354477.

160. Edlund S, Landstrom M, Heldin CH, Aspenstrom P. Transforming growth factor-beta-induced mobilization of actin cytoskeleton requires signaling by small GTPases Cdc42 and RhoA. Molecular biology of the cell. 2002;13(3):902-14. Epub 2002/03/22. doi: 10.1091/mbc.01-08-0398. PubMed PMID: 11907271; PubMed Central PMCID: PMCPMC99608.

161. Seki E, De Minicis S, Osterreicher CH, Kluwe J, Osawa Y, Brenner DA, et al. TLR4 enhances TGF-beta signaling and hepatic fibrosis. Nat Med. 2007;13(11):1324-32. Epub 2007/10/24. doi: 10.1038/nm1663. PubMed PMID: 17952090.

162. Onichtchouk D, Chen YG, Dosch R, Gawantka V, Delius H, Massague J, et al. Silencing of TGF-beta signalling by the pseudoreceptor BAMBI. Nature. 1999;401(6752):480-5. Epub 1999/10/16. doi: 10.1038/46794. PubMed PMID: 10519551.

163. Liu C, Chen X, Yang L, Kisseleva T, Brenner DA, Seki E. Transcriptional repression of the transforming growth factor beta (TGF-beta) Pseudoreceptor BMP and activin membrane-bound inhibitor (BAMBI) by Nuclear Factor kappaB (NF-kappaB) p50 enhances TGF-beta signaling in hepatic stellate cells. The Journal of biological chemistry. 2014;289(10):7082-91. Epub 2014/01/23. doi: 10.1074/jbc.M113.543769. PubMed PMID: 24448807; PubMed Central PMCID: PMCPMC3945368.

164.   Dallas SL, Sivakumar P, Jones CJ, Chen Q, Peters DM, Mosher DF, et al. Fibronectin regulates latent transforming growth factor-beta (TGF beta) by controlling matrix assembly of latent TGF beta-binding protein-1. The Journal of biological chemistry. 2005;280(19):18871-80. Epub 2005/01/29. doi: 10.1074/jbc.M410762200. PubMed PMID: 15677465.

165.   Leask A, Abraham DJ. TGF-beta signaling and the fibrotic response. FASEB J. 2004;18(7):816-27. Epub 2004/05/01. doi: 10.1096/fj.03-1273rev. PubMed PMID: 15117886.

166.   Friedman SL. Hepatic stellate cells: protean, multifunctional, and enigmatic cells of the liver. Physiol Rev. 2008;88(1):125-72. Epub 2008/01/16. doi: 10.1152/physrev.00013.2007. PubMed PMID: 18195085; PubMed Central PMCID: PMCPMC2888531.

167.   Nunez Lopez O, Bohanon FJ, Wang X, Ye N, Corsello T, Rojas-Khalil Y, et al. STAT3 Inhibition Suppresses Hepatic Stellate Cell Fibrogenesis: HJC0123, a Potential Therapeutic Agent for Liver Fibrosis. RSC advances. 2016;6(102):100652-63. Epub 2016/01/01. doi: 10.1039/c6ra17459k. PubMed PMID: 28546859; PubMed Central PMCID: PMCPMC5440088.

168.   Xu MY, Hu JJ, Shen J, Wang ML, Zhang QQ, Qu Y, et al. Stat3 signaling activation crosslinking of TGF-beta1 in hepatic stellate cell exacerbates liver injury and fibrosis. Biochimica et biophysica acta. 2014;1842(11):2237-45. Epub 2014/08/06. doi: 10.1016/j.bbadis.2014.07.025. PubMed PMID: 25092172.

169.   Turner CE. Paxillin and focal adhesion signalling. Nature cell biology. 2000;2(12):E231-6. Epub 2001/01/09. doi: 10.1038/35046659. PubMed PMID: 11146675.

170.   Oakes PW, Beckham Y, Stricker J, Gardel ML. Tension is required but not sufficient for focal adhesion maturation without a stress fiber template. The Journal of cell biology. 2012;196(3):363-74. Epub 2012/02/01. doi: 10.1083/jcb.201107042. PubMed PMID: 22291038; PubMed Central PMCID: PMCPMC3275371.

171.   Anthony B, Allen JT, Li YS, McManus DP. Hepatic stellate cells and parasite-induced liver fibrosis. Parasites & vectors. 2010;3(1):60. Epub 2010/07/29. doi: 10.1186/1756-3305-3-60. PubMed PMID: 20663176; PubMed Central PMCID: PMCPMC2915969.

172.   Liu XY, Liu RX, Hou F, Cui LJ, Li CY, Chi C, et al. Fibronectin expression is critical for liver fibrogenesis in vivo and in vitro. Mol Med Rep. 2016;14(4):3669-75. Epub 2016/08/31. doi: 10.3892/mmr.2016.5673. PubMed PMID: 27572112; PubMed Central PMCID: PMCPMC5042748.

173.   Hata A, Chen YG. TGF-beta Signaling from Receptors to Smads. Cold Spring Harbor perspectives in biology. 2016;8(9). Epub 2016/07/28. doi: 10.1101/cshperspect.a022061. PubMed PMID: 27449815.

174.   Zhang YE. Non-Smad Signaling Pathways of the TGF-beta Family. Cold Spring Harbor perspectives in biology. 2017;9(2). Epub 2016/11/20. doi: 10.1101/cshperspect.a022129. PubMed PMID: 27864313.

175.   Zhang C, Meng X, Zhu Z, Liu J, Deng A. Connective tissue growth factor regulates the key events in tubular epithelial to myofibroblast transition in vitro. Cell

biology international. 2004;28(12):863-73. Epub 2004/11/30. doi: 10.1016/j.cellbi.2004.09.003. PubMed PMID: 15566956.

176.   Silver DL, Naora H, Liu J, Cheng W, Montell DJ. Activated signal transducer and activator of transcription (STAT) 3: localization in focal adhesions and function in ovarian cancer cell motility. Cancer research. 2004;64(10):3550-8. Epub 2004/05/20. doi: 10.1158/0008-5472.can-03-3959. PubMed PMID: 15150111.

177.   Hinz B, Dugina V, Ballestrem C, Wehrle-Haller B, Chaponnier C. Alpha-smooth muscle actin is crucial for focal adhesion maturation in myofibroblasts. Molecular biology of the cell. 2003;14(6):2508-19. Epub 2003/06/17. doi: 10.1091/mbc.E02-11-0729. PubMed PMID: 12808047; PubMed Central PMCID: PMCPMC194898.

178.   Farrell GC, van Rooyen D, Gan L, Chitturi S. NASH is an Inflammatory Disorder: Pathogenic, Prognostic and Therapeutic Implications. Gut and liver. 2012;6(2):149-71. Epub 2012/05/10. doi: 10.5009/gnl.2012.6.2.149. PubMed PMID: 22570745; PubMed Central PMCID: PMCPMC3343154.

179.   Liang S, Kisseleva T, Brenner DA. The Role of NADPH Oxidases (NOXs) in Liver Fibrosis and the Activation of Myofibroblasts. Frontiers in physiology. 2016;7:17. Epub 2016/02/13. doi: 10.3389/fphys.2016.00017. PubMed PMID: 26869935; PubMed CentralPMCID:PMCPMC4735448.

APPENDIX A: COPYRIGHT PERMISSION FOR CHAPTERS 2 AND 3

Copyright

The APS Journals are copyrighted for the protection of authors and the Society. The Mandatory Submission Form serves as the Society's official copyright transfer form.

Rights of Authors of APS Articles

- For educational purposes only:
  - Authors may republish parts of their final-published version articles (e.g., figures, tables), without charge and without requesting permission, provided that full acknowledgement of the source is given in the new work.
  - Authors may use their articles (in whole or in part) for presentations (e.g., at meetings and conferences). These presentations may be reproduced on any type of media in materials arising from the meeting or conference such as the proceedings of a meeting or conference. A copyright fee will apply if there is a charge to the user or if the materials arising are directly or indirectly commercially supported.

- Posting of the accepted or final version of articles or parts of articles is restricted and subject to the conditions below:
  - *Theses and dissertations.* APS permits whole published articles to be reproduced without charge in dissertations and posted to thesis repositories. Full citation is required.
  - *Open courseware.* Articles, or parts of articles, may be posted to a public access courseware website. Permission must be requested from the APS. A copyright fee will apply during the first 12 months of the article's publication by the APS. Full citation is required.
  - *Websites.* Authors may not post a PDF of the accepted or final version of their published article on any website including social and research networking platforms; instead, links may be posted to the article on the APS journal website (see exception to authors' own institution's repository, as note below).
  - *Institutional repositories (non-theses).* Authors may deposit their accepted, peer-reviewed manuscripts into an institutional repository providing:
    - the APS retains copyright to the article[1]
    - a 12 month embargo period from the date of final publication of the article is observed by the institutional repository and the author
    - a link to the published article on the APS website is prominently displayed with the article in the institutional repository
    - the article is not used for commercial purposes
    - Self-archived articles posted to repositories are without warranty of any kind

[1]Unless it is published under the APS *AuthorChoice* open access option, which allows for immediate public access under a Creative Commons license (CC BY)

(See also the APS Policy on Depositing Articles in PMC.)

157